WT-902 (EX)
EXTRACTED VERSION

OPERATION CASTLE

Projects 1.1a, 1.1b, and 1.1d
Blast Pressures and Shock Phenomena Measurements by Photography

March-May 1954

Headquarters Field Command
Armed Forces Special Weapons Project
Sandia Base, Albuquerque, New Mexico

September 1955

NOTICE

This is an extract of WT-902, Operation CASTLE, which remains classified SECRET/RESTRICTED DATA as of this date.

Extract version prepared for:

Director
DEFENSE NUCLEAR AGENCY
Washington, D.C. 20305

1 April 1981

Approved for public release; distribution unlimited.

REPRODUCED BY
NATIONAL TECHNICAL
INFORMATION SERVICE
U.S. DEPARTMENT OF COMMERCE
SPRINGFIELD, VA. 22161

(9) Rept. for Mar-May 54,

UNCLASSIFIED
SECURITY CLASSIFICATION OF THIS PAGE (When Data Entered)

REPORT DOCUMENTATION PAGE	READ INSTRUCTIONS BEFORE COMPLETING FORM
1. REPORT NUMBER: WT-902 (EX)	2. GOVT ACCESSION NO.: AD-A995102	3. RECIPIENT'S CATALOG NUMBER
4. TITLE (and Subtitle): (6) Operation CASTLE.- Projects 1.1a, 1.1b, and 1.1d, Blast Pressures and Shock Phenomena Measurements by Photography.	5. TYPE OF REPORT & PERIOD COVERED: (14) DOE
	6. PERFORMING ORG. REPORT NUMBER: (14) WT-902 (EX)
7. AUTHOR(s): (10) P. Hanlon, J. F. Moulton, Jr., S. L. Woolley, C. J. Aronson	8. CONTRACT OR GRANT NUMBER(s): (15) DNA001-79-C-0455
9. PERFORMING ORGANIZATION NAME AND ADDRESS: Headquarters Field Command, Armed Forces Special Weapons Project, Sandia Base, Albuquerque, N.M. (11)	10. PROGRAM ELEMENT, PROJECT, TASK AREA & WORK UNIT NUMBERS: 1 Apr 81
11. CONTROLLING OFFICE NAME AND ADDRESS	12. REPORT DATE: ~~September 1955~~
	13. NUMBER OF PAGES: ~~98~~ (12) 99
14. MONITORING AGENCY NAME & ADDRESS (if different from Controlling Office)	15. SECURITY CLASS. (of this report): Unclassified
	15a. DECLASSIFICATION/DOWNGRADING SCHEDULE

16. DISTRIBUTION STATEMENT (of this Report)

Approved for public release; unlimited distribution.

17. DISTRIBUTION STATEMENT (of the abstract entered in Block 20, if different from Report)

18. SUPPLEMENTARY NOTES

This report has had the classified information removed and has been republished in unclassified form for public release. This work was performed by Kaman Tempo under contract DNA001-79-C-0455 with the close cooperation of the Classification Management Division of the Defense Nuclear Agency.

19. KEY WORDS (Continue on reverse side if necessary and identify by block number)

Operation CASTLE
Blast Pressures
Shock Phenomena Measurements
Instrumentation

20. ABSTRACT (Continue on reverse side if necessary and identify by block number)

DD FORM 1 JAN 73 1473 EDITION OF 1 NOV 65 IS OBSOLETE

NOTICE

THIS DOCUMENT HAS BEEN REPRODUCED FROM THE BEST COPY FURNISHED US BY THE SPONSORING AGENCY. ALTHOUGH IT IS RECOGNIZED THAT CERTAIN PORTIONS ARE ILLEGIBLE, IT IS BEING RELEASED IN THE INTEREST OF MAKING AVAILABLE AS MUCH INFORMATION AS POSSIBLE.

FOREWORD

This report has had classified material removed in order to make the information available on an unclassified, open publication basis, to any interested parties. This effort to declassify this report has been accomplished specifically to support the Department of Defense Nuclear Test Personnel Review (NTPR) Program. The objective is to facilitate studies of the low levels of radiation received by some individuals during the atmospheric nuclear test program by making as much information as possible available to all interested parties.

The material which has been deleted is all currently classified as Restricted Data or Formerly Restricted Data under the provision of the Atomic Energy Act of 1954, (as amended) or is National Security Information.

This report has been reproduced directly from available copies of the original material. The locations from which material has been deleted is generally obvious by the spacings and "holes" in the text. Thus the context of the material deleted is identified to assist the reader in the determination of whether the deleted information is germane to his study.

It is the belief of the individuals who have participated in preparing this report by deleting the classified material and of the Defense Nuclear Agency that the report accurately portrays the contents of the original and that the deleted material is of little or no significance to studies into the amounts or types of radiation received by any individuals during the atmospheric nuclear test program.

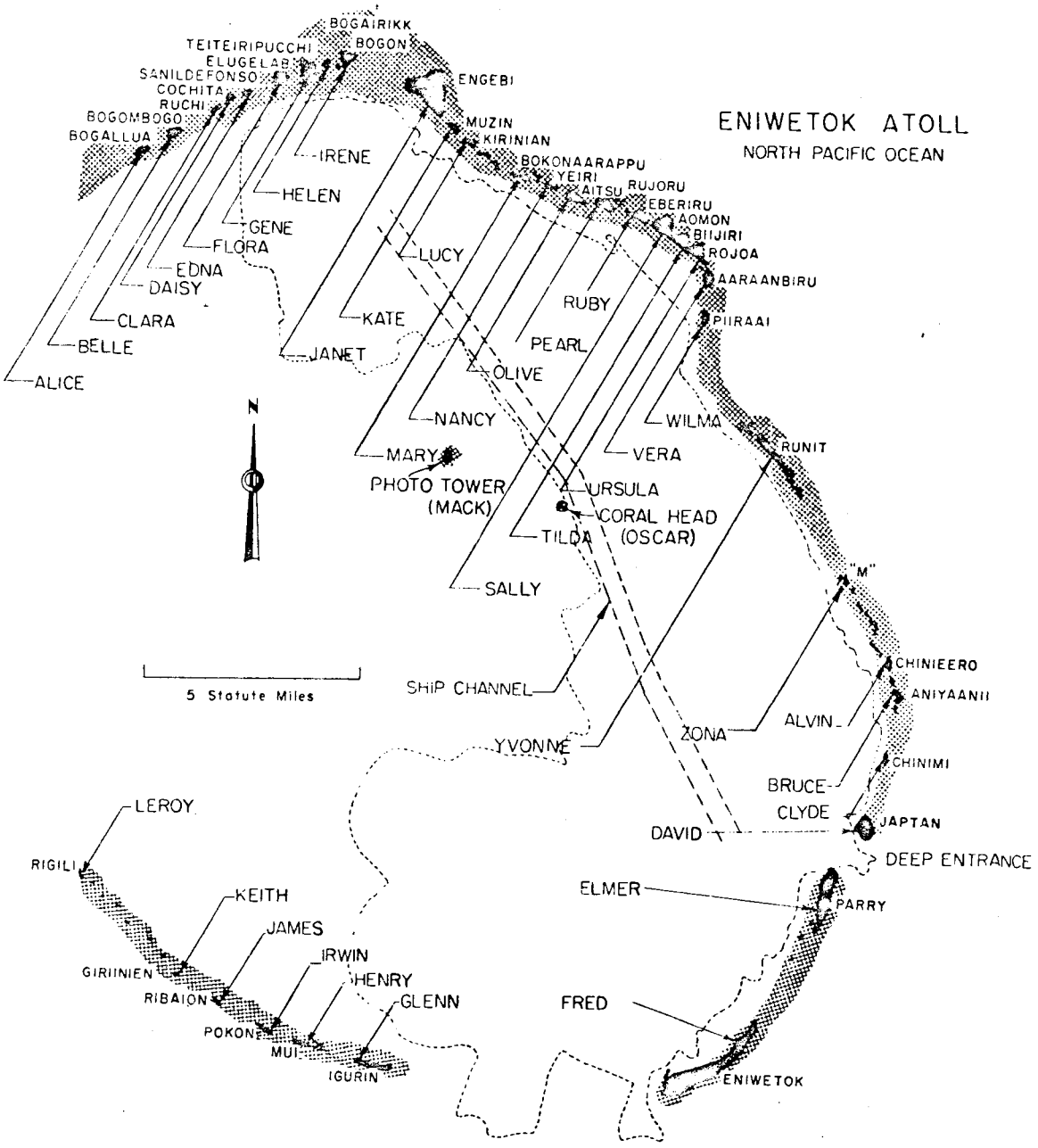
ENIWETOK ATOLL
NORTH PACIFIC OCEAN
BOGAIRIKK
TEITEIRIPUCCHI
BOGON
ELUGELAB
SANILDEFONSO
COCHITA
RUCHI
BOGOMBOGO
BOGALLUA
ENGEBI
MUZIN
KIRINIAN
BOKONAARAPPU
YEIRI
AITSU
RUJORU
EBERIRU
AOMON
BIIJIRI
ROJOA
AARAANBIRU
PIIRAAI
IRENE
HELEN
GENE
FLORA
EDNA
DAISY
CLARA
BELLE
ALICE
LUCY
KATE
JANET
RUBY
PEARL
OLIVE
NANCY
MARY
PHOTO TOWER
(MACK)
WILMA
VERA
RUNIT
URSULA
CORAL HEAD
(OSCAR)
TILDA
SALLY
"M"
CHINIEERO
ANIYAANII
CHINIMI
SHIP CHANNEL
YVONNE
ZONA
ALVIN
BRUCE
CLYDE
DAVID
JAPTAN
DEEP ENTRANCE
ELMER
PARRY
FRED
ENIWETOK
LEROY
RIGILI
KEITH
JAMES
IRWIN
HENRY
GLENN
GIRIINIEN
RIBAION
POKON
MUI
IGURIN
N
5 Statute Miles

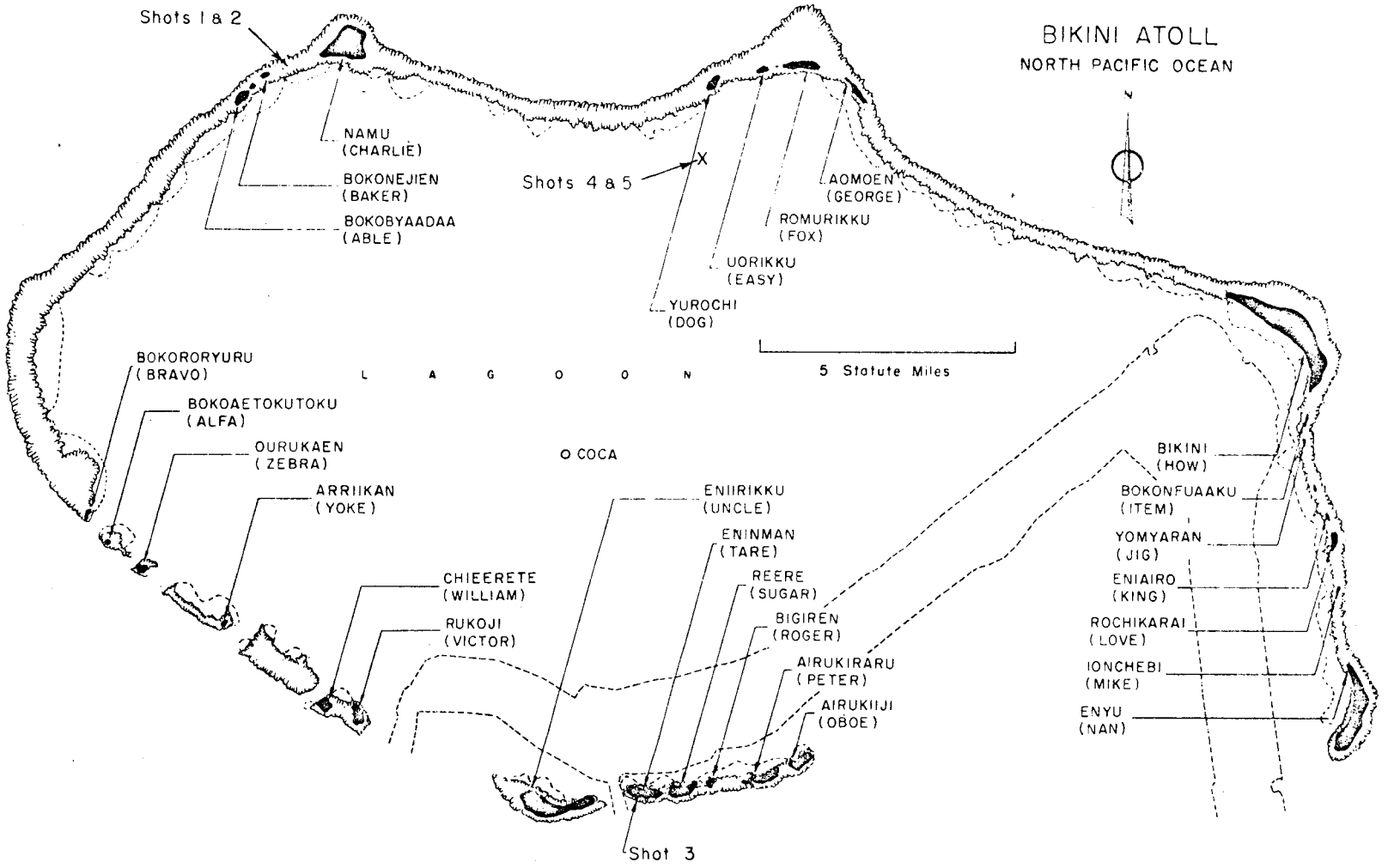
BIKINI ATOLL
NORTH PACIFIC OCEAN
Shots 1 & 2
Shots 4 & 5
Shot 3
NAMU (CHARLIE)
BOKONEJIEN (BAKER)
BOKOBYAADAA (ABLE)
AOMOEN (GEORGE)
ROMURIKKU (FOX)
UORIKKU (EASY)
YUROCHI (DOG)
BOKORORYURU (BRAVO)
BOKOAETOKUTOKU (ALFA)
OURUKAEN (ZEBRA)
ARRIIKAN (YOKE)
CHIEERETE (WILLIAM)
RUKOJI (VICTOR)
ENIIRIKKU (UNCLE)
ENINMAN (TARE)
REERE (SUGAR)
BIGIREN (ROGER)
AIRUKIRARU (PETER)
AIRUKIIJI (OBOE)
BIKINI (HOW)
BOKONFUAAKU (ITEM)
YOMYARAN (JIG)
ENIAIRO (KING)
ROCHIKARAI (LOVE)
IONCHEBI (MIKE)
ENYU (NAN)
COCA
LAGOON
5 Statute Miles

GENERAL SHOT INFORMATION

	Shot 1	Shot 2	Shot 3	Shot 4	Shot 5	Shot 6
DATE	1 March	27 March	7 April	26 April	5 May	14 May
CODE NAME (Unclassified)	Bravo	Romeo	Koon	Union	Yankee	Nectar
TIME*	06:40	06:25	06:15	06:05	06:05	06:15
LOCATION	Bikini, West of Charlie (Namu) on Reef	Bikini, Shot 1 Crater	Bikini, Tare (Eninman)	Bikini, on Barge at Intersection of Arcs with Radii of 6900' from Dog (Yurochi) and 3 Statute Miles from Fox (Aomoen).		Eniwetok, IVY Mike Crater, Flora (Elugelab)
TYPE	Land	Barge	Land	Barge	Barge	Barge
HOLMES & NARVER COORDINATES	N 170,617.17 E 76,163.98	N 170,635.05 E 75,950.46	N 100,154.50 E 109,799.00	N 161,698.83 E 116,800.27	N 161,424.43 E 116,688,15	N 147,750.00 E 67,790.00

* APPROXIMATE

ABSTRACT

The objective of Project 1.1a was to determine by smoke rocket photography, the peak shock overpressure as a function of distance.

The objective of Project 1.1b was to obtain, by direct shock photography, information on precursors and surface effects that might be formed as well as to obtain peak shock overpressure data on those shots not instrumented by Project 1.1a.

The objective of Project 1.1d was to extend by aerial photography the range of measurements to regions not observable in Projects 1.1a and 1.1b.

The results and conclusions may be summarized as follows:

GENERAL

The photographic methods of Projects 1.1a and 1.1b proved to be successful, particularly on Shots 1, 2, 4, and 6.

Project 1.1d was not successful. The films obtained were not usable for one or more of the following reasons:

a. Cloud obscuration.
b. Overexposed films.
c. Large timing and spatial uncertainties.

THE FIREBALL REGION

On all observed shots the growth of the fireball was greater vertically than that along the surface; and on all barge shots, a nipple-like protrusion appeared at the top of the fireball. This protrusion grew until about the time of shock breakaway when it ruptured and appeared to release the detonation products of the fireball. (On Shot 1 the top of the fireball was obscured by clouds and it is not known whether or not the effect existed.)

With the exception of Shot 5, on which the photography was considered to be unreliable, no asymmetry was detected in the fireball growth along the surface.

THE SHOCK REGION

With the exception of the Shot 2 land-surface data, which were known to be high, the pressure-distance data appeared to be trustworthy; the maximum uncertainty for Shots 1, 2 (water surface data), and 6 was 10%; the maximum uncertainty for Shot 4 was 7%. All pressures obtained were in the 500 psi to 10 psi region.

The use of the cube law for scaling pressure-distance curves for weapons of large yields (1.7 MT to 15 MT) in this region over a water surface was satisfactory. The reduced data were self-consistent to within 5% which was less than the experimental uncertainty (10%) and compared favorably with the free-air composite scaled to 2 KT (~ 10% to 15% low).

These CASTLE data, the IVY Mike data, and the JANGLE Surface data appeared compatible in common pressure regions.

No vertical shock data were obtained, except on Shot 2 where pressure-distance data in the 10,000 to 15,000 ft region were obtained. The uncertainties of these data ranged from 20% at 10,000 to 15% at 15,000 ft, which were too large to confirm NOL predicted pressures which had values within the spread of the experimental data.

On Shot 2, two wave fronts were observed at altitudes of ~265,000 ft to ~335,000 ft. The first was apparently the shock; the second was presumed to have been an acoustic wave.

SURFACE EFFECTS

No precursors were observed in any of the films, but a dense water cloud, believed to be the result of the interaction of the shock and the rough water surface, was generated immediately behind the shock of Shot 4. On the other shots, particularly Shot 2, in which the surface could not be viewed directly, there were strong indications of this effect, which is believed to have persisted to at least the 10 psi region.

This seems to confirm the existence of water droplets which Project 1.3 postulated as one of the causes for the anomalies observed in the wave forms and in the dynamic pressures obtained for Shots 4 and 5.

FOREWORD

This report is one of the reports presenting the results of the 34 projects participating in the Military Effects Tests Program of Operation CASTLE, which included six test detonations. For readers interested in other pertinent test information, reference is made to WT-934, Summary Report of the Commander, Task Unit 13, Programs 1-9, Military Effects Program. This summary report includes the following information of possible general interest.

a. An over-all description of each detonation, including yield, height of burst, ground zero location, time of detonation, ambient atmospheric conditions at detonation, etc., for the six shots.
b. Discussion of all project results.
c. A summary of each project, including objectives and results.
d. A complete listing of all reports covering the Military Effects Tests Program.

ACKNOWLEDGEMENTS

The authors are deeply indebted to Edwin G. Nacke of the U. S. Naval Ordnance Laboratory, A/3c Jack A. Martin, USAF, and A/3c William R. Rogers, USAF, all of whom contributed immeasurably to the success of the project. Their attention to detail in the preparatory and the field phases of the project simplified the effort considerably.

James R. Mitchell of NOL is to be commended for his part in the handling of the logistics of this project both in the laboratory and in the field.

The authors wish to express their gratitude to Walter Malmborg of NOL, who performed the machine analysis of the data and to M/Sgt Arlington E. McGee, USAF, for his efforts in preparing the report for publication.

Appreciation is expressed to the personnel of Edgerton, Germeshausen, and Grier, Inc., for their willing cooperation in all phases of the project.

CONTENTS

ABSTRACT 5

FOREWORD 7

ACKNOWLEDGMENTS 7

ILLUSTRATIONS 11

TABLES 12

CHAPTER 1 INTRODUCTION 13

1.1 Objectives and Scope 13
1.2 Background 14
1.2.1 History 14
1.3 Theory 15
1.3.1 The Methods of Measurement 15
1.3.2 Determination of the Arrival Time Data . . . 15
1.3.3 Determination of the Peak Shock Overpressure by the Velocity Method 19
1.3.4 Scaling Factors 21

CHAPTER 2 INSTRUMENTATION 23

2.1 Shot Summary and Participation 23
2.2 Rocket Instrumentation 23
2.2.1 The Smoke Rocket and the Rocket Launcher. . . 23
2.2.2 The Launching Site 25
2.2.3 Power and Timing at Launching Sites 26
2.3 Photographic Instrumentation 26

CHAPTER 3 RESULTS 30
3.1 Instrumentation 30
3.1.1 Projects 1.1a and 1.1b 30
3.1.2 Project 1.1d 30
3.2 Shot 1 32
3.2.1 Arrival Time Data 32
3.2.2 The Velocity and Peak Shock Overpressure-Distance Data 33
3.2.3 The Jet 38

Preceding page blank

3.3 Shot 2 39
3.3.1 The Arrival Time Data 39
3.3.2 The Velocity and Peak Shock Overpressure-Distance Data 52
3.4 Shot 3 53
3.5 Shot 4 53
3.5.1 Arrival Time Data 59
3.5.2 The Velocity, and Peak Shock Overpressure-Distance Data 63
3.6 Shot 5 63
3.6.1 Fireball Data 64
3.7 Shot 6 64
3.7.1 Arrival Time Data 64
3.7.2 The Peak Shock Overpressure-Distance Data. . 72
3.8 Surface Effects 72
3.9 Accuracy of Results 73
3.9.1 Sources of Error 73
3.9.2 Spatial Accuracy 77
3.9.3 Timing Accuracy. 78
3.9.4 The Accuracy of Peak Shock Overpressures . . 79
3.9.5 The Accuracy of the Vertical Data of Shot 2. 79

CHAPTER 4 DISCUSSION OF RESULTS 80

4.1 Scaled Results 80
4.1.1 Scaled Peak Shock Overpressure-Distance Data 80
4.1.2 Scaled Arrival Time Data 82
4.2 The Vertical Data of Shot 2 82
4.2.1 The Low-Altitude Data 82
4.2.2 The High-Altitude Data 84
4.3 Surface Effects 90

CHAPTER 5 CONCLUSIONS AND RECOMMENDATIONS 91
5.1 Instrumentation 91
5.1.1 Photography 1.1a and 1.1b 91
5.1.2 Photography 1.1d 91
5.1.3 Smoke Rockets 91
5.2 Experimental Results. 92
5.2.1 Surface Pressure-Distance Data 92
5.2.2 The Vertical Data of Shot 2. 92
5.2.3 Surface Effects 92

APPENDIX A DETERMINATION OF THE HORIZONTAL AIMING ANGLES . . 93

A.1.1 Shot 2 93
A.1.2 Shot 4 96

APPENDIX B METEOROLOGICAL DATA ALOFT FOR SHOT 2 97

BIBLIOGRAPHY 98

ILLUSTRATIONS

1.1 Geometry of the Primary and Secondary Planes of Measurement 17
1.2 Plan and Elevation Views of the nth Plane of Measurement. . 20
2.1 Instrumentation layout, Bikini 24
2.2 Instrumentation Layout, Eniwetok 25
2.3 The Variable Elevation Launcher and Associated Equipment. . 27
2.4 The Fan Grid Rocket Launching Station 27
2.5 Firing Circuit and Associated Equipment 28
3.1 Fireball Arrival Time Data, Shot 1 34
3.2 Surface Shock Arrival Time Data, Shot 1 36
3.3 Surface Fireball Velocity vs Distance, Shot 1 38
3.4 Surface Peak Shock Overpressure vs Distance, Shot 1 39
3.5 The Assumed Form of the Horizontal Jet, Shot 1 40
3.6 Horizontal Jet Data, Shot 1 41
3.7 Fireball Photographs Showing the Jet of Shot 1 42
3.8 Fireball Photographs Showing the Vertical Protrusion of Shot 2 43
3.9 High Altitude Arrival Time Data, Shot 2 45
3.10a Photographs of the First Wave Observed at Great Altitudes 46
3.10b Photographs of the Second Wave Observed at Great Altitudes 47
3.11 Fireball Arrival Time Data, Shot 2 51
3.12 Shock Arrival Time Data, Shot 2 52
3.13 Fireball Velocity vs Distance, Shot 2 54
3.14 Peak Shock Overpressure vs Distance, Shot 2 55
3.15 Fireball Photographs Showing the Vertical Protrusion of Shot 4 60
3.16 Fireball Arrival Time Data, Shot 4 61
3.17 Surface Shock Arrival Time Data, Shot 4 62
3.18 Fireball Velocity vs Distance, Shot 4 66
3.19 Surface Peak Shock Overpressure vs Distance, Shot 4 . . . 67
3.20 Fireball Arrival Time Data, Shot 5 68
3.21 Fireball Photographs Showing the Vertical Protrusion of Shot 6 69
3.22 Fireball Arrival Time Data, Shot 6 73
3.23 Surface Shock Arrival Time Data, Shot 6 74
3.24 Surface Peak Shock Overpressure vs Distance, Shot 6. . . . 75
3.25 The Growth of the Water Cloud Behind the Shock Front of Shot 4 76
4.1 Surface Pressure-Distance Data Scaled to 1 KT at Sea Level 81
4.2 Surface Arrival Time Data Scaled to 1 KT at Sea Level . . 83
4.3 Theoretical Surface Curves Derived from Shot 2 and IVY Mike Data 85

4.4 Vertical Pressure-Distance Data of Shot 2 Shown with Curves Predicted from NOL Theory 86

A.1 Plan and Elevation Views of the Geometry of the Optical Axis of the Primary Camera 94
A.2 Use of a Fiducial Marker of Unknown Location 95

TABLES

1.1 Summary Data for All Shots 22
2.1 Shot Participation 23
2.2 Rocket Instrumentation 26
2.3 Photographic Instrumentation 29
3.1 Photographic Instrumentation Results 31

3.2 Observed Arrival Time Data, Shot 1 35
3.3 Arrival Time, Velocity and Peak Shock Overpressure, Shot 1 37
3.4 Jet Data, Shot 1 37
3.5 Observed High Altitude Arrival Time Data, Shot 2 44
3.6 Observed Surface Arrival Time Data, Shot 2 48
3.7 Observed Vertical Arrival Time Data, Shot 2 50
3.8 Arrival Time, Velocity, and Peak Shock Overpressure, Shot 2 56
3.9 Observed Arrival Time Data, Shot 4 57
3.10 Arrival Time, Velocity, and Peak Shock Overpressure, Shot 4 59
3.11 Observed Arrival Time Data, Shot 5 65
3.12 Calculated Arrival Time, Shot 5 65
3.13 Observed Arrival Time Data, Shot 6 70
3.14 Arrival Time, Velocity, and Peak Shock Overpressure, Shot 6 71
4.1 Scaled Pressure-Distance Data 87
4.2 Composite Free-Air Arrival Time Data for 1 KT 88
4.3 Arrival Time Data Scaled to 1 KT at Sea Level 89

Meteorological Data Aloft for Shot 2 97

CHAPTER 1

INTRODUCTION

1.1 OBJECTIVES AND SCOPE

At the request of the Armed Forces Special Weapons Project, (AFSWP), the U. S. Naval Ordnance Laboratory (NOL) instituted Project 1.1 on Operation CASTLE. This project was designed to aid in the accomplishment of the mission of the Department of Defense Weapons Effects Test Program. [1]

The objectives of Project 1.1a were to determine the peak shock overpressure in air as a function of distance in regions:

a. Along the surface, and

b. Vertically above ground zero.*

The objective of Project 1.1b was to obtain further information relative to the formation, growth, and magnitude of precursors and other visible observable effects that might be formed as well as to obtain peak shock overpressure data on shots not instrumented by 1.1a.

The objectives of Project 1.1d, Aerial Photography, were two-fold. Only one was intimately connected with Projects 1.1a and 1.1b, namely to measure the motion of the shock wave on the water's surface as recorded on aerial motion pictures to obtain a pressure-distance relation. These measurements were to be made to extend the range of pressures well beyond that obtained under Projects 1.1a and 1.1b, and to obtain pressure-distance data in radial directions not observable in the records of Projects 1.1a and 1.1b. The second objective, which is discussed in the report on Project 1.1c, "Base Surge Measurements by Photography" was to take aerial photographs of the base surge to enable its motion to be measured in directions not covered by the conventional tower photography.

*. The Rankine-Hugoniot relation between shock pressure and velocity can be used only if the direction of shock propagation is known; consequently the measurements were restricted to the horizontal and the vertical.

1.2 BACKGROUND

With respect to a study of military effects, the importance of pressure-distance data in air is well founded. These data, used in conjunction with other information, namely knowledge of the formation and magnitude of precursors and other thermal effects and knowledge of the mechanical effects of the surface, contribute to the general understanding of shock wave behavior and enhance the ability to predict the blast fields resulting from explosions. When this information is correlated with damage studies it aids in predicting the effects that may be expected from the actual use of nuclear or thermonuclear weapons.

The pressure-distance data obtained on IVY Mike were limited to pressures less than 20 psi. Thus data obtained at higher pressures would be of use for verification of the scaling methods at these higher levels.

Recently at the NOL a theory [2,3] concerning the transmission of blast from high yield weapons (of the order of 1 MT or greater) through a non-homogeneous atmosphere was postulated. The theory indicates that the effects of the non-homogeneous atmosphere become apparent at relatively low altitudes. Operation CASTLE, then, presented an opportunity to make measurements of the effect of altitude on blast which it was hoped could be correlated with the theory.

1.2.1 History

The smoke-rocket trail photographic technique used on Project 1.1a to obtain peak overpressure in air was felt to be a suitable method on this operation in light of the results achieved on the JANGLE surface shot. The technique, developed at the NOL, was first used on Operation GREENHOUSE [4] and proved to be a success. On subsequent operations, JANGLE,[5] TUMBLER,[6] IVY,[7] and UPSHOT-KNOTHOLE,[8] satisfactory results were obtained. The technique was modified slightly for use on IVY, as it was for this operation, to conform to geographic limitations.

Project 1.1b utilized the method of direct shock photography to obtain its objectives. The method has been used with gratifying results by the NOL and other organizations on previous operations.

Aerial photography, Project 1.1d, was used on CROSSROADS [9] and GREENHOUSE [10] with limited success and accuracy because of cloud interference, low observation angles, and other distorting effects. Even though such difficulties were anticipated on CASTLE, NOL was asked to include the project chiefly because this technique might have been able to provide a means to confirm and extend the measurements made from the tower camera records under somewhat different experimental conditions. Nevertheless for reasons discussed in Section 3.1.2 the records obtained for Project 1.1d were not useful for extending or confirming the surface measurements obtained through Projects 1.1a and 1.1b.

1.3 THEORY

1.3.1 The Methods of Measurement

The method of measurement and the subsequent pressure calculations for Projects 1.1a and 1.1b were essentially the measurement of shock position or radius in time. From these direct measurements shock velocity and in some instances shock pressure were compiled. The methods of measurements and the smoke rocket technique are described in detail in reference (4) and to a lesser degree in references (5, 6, 7, and 8).

The shock front in many cases can be photographed directly; this is a result of light refracted by the shock front. Project 1.1b* (Direct Shock Photography) was totally dependent upon this effect. The films obtained for Project 1.1a (Smoke Rocket Photography) were not, because the shock front did not need to be rendered visible to be detected. The position of the shock front was established through the grid of smoke trails established behind the burst. The light rays which were reflected from the grid and passed tangentially to the shock front were refracted and caused breaks to appear in the otherwise continuous grid lines.

All of the films were measured in the same general manner. The position of ground zero was established and the position of the shock front was determined with respect to it. These measurements were made with respect to time on 20X magnified projections which were obtained through a direct projection Recordak.

1.3.2 The Determination of the Arrival Time Data

From past experience it was known that to obtain accurate results with either the smoke rocket or the direct shock photographic technique, the magnification factor** should not be much greater than 300 ft/mm*** (this figure does not apply to measurements made in the

---

* Films obtained for Project 13.2, which were used to extend the coverage of the Project 1.1 films, were also dependent upon this effect.

** The magnification factor is the ratio of the perpendicular distance from the camera to the plane of measurement to the focal length of the optical system. It may also be expressed as the ratio of a given distance in the plane of measurement to the same distance as it is reproduced in the focal plane of the lens.

*** The Project 13.2 films had magnification factors considerably larger than the stipulated 300 ft/mm (refer to Table 2.3). The resulting distance uncertainties were very large on these films compared to those of the Project 1.1 films. See Section 3.9.2.

region of the fireball), even though the resolving power of the system might seem to be adequate at somewhat higher values. If this figure is exceeded the accuracy of the method fails rapidly because of the inability to detect the position of the shock or the apparent breaks in the smoke trails and hence the location of the shock. For this reason, lenses of large focal lengths were used for Projects 1.1a and 1.1b. These limited the field of view, and because of the magnitude of the effects, it was necessary to use a series of cameras to cover the event. The Project 1.1 cameras for any given shot were all located at one station; therefore, to obtain adequate horizontal coverage without loss of continuity, the horizontal aiming angle of each camera used for this purpose was such that the field of view of each camera slightly overlapped those of adjacent cameras. Consequently the planes of measurement* did not constitute portions of a single plane. Ground zero was visible in the field of at least one of the cameras. See Fig. 1.1.

The chief problem encountered in the determination of the arrival time curve was the correlation of the data obtained from the discontinuous planes of measurement of the 1.1a and 1.1b films. It was found that the effects of elongation[4] normally encountered in non-linear photogrammetry could be neglected on the 1.1a and 1.1b films but it was necessary to make these corrections on the Project 13.2 films.

The data obtained from the discontinuous measurement planes could be correlated if the following conditions were met:

a. The fireball was symmetric about the origin in the region of the surface in which the correlation was to be made.

With the exception of Shot 6, films obtained from different camera stations were available for each shot (refer to Tables 2.3 and 3.1). Through these films it was possible to check for gross asymmetries in the fireball growth along the surface (see Section 3.9.2). No asymmetry** of this nature was noted in two of the shots requiring correlation.***

b. The horizontal aiming angle of each camera was known and the position of ground zero was known in one of the films.

On Shots 2 and 4 it was found that the horizontal aiming angles were not correct. The methods used for correcting the aiming angles may be found in Appendix A. The nominal aiming angles and the corrected aiming angles are given in Table 2.3. The nominal aiming

---

* The plane of measurement is defined as that plane which is perpendicular to the principal optical axis and includes the origin of the event. The baseline of this plane lies on the surface. Consequently ground zero lies on the baseline.

** Shot 5 data from the two usable films which were obtained from different camera stations showed different rates of growth along the surface, but this could be accounted for by film anomalies. Refer to Section 3.6.

*** Shots 2 and 4. Films were not available to check Shot 6.

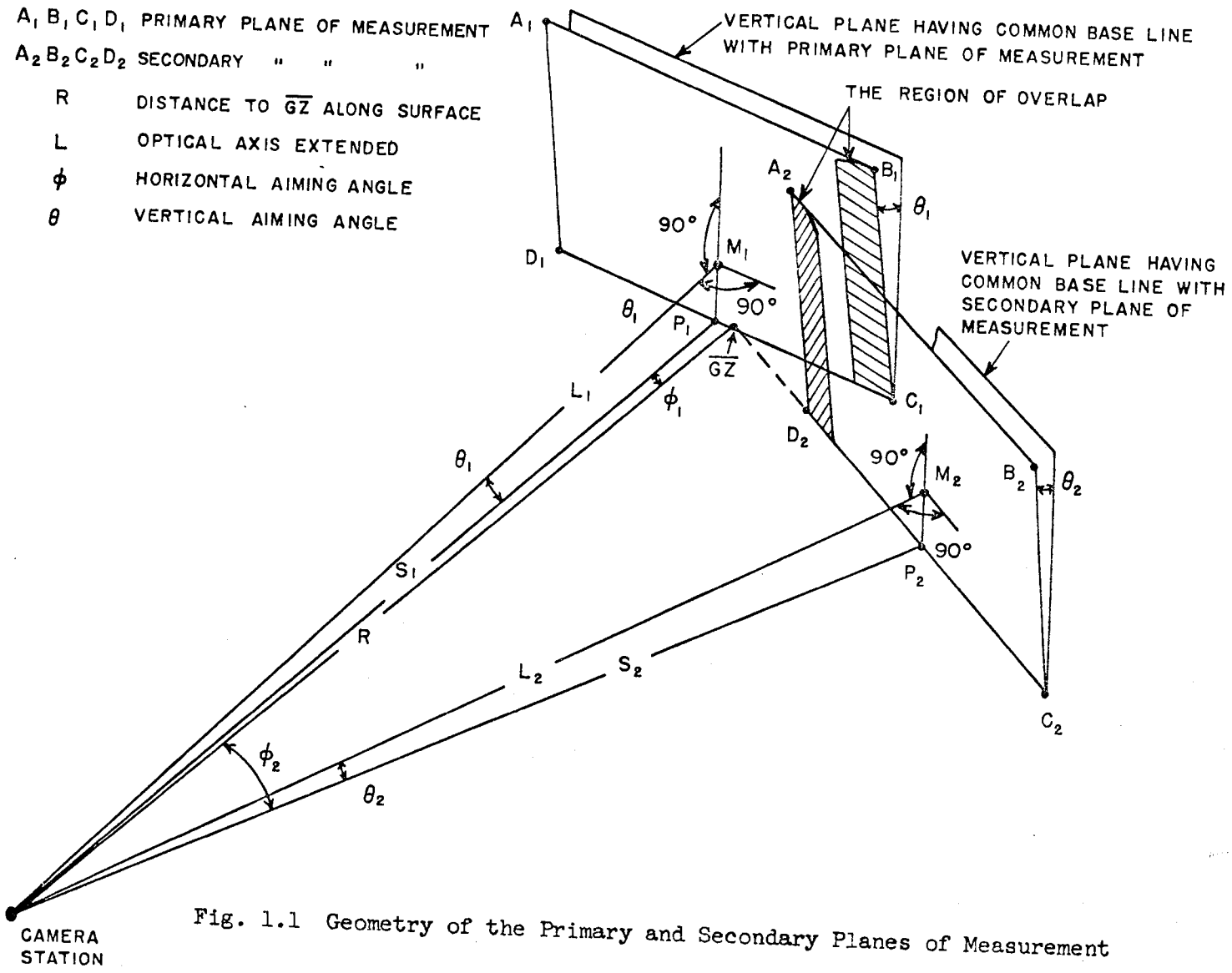

Fig. 1.1 Geometry of the Primary and Secondary Planes of Measurement

angles lead to large discrepancies* in the position of ground zero in the measurement planes of the subsequent** cameras. Further the primary*** cameras were not aimed at ground zero and as a result ground zero had to be assumed to be at the midpoint of the fireball diameter along the surface.

After the position of ground zero was established in the plane of measurement of the primary camera, and the horizontal aiming angles were found, the data were correlated as follows:

The primary record was measured directly by the methods outlined in Section 1.3.1. The subsequent records were measured in the same manner except that the position of the shock front was measured with respect to the point, P_n, at which the vertical centerline**** of each frame intersected the surface***** (refer to Fig. 1.2******).

The distance from ground zero to this point ($\overline{GZP_n}$) was easily determined.

The offset is given by

$$\overline{GZP_n} = R \sin \phi_n \qquad (1.1)$$

The film scaling factor is given by

$$m_{Fn} = \frac{L_n}{f_n}$$

and the drawing scaling factor by

$$m_{Dn} = \frac{L_n}{f_n \, m_r} \qquad (1.2)$$

---

* On Shot 2 the discrepancy was of the order of 350 feet; on Shot 4 the discrepancy for film 24181 was ~ 2,800 feet and for film 24182 it was ~ 4,800 feet.

** The overlapping cameras.

*** The primary camera was that camera which was most nearly (horizontally) aimed at ground zero. The data obtained from the subsequent cameras were referred to this camera for correlation.

**** The principal optical axis of any lens was assumed to intersect the vertical centerline of the frame. Later calibration of lenses and cameras bore out this assumption. On Shot 2 it was found that the divergence was less than 1 minute of arc. On Shot 4 the maximum divergence was found to be 5 minutes. On Shot 6 calibration for the camera used to obtain film 24478 was not available. Corrections were made for the known divergences.

***** On Shots 2 and 6 the surface was below the horizon and the horizon was used as the baseline. As a result these measurements were actually made 10 ft and 50 ft, respectively, above the real surface.

****** Camera towers are not shown. The effect of these towers on the ranges and aiming angles was negligible.

Where $\overline{GZP}_n$ = the offset of the nth camera (ft)

m_{Fn} = the film scaling factor of the nth camera (ft/mm)

$L_n = R \cos \phi_n \cos\theta_n$ (ft)

f_n = the effective focal length of the lens of the nth camera (mm)

m_{Dn} = the drawing scaling factor of the nth camera (ft/mm)

m_R = the magnification of the Recordak

The distance from ground zero to the shock front is given by

$$r = \overline{GZP}_n \pm d_n \qquad (1.3)$$

where r = the distance from ground zero to the shock front, and d_n = the distance from P_n to the shock front. (The distance from ground zero to the shock front was determined frame by frame and a relative time base was established by the timing marks on the film.)

The distance-time data obtained from the measurement of the subsequent records were correlated by establishing a common absolute time base for all records. The absolute time base was established through the data obtained from the primary record, which was expressed in terms of zero time.* The arrival time data obtained from the primary record in the region overlapping the data of the first subsequent record were plotted. The times corresponding to the distances taken from the subsequent record were read from the curve. In this manner the timing of the first few frames of the subsequent record was adjusted to the absolute time scale. The relative time base of the second subsequent record was obtained in the same way via the first subsequent record.

The films obtained for Project 13.2 were measured in the same manner as the primary film. The resultant data were expressed in terms of zero time through a comparison to distances as described above.

1.3.3 The Determination of Peak Shock Overpressure by the Velocity Method

From the shock arrival time data, instantaneous shock velocities were determined. This was done by fitting the data with a smooth curve which could be expressed in closed mathematical form. Differentiation of the empirical equation gave velocity as a function of distance.

---

* The primary records of Shots 1, 2, and 4 were used in conjunction with other films by EG&G in the fireball analysis and the time of each frame was established in terms of absolute time.

This equation was fitted, by the method of least squares, to the arrival time data on IBM equipment. Upon differentiation, the following equation was obtained for the instantaneous shock velocity:

$$U = A \left[1 + \left(\frac{B}{r}\right)^{1.5}\right] \tag{1.7}$$

A complete explanation of the derivation of the equation and the method of fitting may be found in reference (7).

The peak pressure of the shock wave was calculated for values of the instantaneous shock velocity by use of the Rankine-Hugoniot relation:

$$P_s = \frac{2\gamma p_o}{\gamma + 1}\left[\left(\frac{U}{C_o}\right)^2 - 1\right] \tag{1.8}$$

where P_s = peak shock overpressure, (psi)

p_o = ambient pressure ahead of the shock (psi)

γ = the ratio of specific heats* for air (1.40)

U = shock velocity (ft/sec)

T_o = ambient temperature (^oC)

C_o = the speed of sound ahead of the shock

$$= 1{,}089\left[1 + \frac{T_o}{273}\right]^{1/2} \text{(ft/sec)}$$

1.3.4 Scaling Factors

All of the scaled data presented were reduced to an equivalent 1 KT burst at standard sea level conditions.** The scaling factors are defined as follows[6]:

$$\text{Pressure:} \quad S_p = \frac{P_2}{P_1} = \frac{14.7}{p_o} \tag{1.9}$$

$$\text{Distance:} \quad S_d = \frac{r_2}{r_1} = \left(\frac{p_o}{14{,}700W}\right)^{1/3} \tag{1.10}$$

$$\text{Time:} \quad S_t = \frac{t_2}{t_1} = \left(\frac{T_o + 273}{293}\right)^{1/2}\left(\frac{p_o}{14{,}700W}\right)^{1/3} \tag{1.11}$$

---

* In regions of very high pressures and temperatures the Rankine-Hugoniot relation as written is not exact because the equation of state upon which it is based no longer applies. The ratio of specific heats, γ, for air becomes meaningless. To avoid introducing errors and to simplify the task of calculation, recourse was made to the Hirschfelder and Curtiss Tables (11) which give $(P_s+p_o)/P$ as a function of U/C_o with all the necessary corrections accounted for.

** Atmospheric pressure was assumed to be 14.7 psi; temperature was assumed to be 20^oC.

where P_1 = unreduced peak shock overpressure (psi)
P_2 = peak shock overpressure reduced to standard atmospheric pressure (psi)
r_1 = unreduced distance (ft)
r_2 = distance reduced to 1 KT at sea level (ft)
t_1 = unreduced time (sec)
t_2 = time reduced to 1 KT at sea level (sec)
W = yield of weapon in megatons
p_o = atmospheric pressure (psi)
T_o = ambient temperature (^oC)

The scaling factors used and those data used to derive them are given in Table 1.1.

TABLE 1.1 - Summary Data for All Shots

	Shot 1	Shot 2	Shot 3	Shot 4	Shot 5	Shot 6
DATE (GMT)	1 March	27 March	7 April	26 April	5 May	14 May
CODE NAME OF SHOT DAY	Bravo	Romeo	Koon	Union	Yankee	Nectar
TIME (GMT-WWV)(Not corrected for delay in transmission)	06:44:59 0.972±10 ms	06:30:00 0.373±1 ms	06:20:00 0.398±1 ms	06:10:00 0.677±1 ms	06:10:00 0.142±1 ms	06:20:00 0.387±2 ms
TYPE	Land	Barge	Land	Barge	Barge	Barge
LOCATION	Bikini, West of Charlie (Namu) on Reef	Bikini, Shot 1 Crater	Bikini, Tare (Eninman)	Bikini, on Barge at Intersection of Arcs with Radii of 6900' from Dog (Yurochi) and 3 Statute Miles from Fox (Aomoen)		Enivetok, IVY Mike Crater, Flora (Elugelab)
YIELD (MT)	15±.5	11±.5	.13±.02	7±.3	13.5±1	1.7±.3
METHOD	Analytical Solution	Analytical Solution	Time Differences	Analytical Solution	Analytical Solution	Analytical Solution
ECHMEN & MARVER COORDINATES	N 170,617.17 E 76,163.98	N 170,635.05 E 75,950.46	N 100,154.50 E 109,799.00	N 161,698.83 E 116,800.27	N 161,424.43 E 116,688.15	N 147,750.00 E 67,790.00
STATION NUMBER	20	90	50	30	40	10
HEIGHT OF CENTER OF GRAVITY OF DEVICE ABOVE BARGE DECK OR FOUNDATION (FT)	7	7	13.6	7	7	7
HEIGHT OF BARGE DECK ABOVE WATER (FT)		7.2		5.8	6.6	7.2
FOUNDATION ABOVE DATUM (6" Below Mean Low Water Spring Tides) (FT)	10		8.0			
TIDE AT ZERO TIME (Datum is 6" Below Mean Low Water Spring Tides)	2.72	3.22	5.92	2.91	5.70	2.35
DEW POINT (°F)	72°	72°	75°	76°	75°	75°
ATMOSPHERIC PRESSURE (mb) at GZ	1006.1	1012.4	1009.7	1007.4	1010.8	1006.4
SURFACE AIR TEMPERATURE (°F)	80°	80°	81°	81°	80.8°	80°
SURFACE RELATIVE HUMIDITY (%)	77	77	82	86	84	85
SURFACE WIND DIRECTION AT SHOT TIME	070	040	090	062	070	090
VELOCITY (Knots)	15	10	13	18	20	17
ATMOSPHERIC TRANSMISSION (Total %)	GZ to George 10.6 GZ to Tare 12.0 GZ to Delta 58.0-65.0	GZ to Tare 22 GZ to Fox 8	GZ to How 0 GZ to Nan 5	GZ to Nan 26 GZ to How 28	GZ to Nan 1.1 GZ to How 28	GZ to Janet 67 GZ to Fred 0
BLAST WAVE SCALING FACTOR Sp	1.008.	1.001		1.006		1.007
DISTANCE SCALING FACTOR Sd	0.0405	0.0450		0.0522		0.0836
TIME SCALING FACTOR St	0.0409	0.0455		0.0528		0.0845

CHAPTER 2

INSTRUMENTATION

2.1 SHOT SUMMARY AND PARTICIPATION

Projects 1.1a, 1.1b, and 1.1d were activated on those shots indicated in Table 2.1.

TABLE 2.1 - Shot Participation

Shot	1	2	3	4	5	6
Projects	1.1 a-b-d	1.1 b-d	1.1 a-b-d	1.1 a-b-d	1.1 b-d	1.1 b-d

On the second and fifth shots it was not feasible to set up rocket stations because all potential launching sites were highly contaminated by lingering radiation from previous detonations. Shot 6 was not instrumented with rockets because of possible interference with other projects. The general layouts of all stations are shown in Figs. 2.1 and 2.2.

2.2 ROCKET INSTRUMENTATION

A summary of the rocket instrumentation may be found in Table 2.2.

2.2.1 The Smoke Rocket and the Rocket Launcher

The smoke trails which formed the background grid were generated by 5.0" spin-stabilized rockets,[12] which were made up of a 5.0" Mark 3 Mod 0 electric-firing motor and a modified 5.0" Mark 10 head loaded with ten pounds of FS chemical smoke mix (55% $HClSO_3$ and 45% SO_3).

The launcher used on this operation consisted of a 5.0" Mark 50 launching tube mounted on a rugged base made of 2" steel pipe. The tube was suspended from the framework by means of a pillow block bolted to a plate which was welded to the tube at the center of

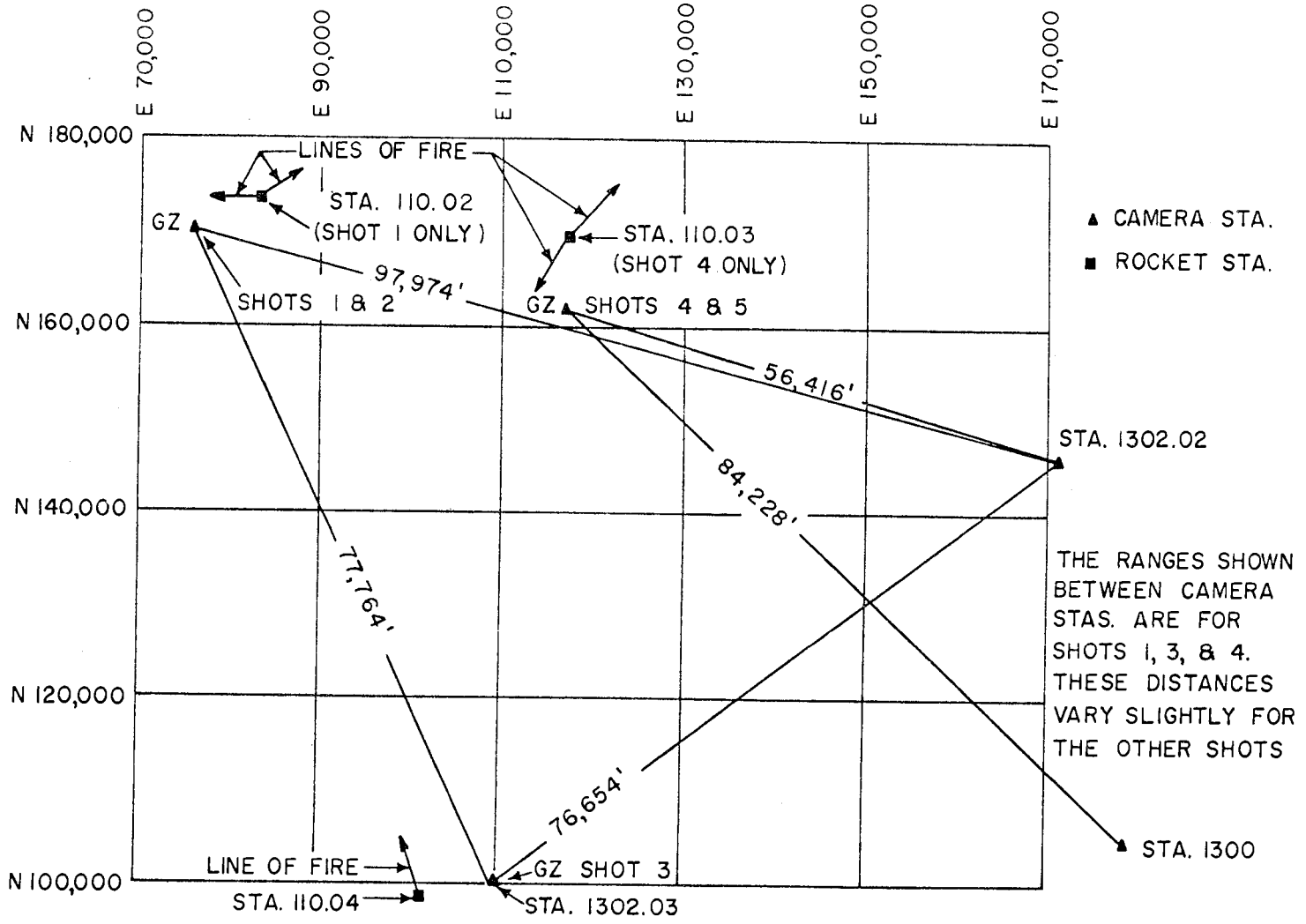

Fig. 2.1 Instrumentation Layout, Bikini

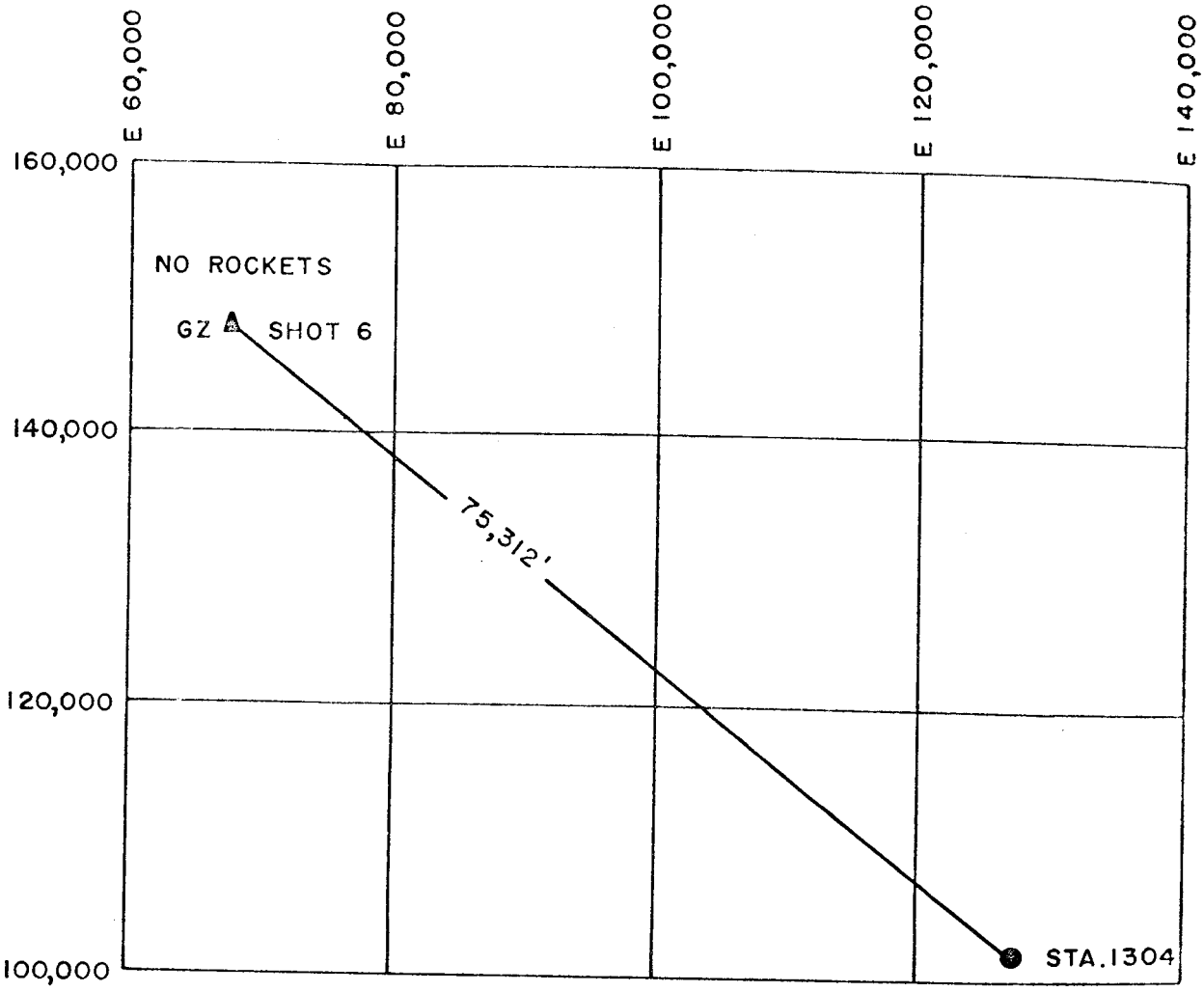

Fig. 2.2 Instrumentation Layout, Eniwetok

gravity (i.e. when loaded). With this type of construction the tube could be rotated to any desired angle of elevation. Reference is made to Fig. 2.3.

2.2.2 The Launching Site

The limited dry land area available for launching sites made it necessary to use the fan grid [7] rather than the usually preferable vertical grid [4,5,6,8].

With the exception of Station 110.04, which used a single battery, there were two identical batteries of eight launchers apiece at each launching site. These batteries were located along opposite sides of a 100 ft x 50 ft plot and were staggered so that launchers were not directly opposite one another. The launchers of each battery were oriented to fire in the same direction at different angles of elevation ranging from 20° to 85°. A typical station is shown in Fig. 2.4

TABLE 2.2 - Rocket Instrumentation

Shot	Rocket Station No. and Location	Direction of Fire	Grid	Power and Timing	Range GZ To Rkt. Sta. (ft)
1	110.02 Bikini N 169,752 E 83,023	65° 347°	Full Fan 16 Rounds	120 VAC -15*, -5 sec	8056
3	110.04 Bikini N 98,707 E 101,698	340°	Half Fan 8 Rounds	120 VAC -15*, -5 sec**	8229
4	110.03 Bikini N 169,752 E 117,014	45° 127°	Full Fan 16 Rounds	120 VAC -15*, -5 sec	8056

* All -15 sec signals operated through a 5 sec delay relay.
** Timing Signals by radio.

2.2.3 Power and Timing at Launching Sites

Power was provided until zero time by an engine-alternator set located at each launching station. Timing signals, available at -15 and -5 sec, were provided by cable from the Edgerton Germeshausen & Grier (EG&G) timing station, except at station 110.04, where they were received by radio, through a receiver furnished by EG&G.

In view of the time of flight of the rockets and the duration of the trails, the optimum firing time was -10 sec. Consequently the -15 sec signals were made to operate a 5 sec delay relay. The -5 sec signal served as a backup signal.

The firing circuit and associated gear are shown in Fig. 2.5.

2.3 PHOTOGRAPHIC INSTRUMENTATION

The basic films of Projects 1.1a and 1.1b were obtained by EG&G. In addition to these, accurate prints of others taken by EG&G for Project 13.2 (Early Cloud Photography) were used to extend the coverage of the basic films. All of the records used were obtained by high speed Mitchell cameras. Timing marks appeared on the original 1.1a and 1.1b records at a rate of 100 cps. Timing marks did not appear on the copies of the 13.2 films used but the velocities of these films were given by EG&G.

The photographic records of Project 1.1d were obtained by the Lookout Mountain Laboratory. One Éclair camera was used for each shot. Timing was provided by a clock appearing in each frame. Reference is made to Section 3.1 and Table 3.1.

The photographic instrumentation plan is found in Table 2.3. This table includes only those records which were used quantitatively.

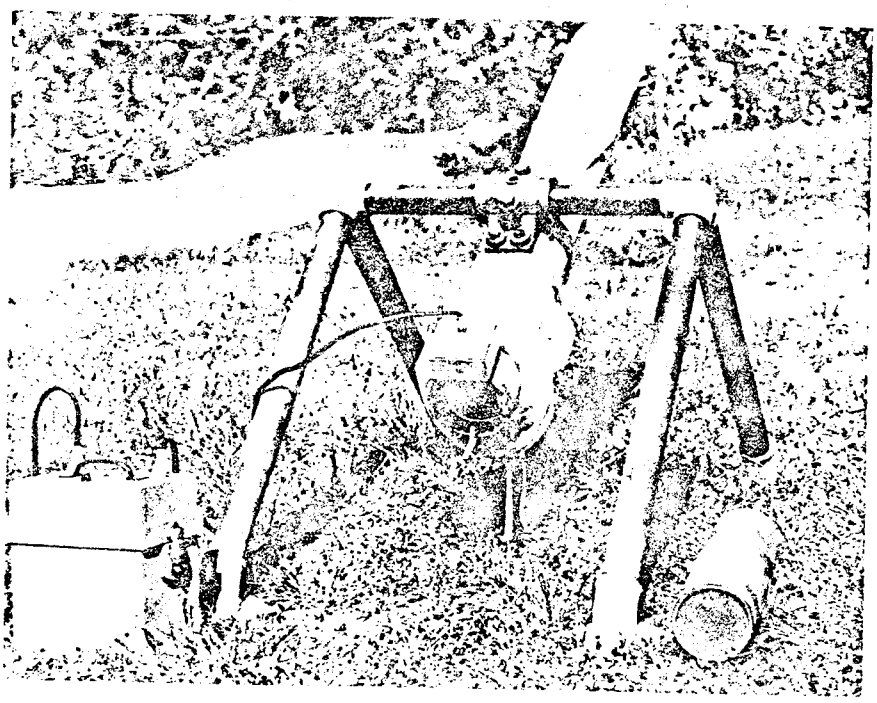

Fig. 2.3 The Variable-Elevation Launcher and Associated Equipment

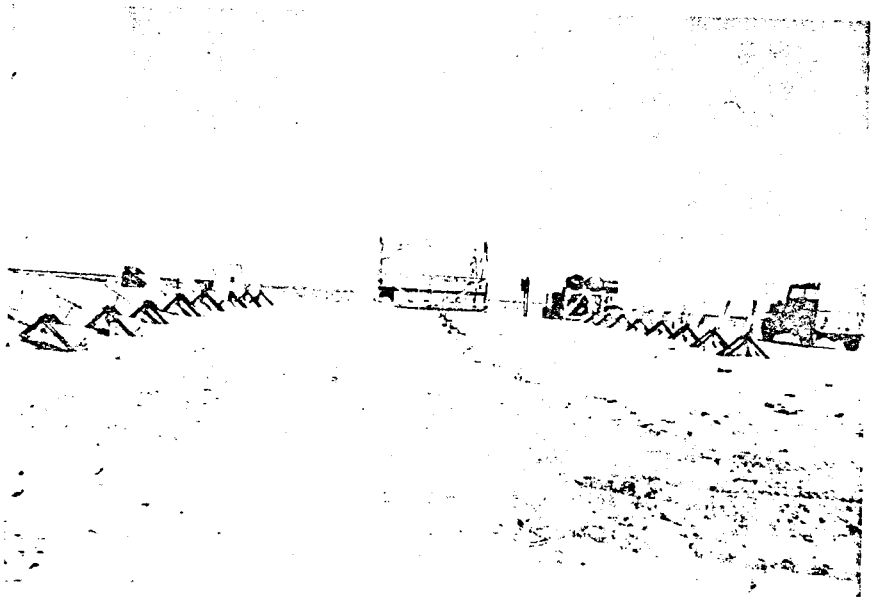

Fig. 2.4 The Fan Grid Rocket Launching Station

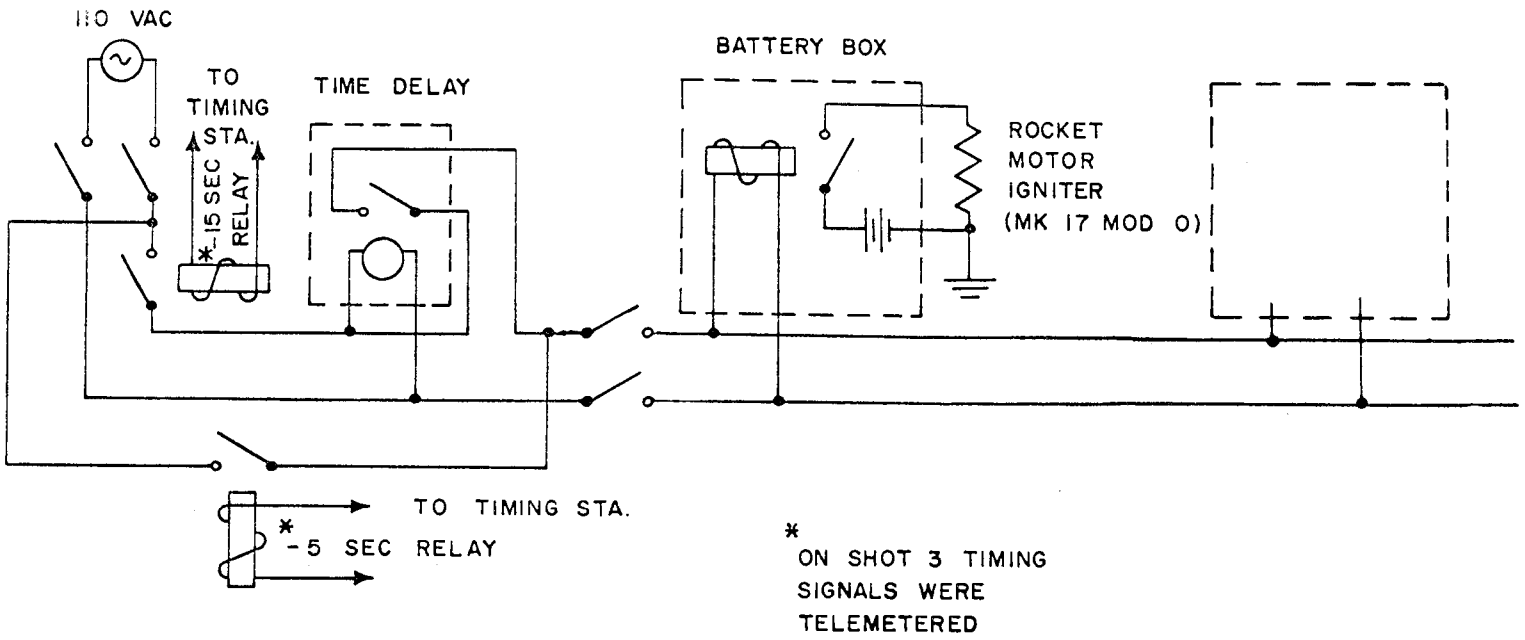

Fig. 2.5 Firing Circuit and Associated Equipment

TABLE 2.3 - Photographic Instrumentation

Film & Proj.	Camera Sta.	Range From GZ (ft)	Lens Focal Length (mm)	Nominal Aim Horiz.	Nominal Aim Vert.	Corrected Aim Horiz.	Resolution (ft)	Magnification ft/mm
SHOT 1								
24054(13.2)	1302.03	77,764	25.29	0°	-	0°	50	3075
24079(1.1a)	Tare Is.	"	152.2	0°	2°30'	0°	10	510
SHOT 2								
24554(13.2)	1302.03	77,872	25.29	0°	0°	0°	50	3079
24575(1.1b)	Tare Is.	77,872	152.2	0°	2°30'	26'R	10	511
24576(1.1b)	" "	77,872	249.6	2°30'R	1°30'	2°14'R	7	312
24577(1.1b)	" "	77,872	248.8	5°45'R	1°30'	5°31'R	7	313
24562(13.2)	1301 Elmer Is.	1,040,900	35.89*	~0°	~4°	-	-	29,000
SHOT 4								
24150(13.2)	1302.02	56,416	25.29	0°	14°50'	-	50	2156
24180(1.1a)	How Is.	56,416	249.2	2°30'R	1°30'	33'R	7	226
24181(1.1a)	" "	56,416	250.0	5°45'R	1°30'	2°37'R	7	226
24182(1.1a)	" "	56,416	250.7	9°R	1°30'	4°04'R	7	225
SHOT 5								
24250(13.2)	1302.02 How Is.	56,450	25.29	0°	14°50'	-	50	2158
24253(13.2)	1300 Nan Is.	84,125	35.34	0°	0°	-	50	2380
SHOT 6								
24477(1.1b)	1304	75,312	248.1	2°35'R	1°30'	-	7	303
24478(1.1b)	Yvonne Is.	75,312	251.1	5°45'R	1°30'	-	7	298

*Focal Length Used to Obtain Part Used.

Camera Station Coordinates:

1300	N 104652	E 178768	Z 300'
1302.02	N 146236	E 171056	Z 75'
1302.03	N 100325	E 109424	Z 75'
1301	N 53572	E 133188	Z 125'
1304	N 101772	E 127438	Z ~ 15'

CHAPTER 3

RESULTS

3.1 INSTRUMENTATION

3.1.1 Projects 1.1a and 1.1b

The smoke rockets of Project 1.1a were fired successfully on the three shots so instrumented.

The films obtained for these projects were satisfactory and the photographic methods employed proved successful. The discrepancies in the horizontal aiming angles of the cameras on Shots 2 and 4 had no serious effects. The chief loss caused by these aiming errors was the restriction of the coverage on Shot 4, but this loss was made up in part by the less accurate data obtained from Project 13.2 films. A list of all films and their uses, including those of Project 13.2, may be found in Table 3.1.

It should be pointed out that the conditions under which the cameras were set up and final adjustments made were very poor. The EG&G personnel were limited in the time that could be spent in the aiming of the cameras as a result of lingering radiation and were handicapped by poor visibility. The work done was highly creditable in light of these conditions.

3.1.2 Project 1.1d

Project 1.1d (Aerial Photography) was not successful and no usable data were obtained. With the exception of Shots 2 and 4 the cloud cover was sufficient to obscure the field of view. On these shots the films were badly overexposed* for approximately the first

* With the exception of the Shot 3 film, all the films obtained for Project 1.1d were badly overexposed in the first 30 sec after zero time. High speed film was used rather than the high latitude film requested.

TABLE 3.1 - Photographic Instrumentation Results

Project	Film	Results
SHOT 1		
1.1d	22 Mag 117C	Not used, Obscured by clouds
1.1a	24079	Fireball and jet data
1.1a	24080	*
1.1a	24081	Not used, obscured by jet
1.1a	24082	" " " " "
13.2	24050	Asymmetry check, qualitative
13.2	24052	jet and fireball observations
13.2	24053	
13.2	24054	Shock measurements
13.2	24055	Same as 050, 052, 053
SHOT 2		
1.1d	Mag 121D	Not used. First 30 sec overexposed
1.1b	24575	Fireball data
1.1b	24576	Shock measurement
1.1b	24577	" "
1.1b	24578	Not used. Shock not visible
13.2	24552	Shock measurements asymmetry check
13.2	24553	Asymmetry check, fireball observations
13.2	24554	Shock meas. both vertical and surface
13.2	24555	Asymmetry check fireball observations
13.2	24562	High altitude effects
SHOT 4		
1.1d	Mag 132a	Not used. First 30 sec overexposed
1.1a	24179	*
1.1a	24180	Fireball data
1.1a	24181	Shock measurements
1.1a	24182	" "
13.2	24150	" " Fireball observations
13.2	24153	Asymmetry check " "
SHOT 5		
1.1d	Mag 125E	Not used. Obscured by clouds
1.1b	24279	*
1.1b	24280	Not used. Film irradiated, $\overline{GZ}$ not known
(Con't)		

* Films not obtained as a result of a mechanical failure.

TABLE 3.1 - Photographic Instrumentation Results (Con't)

Project	Film	Results
SHOT 5 (Con't)		
1.1b	24281	*
1.1b	24282	*
13.2	24250	Fireball data
13.2	24253	" "
SHOT 6		
	24408	Fireball observations
1.1b	24475	Not used. GZ not known
1.1b	24476	" " " " "
1.1b	24477	Fireball data
1.1b	24478	Shock measurements

* Films not obtained as a result of a mechanical failure.

30 sec, which was the region of interest. The Shot 2 film was analyzed but the resultant data were not usable, chiefly because of the large uncertainties* in timing and the position of the aircraft with respect to ground zero. It was not possible to analyze the Shot 4 film because of the inability to establish ground zero in the film.

3.2 SHOT 1

As a result of the unexpectedly high yield, the cloud cover, and the jet which emanated from the east side of the fireball, a great deal of potential information was lost. The cloud cover precluded the possibility of obtaining much vertical data and the growth of the jet along the line of coverage rendered two of the three 1.1a films useless.

3.2.1 Arrival Time Data

It was noted that the growth of the fireball was not the same along the surface as it was vertically above ground zero. The vertical growth was greater than that along the surface. In the early frames of film 24,079, a bulging on the west side of the fireball was apparent. (See Fig. 3.7)

Because the top of the fireball was obscured by the clouds after about 30 msec, it is not known whether the vertical protrusion, observed on all of the barge shots, existed.

* The spatial uncertainties were of the order of 3 to 5 per cent.

The surface arrival time data presented were derived from films 24,079 (Project 1.1) and 24,054* (Project 13.2). The data obtained from the Project 1.1 film covered the first 5300 ft and the Project 13.2 film data extended from 7500 ft to 10,500 ft. The shock front was not visible in the region not covered.

The type of surface** over which these data were obtained could not be clearly ascertained. Ground zero was on a causeway that ran from Charlie Island toward Baker Island. The baselines of the planes of measurement of the two films extended over the reef. Consequently it was impossible to know precisely what type of surface it was. It was assumed to be primarily water.

As a result of the variations in the slope of the fireball surface arrival-time curve, it was necessary to fit this region in three parts. The data were fitted by an empirical equation of the form of 1.4. The equations for these parts of the fireball region were found to be:

Surface	$r = 9287t^{0.430}$	$500 \leq r_h \leq 1350$ (ft)
Surface	$r = 7260t^{0.376}$	$1350 \leq r_h \leq 3400$ (ft)
Surface	$r = 7576t^{0.397}$	$3400 \leq r_h \leq 4500$ (ft)
Vertical	$r = 8338t^{0.402}$	$500 \leq r_v \leq 1500$ (ft)

(Subscripts "h" and "v" refer to horizontal and vertical distances respectively.)

The arrival time data obtained after shock breakaway which occurred sometime between 0.3 and 0.4 sec were fitted by equation 1.6 and the constants were found to be:

$A = 990$ $B = 13,908$ $C = -20.2$ $7500 \leq r \leq 10,500$ (ft)

The observed arrival time data are presented in Table 3.2. The fitted data are given in Table 3.3 and are shown with the observed data in Fig. 3.1 (fireball region) and Fig. 3.2.

3.2.2 The Velocity and Peak Shock Overpressure-Distance Data

The fitting functions were differentiated to obtain the expressions for the instantaneous velocities, U, at the desired distances. The following were obtained in the fireball region:

Surface $U_h = 2728t^{-0.624} = 7061 \times 10^6 r_h^{-1.661}$ $1350 \leq r_h \leq 3400$ (ft) (3.1)

Surface $U_h = 3007t^{-0.603} = 2371 \times 10^6 r_h^{-1.520}$ $3400 \leq r_h \leq 4500$ (ft) (3.1a)

* There were several 13.2 films available for this shot. Film 24,054 was found to be best suited for shock measurements.

** Ground zero was 10 ft below the horizon. As a result all horizontal measurements were effectively made 10 ft above the surface.

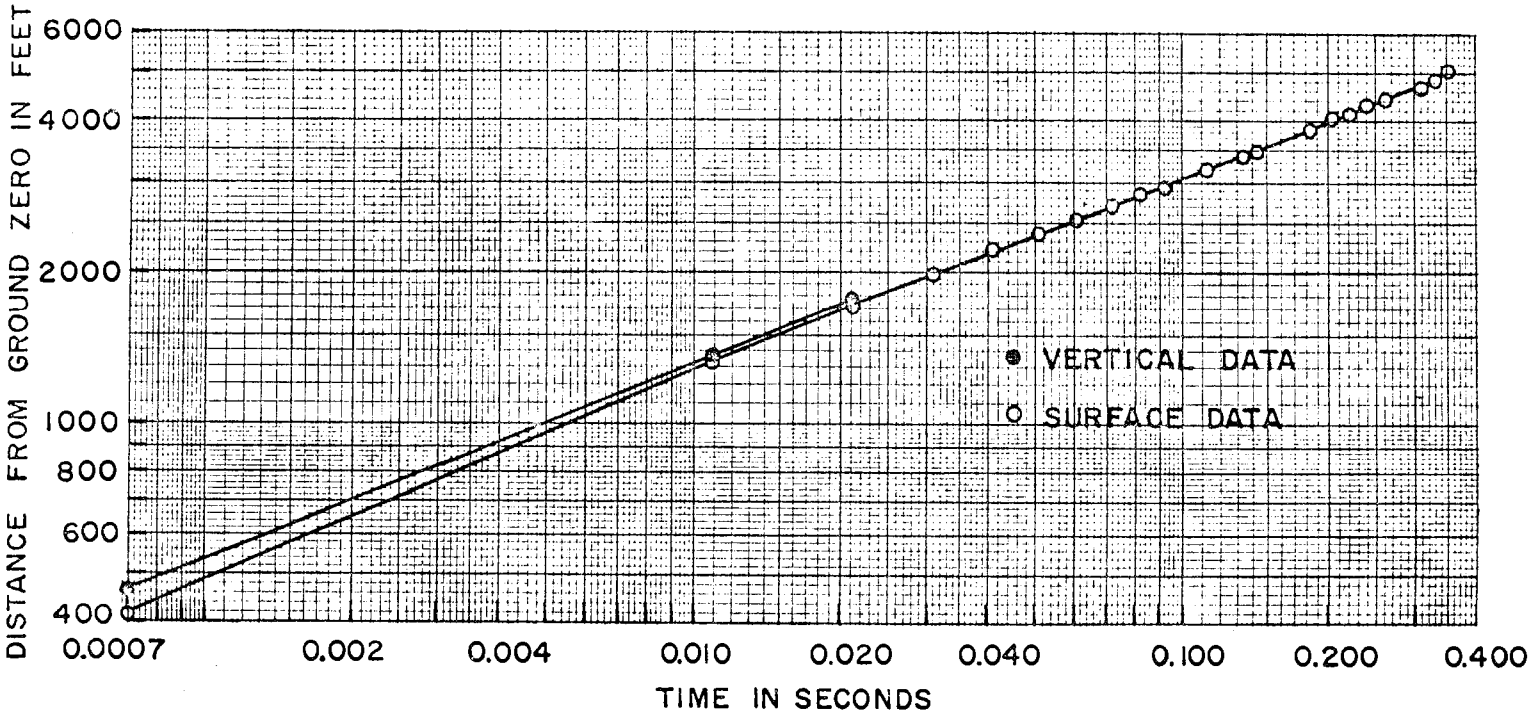

Fig. 3.1 Fireball Arrival Time Data, Shot 1

TABLE 3.2 - Observed Arrival Time Data, Shot 1

Time (Sec)	Distance From GZ (ft) Surface	Vertical	Time (Sec)	Distance From $\overline{GZ}$, (ft) Surface	Time (Sec)	Distance From $\overline{GZ}$, (ft) Surface
0.0007	413	463				
0.0108	1325	1368	1.3252	8613	2.1092	10,972
0.0210	1730	1752	1.2976	8699	2.2495	11,129
0.0311	2000		1.3076	8730	2.5000	11,750
0.0412	2230		1.3677	8777		
0.0513	2412		1.3855	8896		
0.0614	2567		1.4457	8926		
0.0716	2701		1.3978	8966		
0.0817	2847		1.3878	8982		
0.0918	2968		1.4178	8997		
0.1120	3197		1.4880	9172		
0.1323	3393		1.4980	9172		
0.1424	3489		1.4679	9234		
0.1829	3854		1.5180	9281		
0.2031	4023		1.5681	9406		
0.2234	4177		1.5762	9411		
0.2436	4317		1.6182	9454		
0.2638	4448		1.5160	9458		
0.3144	4695		1.5982	9580		
0.3347	4851		1.6365	9630		
0.3549	5028		1.5882	9673		
0.3958	5304		1.6867	9677		
0.9970	7405		1.6884	9799		
0.9236	7466		1.6683	9799		
0.9939	7625		1.7184	9799		
0.9970	7640		1.7570	9801		
1.0070	7782		1.7084	9815		
1.0972	7924		1.7685	9878		
1.0371	7972		1.7986	9893		
1.0943	7985		1.8272	9942		
1.0872	8067		1.8186	10,004		
1.1345	8096		1.7886	10,051		
1.1473	8129		1.8888	10,207		
1.0872	8146		1.8875	10,254		
1.1847	8268		1.8687	10,270		
1.2074	8383		1.9288	10,270		
1.2248	8409		1.9088	10,316		
1.1974	8414		1.9890	10,348		
1.2475	8446		2.0090	10,411		
1.2750	8534		1.9990	10,536		
1.3076	8556		2.0892	10,957		

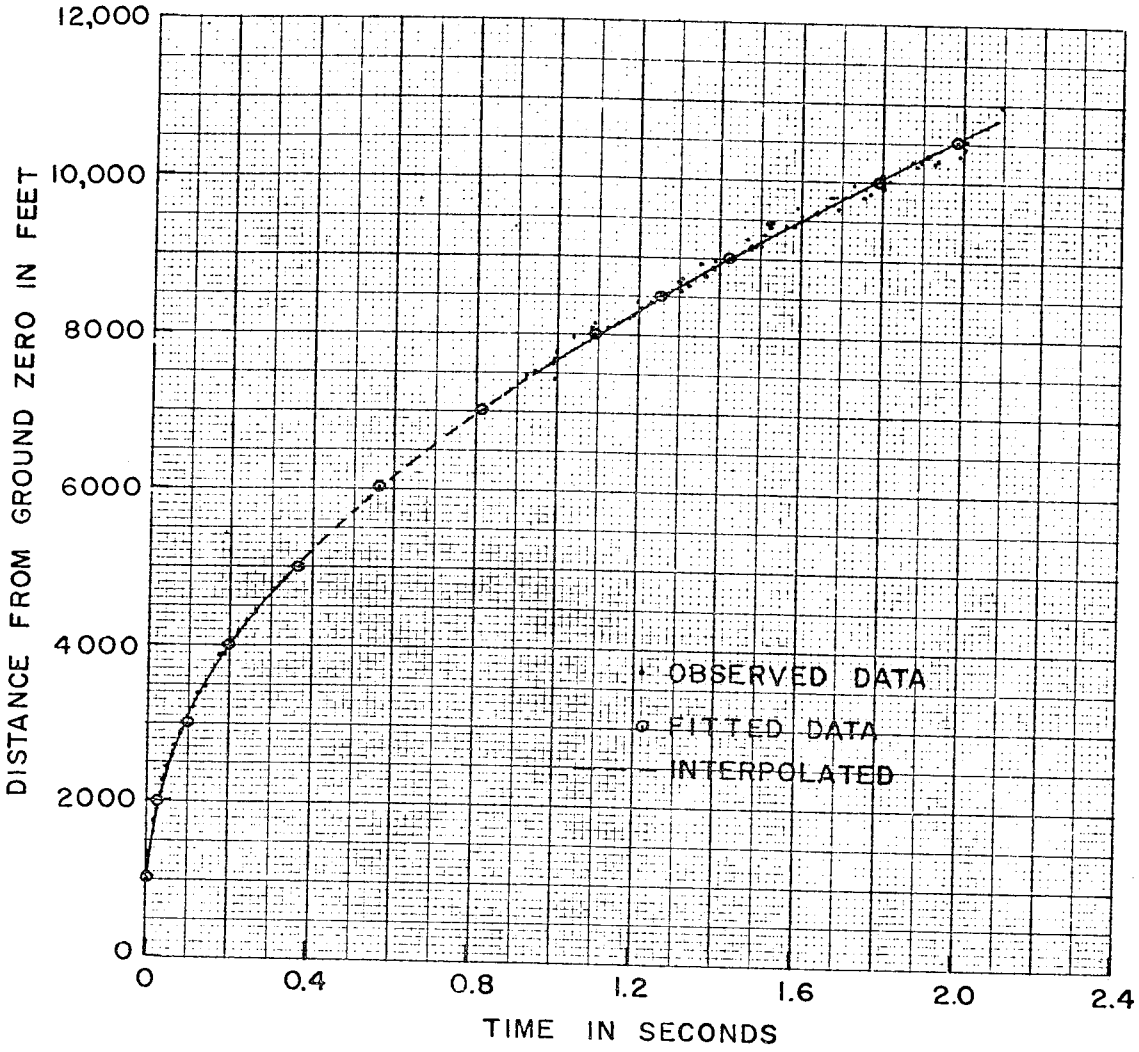

Fig. 3.2 Surface Shock Arrival Time Data, Shot 1

The vertical data and the early surface data were not differentiated because there were not sufficient data in this region to justify it. Pressures are not presented in the fireball region. The surface velocity-distance data are presented in Table 3.3 and Fig. 3.3

For the region after shock breakaway the following was obtained:

$$U = 990 \left[1 + \left(\frac{13{,}908}{r} \right)^{1.5} \right] \qquad 7{,}500 \leq r \leq 10{,}500 \text{ (ft)} \qquad (3.2)$$

The horizontal velocities were used in conjunction with the ambient conditions* to derive the peak shock overpressures for the corresponding distances. These data may be found in Table 3.3 and Fig. 3.4.

* All surface meteorological data are found in Table 1.1.

TABLE 3.3 - Arrival Time, Velocity and Peak Shock Overpressure, Shot 1

Distance From $\overline{GZ}$ (ft)	Arrival Time (Sec) Surface	Vertical	Velocity (ft/sec) Surface	Peak Shock Overpressure (psi)
500	0.0012	0.0009		
1000	0.0056	0.0051		
1500	0.0150	0.0140	37460	
2000	0.0324		23220	
2500	0.0586		16030	
3000	0.0952		11840	
3400	0.1323*		9911*	
4000	0.2003		7930	
4500	0.2696		6630	
5000	0.3643		5585	397
**5500	0.4594		4973	314
**6000	0.5654		4486	251
**6500	0.6822		4090	206
**7000	0.8098		3764	171
7500	0.9478		3491	140
8000	1.0961		3260	124
9000	1.4225		2893	94.5
10000	1.7867		2615	73.0
10500	1.9823		2500	64.9

* Average of the two fitted curves.
** Interpolated from equation 3.2.

TABLE 3.4 - Jet Data*, Shot 1

Time (Sec)	Distance (ft) L_o	$(L_o - R)$	Height of Jet h_a (ft)	h_b	Approximate Volume ft^3
0.0108	1691	366	144	27	9.7×10^6
0.0210	2227	497	208	59	30.7 x "
0.0311	2576	576	257	67	50.2 x "
0.0412	2891	661	311	53	80.3 x "
0.0513	3120	708	351	75	115 x "
0.0614	3327	760	377	61	134 x "
0.0716	3492	791	411	53	160 x "
0.0817	3659	812	435	53	183 x "
0.0918	3793	825	448	67	204 x "

* See Fig. 3.5

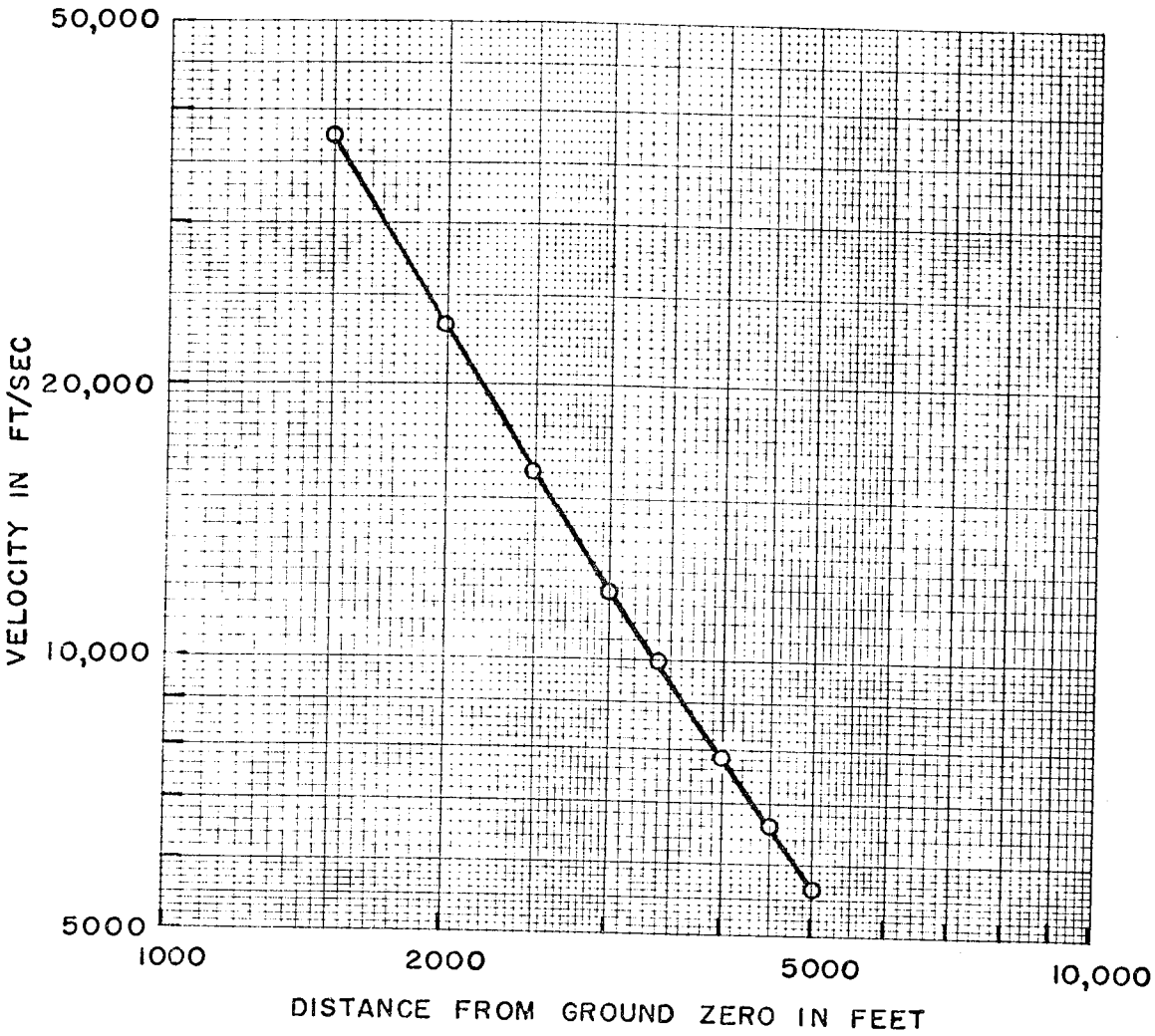

Fig. 3.3 Surface Fireball Velocity vs Distance, Shot 1

3.2.3 The Jet

A jet emanated from the east side of the fireball and grew along the pipeline that extended from ground zero to Station 1201. The growth of the jet was almost parallel* to the plane of measurement of film 24,079, and it was possible to make measurements of its growth for the first 100 msec. During this time (10 to 100 msec) the velocity of the jet with respect to GZ was 1.29 times that of the main fireball. Comparison was made at nine points in time during the interval and the ratio varied only between the limits of 1.28 to 1.30.

* The azimuth of the pipeline from ground zero was $65^{\circ}52'\ 03"$ and the azimuth of the plane of measurement of film 24,079 was $64^{\circ}40'\ 41"$. Corrections were made for the small angular difference.

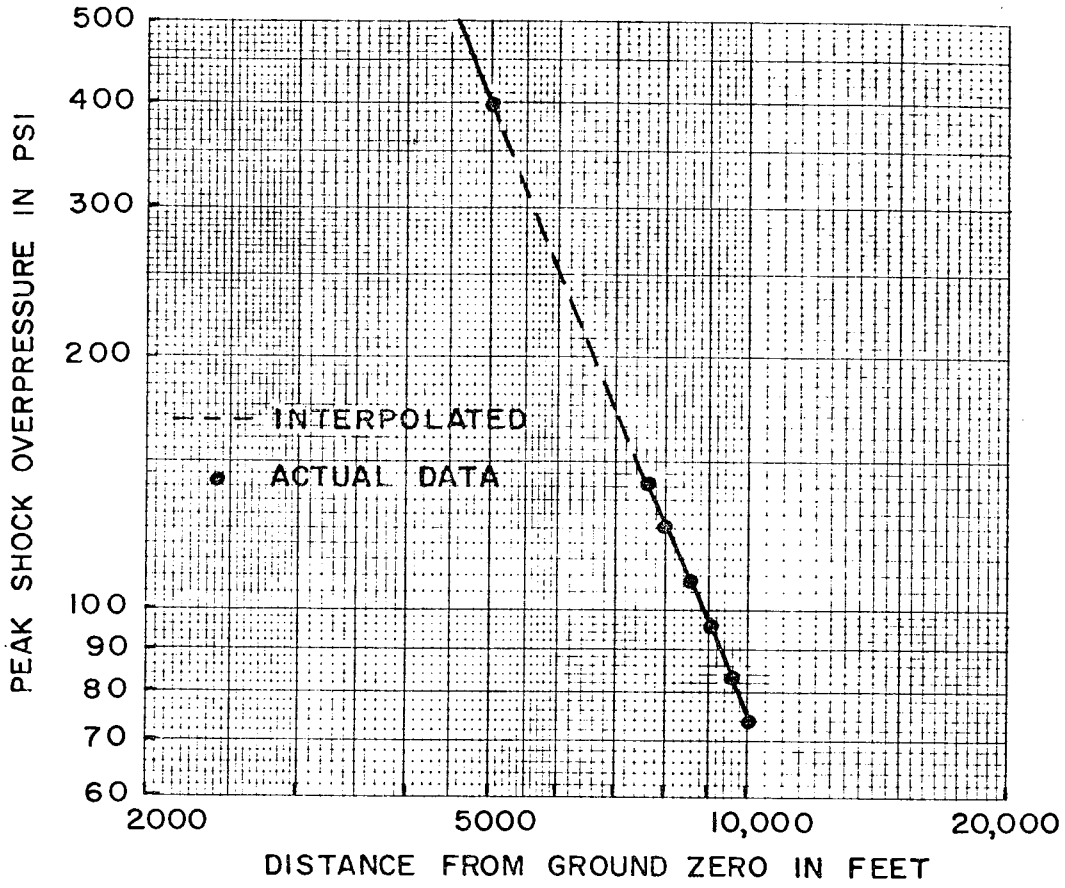

Fig. 3.4 Surface Peak Shock Overpressure vs Distance, Shot 1

The jet was assumed to take the form of a truncated semicircular cone* in order to determine the volume (see Fig. 3.5). The jet data are presented in Table 3.4 and Fig. 3.6. Photographs are shown in Fig. 3.7.

3.3 SHOT 2

Three of the films obtained for Project 1.1 were of fair quality and were used in the analysis. The horizontal aiming angles were not as indicated in the instrumentation plan, but it was possible to make the necessary corrections. Films taken for Project 13.2 were used to extend the coverage of the 1.1 films.

3.3.1 Arrival Time Data

It was noted that the fireball growth was greater vertically than it was along the surface. A nipple-like protrusion appeared at the top of the fireball at about 40 msec and it continued to grow

* Various views of the jet were available (from Stations 1302.03, 1302.02, and 1300.) Accurate measurements of the jet were possible on only the 1.1 film taken from 1302.03 but the appearance of the jet in the 13.2 films taken from the other stations indicated this form.

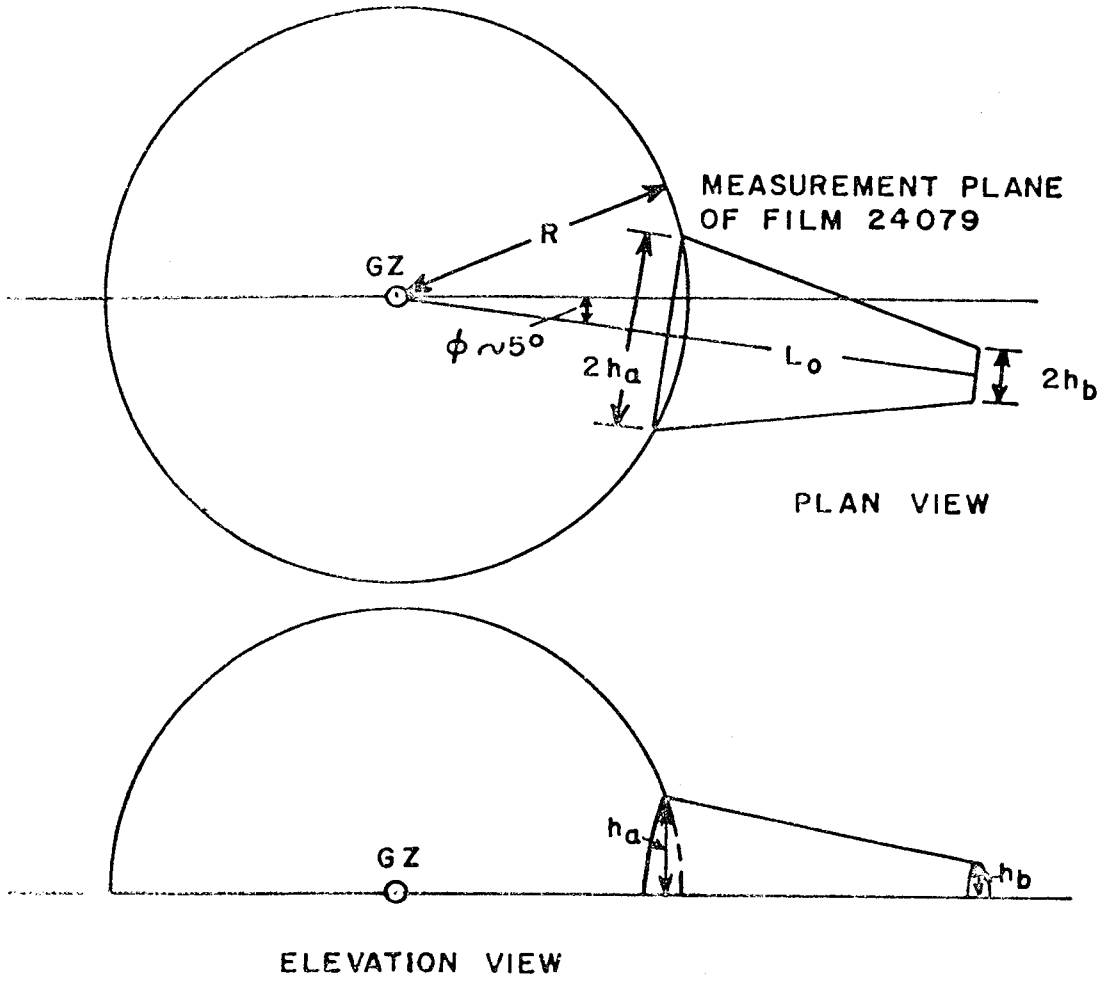

Fig. 3.5 The Assumed Form of the Horizontal Jet, Shot 1

throughout the fireball period. The protrusion began to rupture and appeared to release the detonation products of the fireball at about 300 msec, which was roughly the time of shock breakaway. Refer to Fig. 3.8.

As a result of the appearance of the vertical protrusion the vertical fireball data were fitted in two parts, before the arrival and after the arrival of the protrusion. Both surface and vertical data were fitted by equation 1.4 and the equations were found to be:

Vertical	$r = 6478t^{0.350}$,	$1100 \leq r_v \leq 2250$ (ft)
Vertical	$r = 7677t^{0.403}$	$2250 \leq r_v \leq 4500$ (ft)
Surface	$r = 6722t^{0.381}$	$1000 \leq r_h \leq 4500$ (ft)

The surface shock-arrival data presented were derived from films 24,575, 24,576, 24,577, 24,552, and 24,554. The baselines of the planes of measurement of these films encompassed both land and water surfaces. Data obtained from film 24,575 (Project 1.1) and

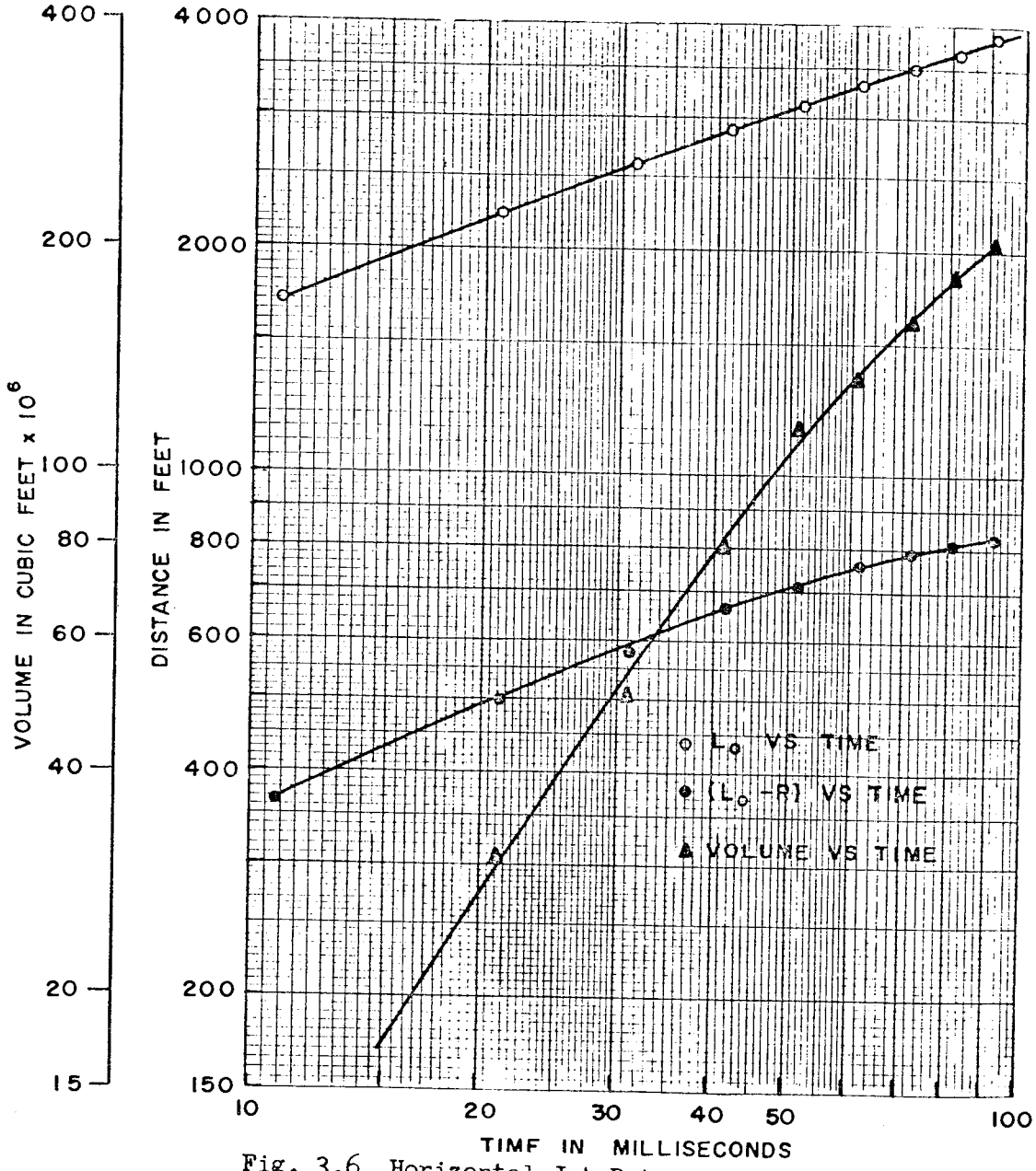

Fig. 3.6 Horizontal Jet Data, Shot 1

films 24,552 and 24,554 (Project 13.2)* were measured over a water surface.** The majority of the data presented that were obtained from the other two usable Project 1.1 films (24,576 and 24,577) were measured over a land surface. The two sets of data were fitted separately.

---

* These two films were taken from different camera stations. No asymmetry was detected in the shock growth along the surface.

** As on Shot 1 ground zero is not visible. It is 10 ft below the horizon. The plane of measurement of film 24,554 was over the reef. The plane of measurement of film 24,552 was chiefly over the lagoon.

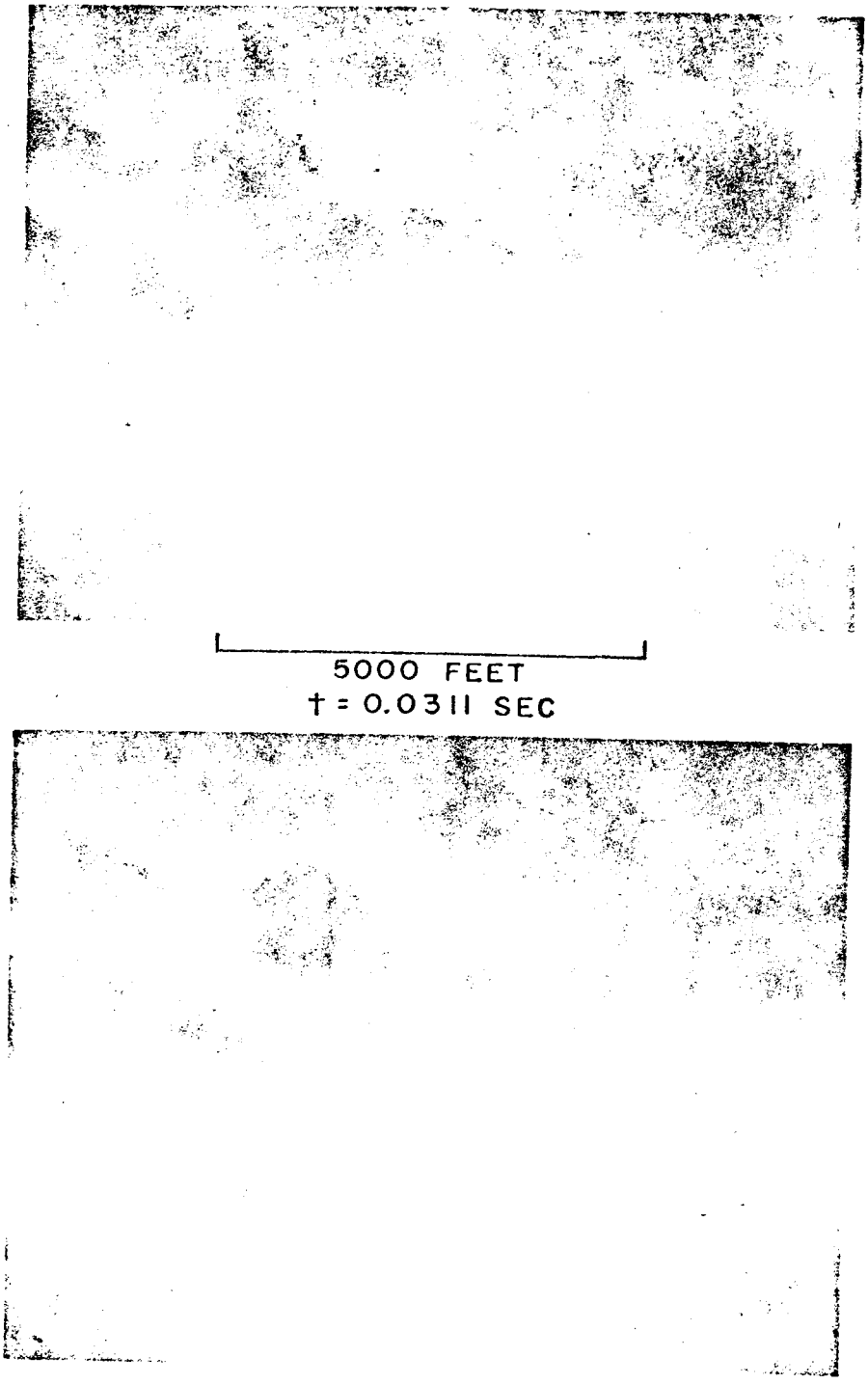

Fig. 3.7 Fireball Photographs Showing the Jet of Shot 1

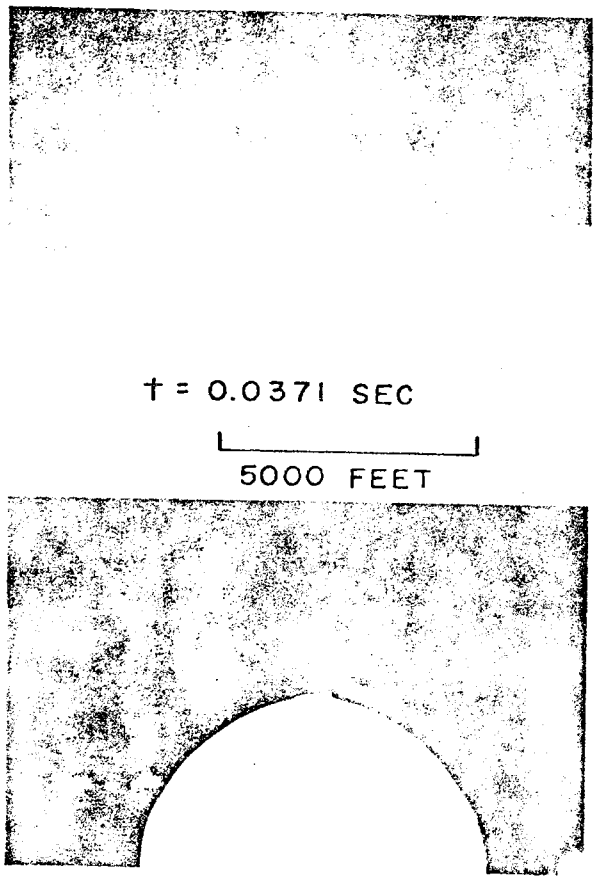

g. 3.8 Fireball Photographs Showing the Vertical Protrusion of Shot 2

TABLE 3.5 - Observed High Altitude Arrival Time Data, Shot 2

Time (Sec)	Distance Above Surface (Thousands of Feet)
205	266
210	270
212	273
213	273
215	280
216	275
217	280
218	278
220	285
221	288
222	288
223	288
225	292
226	295
228	298
230	300
231	300
232	303
233	301
235	304
236	309
237	309
238	311
240	314
241	314
242	318
243	321
245	325
246	323
250	332

Vertical data beyond the fireball region were obtained from film 24,554 in the region from 10,000 ft to 15,000 ft directly above ground zero. The spatial uncertainty of these data was of the order of 400 ft. (See Sections 3.9.2 and 3.9.5)

Two wave fronts were observed* at very great altitudes ($\sim$ 265,000 ft to $\sim$ 335,000 ft) on film 24,562. The arrival time of the first wave was measured from $\sim$ + 205 sec to $\sim$ + 250 sec, at which time the top of the wave went beyond the range of the film. No usable data were obtained for the second wave front because it was very difficult to discern on the copy of film 24,562 used for the measurement.

* This effect was visible to the unaided eye from Elmer Island, about 200 miles away.

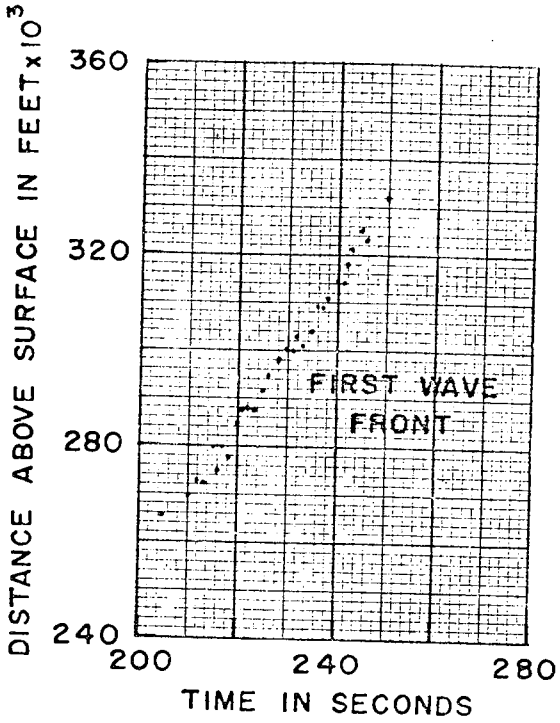

Fig. 3.9 High Altitude Arrival Time Data, Shot 2

The spatial uncertainty of the measurements made of the first wave was large* and the velocities obtained from these data should be considered as approximations only. The velocities obtained by NOL and EG&G for the first wave front differed by about 20 per cent (See 4.2.2.) This large difference can easily be accounted for through the large spatial uncertainty.

These data are shown in Table 3.5 and are plotted in Fig. 3.9. Photographs obtained from the film are found in Fig. 3.10a and 3.10b. These prints are negatives; the wave front is more easily seen in them than it would be in positive prints.

The shock arrival time data near the surface, both surface and vertical, were fitted by equation 1.6 and the constants were found to be:

---

* This film was obtained from Elmer Island, 200 miles away from $\overline{GZ}$. Thus the film scale was large ($\sim$ 20,000 ft/mm). Further the film was overexposed and therefore grainy. The external geometry of the system was not completely known and it was necessary to make several approximations to determine the altitudes. The wave front was non-spherical and as a result the proper corrections to be made for elongation in the measurement plane were not known. However, the normal corrections[4] for the spherical case were made. It should also be pointed out that the film used for the measurements was a copy.

The maximum spatial uncertainty was unknown, but it is believed to be of the order of 10 per cent.

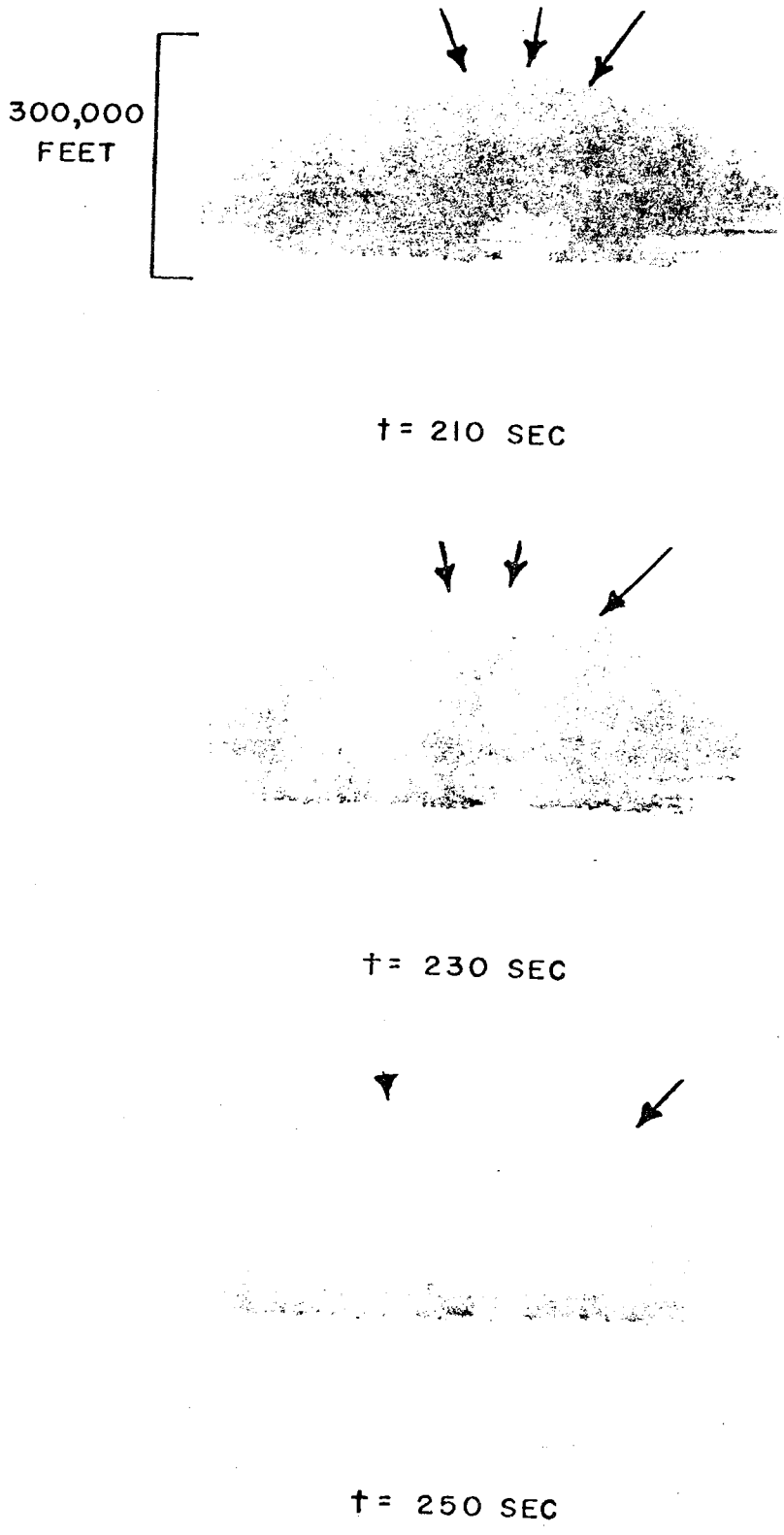

Fig. 3.10a Photographs of the First Wave Observed at Great Altitudes

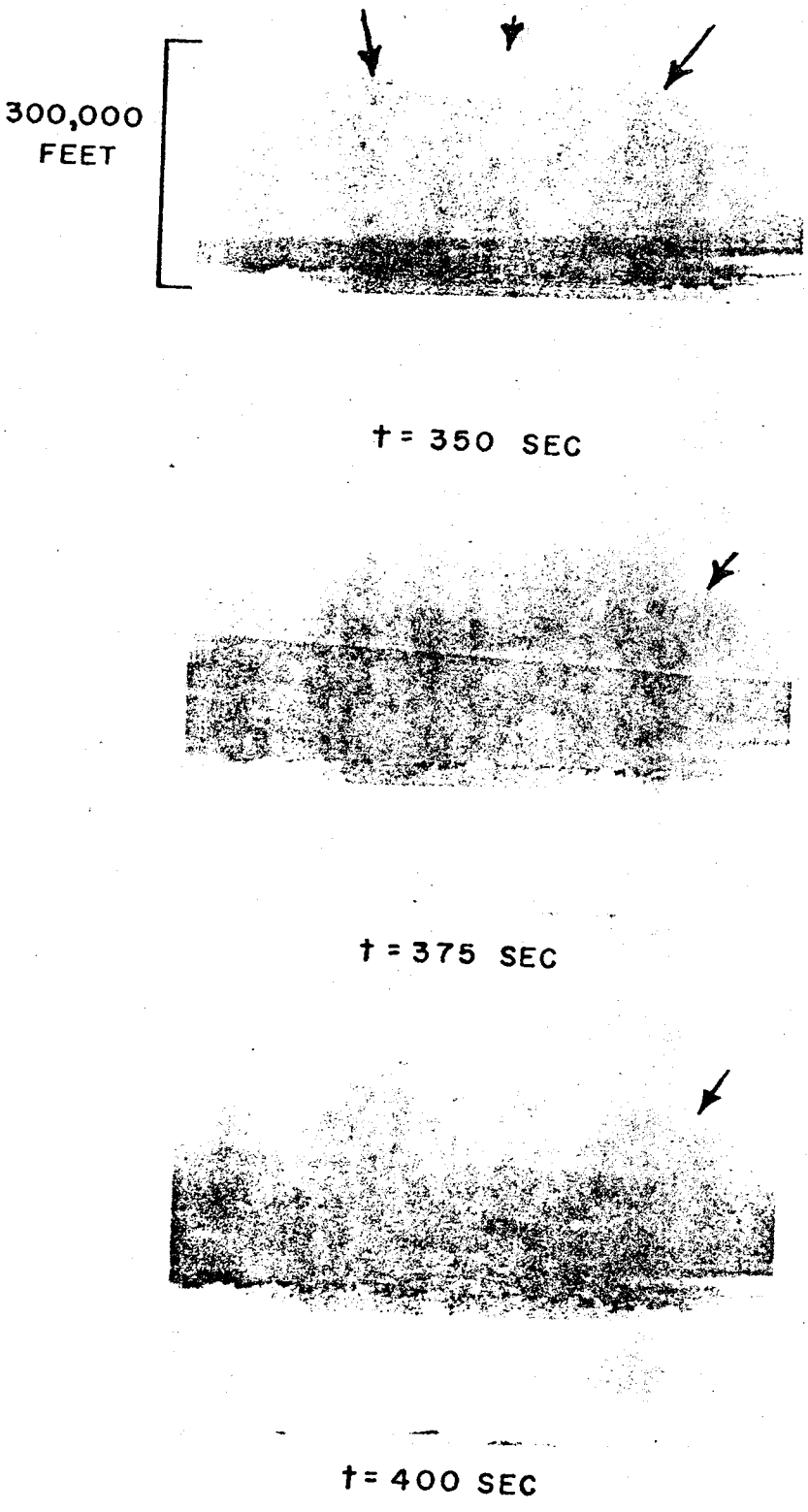

THIS PAGE IS BEST QUALITY PRACTICABLE
FROM COPY FURNISHED TO DDC

3.10b Photographs of the Second Wave Observed at Great Altitudes

TABLE 3.6 - Observed Surface Arrival Time Data, Shot 2

Time (sec)	Distance From $\overline{GZ}$ (ft)	
0.0066	987	FIREBALL
0.0168	1410	
0.0269	1690	
0.0371	1916	
0.0473	2106	
0.0574	2263	
0.0676	2408	
0.0777	2535	
0.0879	2660	
0.0981	2775	
0.1082	2880	
0.1184	2988	
0.1387	3170	
0.1590	3350	
0.1793	3504	
0.1997	3652	
0.2200	3794	
0.2403	3926	
0.2606	4035	
0.2809	4133	
0.3013	4236	
0.3216	4319	SHOCK BREAK-AWAY REGION
0.3311	4411	
0.3521	4509	
0.3501	4553	
0.3716	4595	LAND SURFACE
0.3686	4600	
0.3818	4691	
0.4055	4786	
0.3919	4789	
0.4020	4825	
0.4240	4877	
0.4223	4881	
0.4332	4928	
0.4426	4945	
0.4424	4979	
0.4628	5051	
0.4794	5164	
0.5033	5225	
0.5163	5315	
0.5347	5390	
0.5439	5407	
0.5641	5447	LAND SURFACE
0.5532	5458	
0.5901	5622	
0.6086	5733	
0.6270	5781	
0.6640	5903	
0.6816	6116	
0.7009	6156	
0.7378	6269	
0.7470	6306	
0.7655	6367	
0.8116	6558	
0.8578	6676	
0.8762	6843	
0.8855	6864	
0.8947	6928	
0.9039	6937	
0.9224	6987	
0.9408	7030	
0.9593	7066	
0.9686	7111	
1.0147	7284	
1.0239	7304	
1.0424	7330	
1.0287	7382	
1.0187	7398	
1.0488	7414	
1.0690	7429	
1.0598	7432	
1.0701	7448	
1.0801	7451	
1.0891	7509	
1.0978	7517	
1.1207	7539	
1.1193	7540	
1.0991	7583	
1.1255	7606	
1.1494	7641	
1.1595	7678	
1.1696	7729	WATER SURFACE
1.1817	7734	
1.1293	7745	

TABLE 3.6 - Observed Surface Arrival Time Data, Shot 2, (Cont'd)

Time (sec)	Distance From $\overline{GZ}$ (ft)		Time (sec)	Distance From $\overline{GZ}$ (ft)	
1.1394	7761		1.7329	9260	
1.1410	7770		1.7128	9321	
1.1796	7805		1.7832	9369	
1.1614	7823		1.7530	9417	
1.1997	7824		1.8738	9417	
1.1987	7852		1.7933	9433	
1.2601	8121		1.8536	9588	
1.3442	8125		1.8335	9604	
1.3506	8173		1.8939	9620	
1.3305	8189		1.9140	9652	
1.3657	8219		1.9542	9777	
1.3808	8234		2.0247	9793	
1.3406	8251		2.0649	9918	
1.3708	8362		2.0448	9950	
1.4110	8394		2.1152	9980	
1.4662	8410		2.0045	9993	
1.4211	8410		1.9744	10,012	
1.4009	8412		2.0850	10,073	
1.4613	8440		2.1957	10,123	
1.4052	8444		2.1253	10,139	
1.4311	8489		2.1655	10,232	
1.4357	8499		2.2158	10,262	
1.4512	8508		2.3063	10,388	
1.4714	8519		2.2359	10,436	
1.4412	8535		2.2762	10,481	
1.5418	8561		2.2057	10,518	
1.4814	8613		2.3466	10,545	
1.5015	8707		2.2560	10,564	
1.5619	8872		2.3667	10,607	
1.5820	8882		2.4170	10,623	
1.6021	9004		2.4069	10,636	
1.6223	9006		2.3501	10,650	
1.6826	9006		2.3868	10,652	
1.6424	9134		2.3907	10,740	
1.6625	9182		2.6081	11,013	
1.6927	9212		2.5075	11,122	
1.7430	9212		2.5578	11,151	

WATER SURFACE

WATER SURFACE

TABLE 3.7 - Observed Vertical Arrival Time Data, Shot 2

Time (sec)	Distance From $\overline{GZ}$ (ft)		Time (sec)	Distance From $\overline{GZ}$ (ft)
0.0066	1121	FIREBALL	2.2359	12,045
0.0168	1534		2.3667	12,045
0.0269	1828		2.4371	12,045
0.0371	2041		2.6081	12,277
0.0473	2249		2.6584	12,509
0.0574	2401		2.8093	12,662
0.0676	2575		3.1614	12,970
0.0777	2748		3.2117	13,030
0.0879	2887		3.3123	13,200
0.0981	3018		3.0608	13,368
0.1082	3148		3.4129	13,582
0.1184	3242		3.3626	13,782
0.1387	3455		3.5638	13,797
0.1590	3655		3.6644	13,952
0.1793	3842		3.5135	14,194
0.2200	4170		3.6141	14,240
0.2403	4303		3.8656	14,498
0.2606	4432		3.8153	14,650
1.5217	8971		4.0668	14,725
1.6223	9552		3.9763	14,803
1.4512	9708		4.0266	14,803
1.5418	9708		4.1876	14,803
1.7933	10,148		4.1976	14,803
2.0949	10,803		4.2177	14,833
2.0045	10,944		3.7650	14,848
1.9844	10,959		3.9461	14,849
2.0448	11,115		4.0165	14,909
2.3164	11,379		4.2580	14,909
2.0850	11,426		3.9361	14,923
2.1655	11,426		4.2379	14,923
2.3063	11,426		4.2680	14,923
2.1856	11,457		4.0568	15,045
2.1152	11,581		4.2882	15,181
2.3265	11,581		4.3183	15,197
2.4874	11,626		4.1171	15,257
2.2963	11,737			
2.2259	11,782			
2.3466	11,813			
2.3968	11,890			
2.5578	12,014			

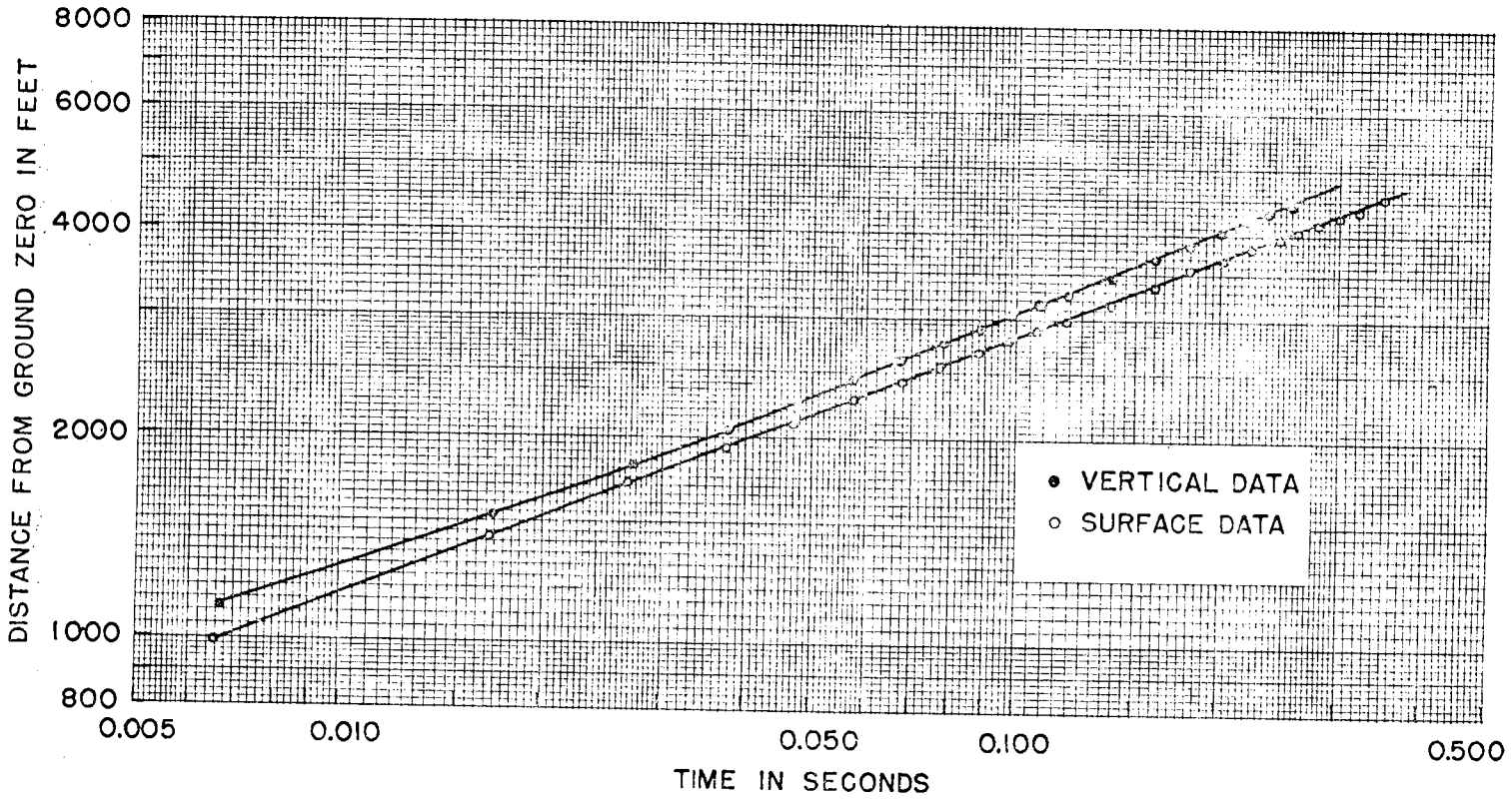

Fig. 3.11 Fireball Arrival Time Data, Shot 2

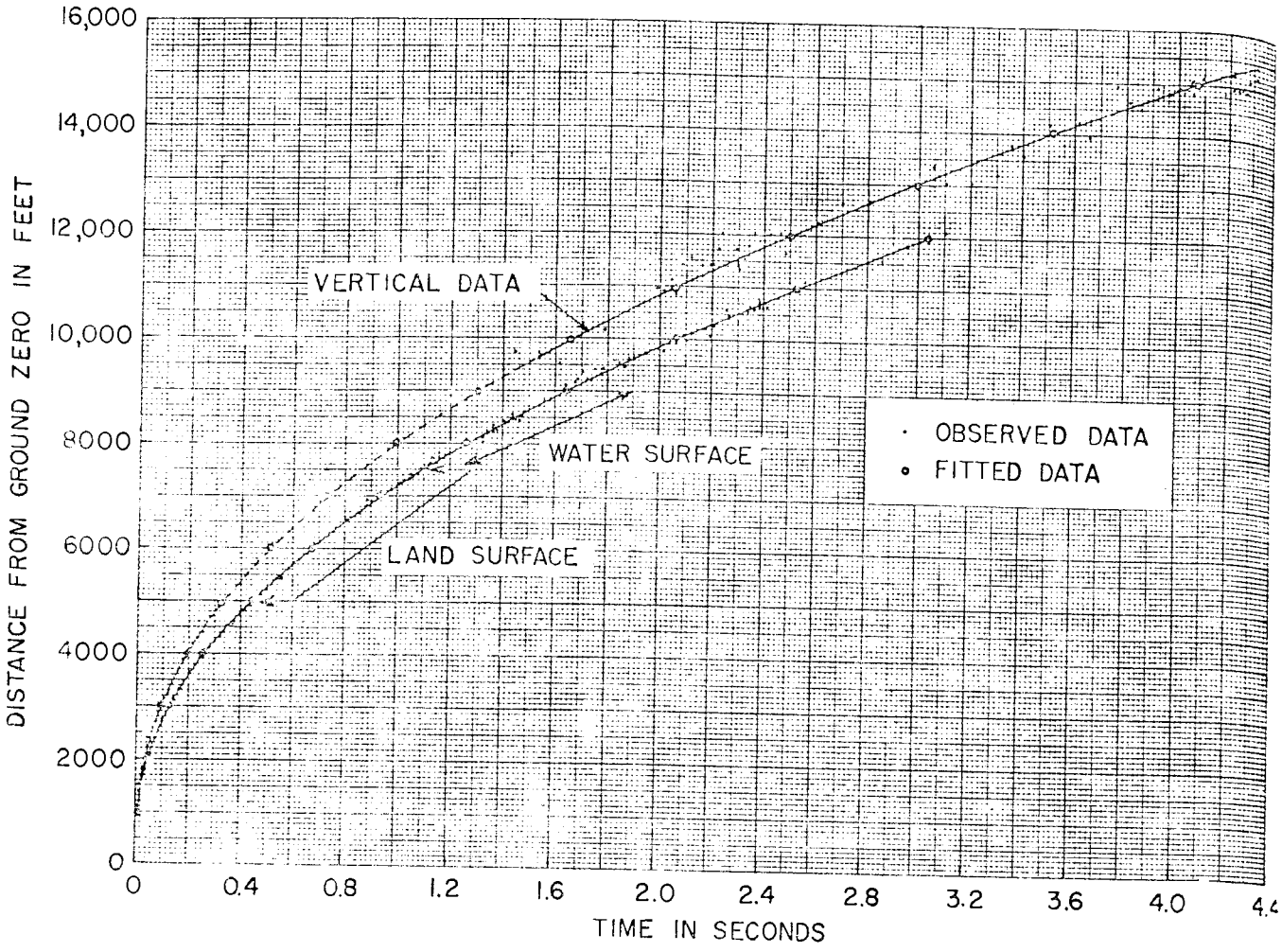

Fig. 3.12 Shock Arrival Time Data, Shot 2

Surface, Water and Land A=1377 B=9592 C=-15.4 $4500 \leq r_h \leq 7500$ (ft)

Surface, Water A= 726 B=16,272 C=3.7 $7500 \leq r_h \leq 11{,}000$ (ft)

Vertical A= 609 B=22,386 C=3.6 $10{,}000 \leq r_v \leq 15{,}000$ (ft)

The observed arrival time data are presented in Tables 3.6 and 3.7. The calculated surface and vertical data are presented in Table 3.8. The calculated and observed data are shown in Figs. 3.11 (fireball) and 3.12.

3.3.2 The Velocity and Peak Shock Overpressure-Distance Data

The fitting functions were differentiated and the following were obtained:

The fireball region:

Vertical $U_v = 2267t^{-0.650} = 27{,}120 \times 10^6 r_v^{-1.857}$ $1100 \leq r_v \leq 2250$ (ft) (3.3)

Vertical $U_v = 3094t^{-0.597} = 1756 \times 10^6 r_v^{-1.481}$ $2250 \leq r_v \leq 4500$ (ft) (3.3a)

Surface $U_h = 2561t^{-0.619} = 4246 \times 10^6 r_h^{-1.625}$ $1000 \leq r_h \leq 4500$ (ft) (3.4)

The region after shock breakaway which occurred sometime between 0.3 and 0.35 sec had the following velocities:

Surface, Water and Land $U_h = 1337 \left[1 + \left(\frac{9592}{r_h}\right)^{1.5}\right]$ $4500 \leq r_h \leq 7500$ (ft) (3.5)

Surface, Water $U_h = 726 \left[1 + \left(\frac{16{,}272}{r_h}\right)^{1.5}\right]$ $7500 \leq r_h \leq 11{,}000$ (ft) (3.6)

Vertical $U_v = 609 \left[1 + \left(\frac{22{,}386}{r_v}\right)^{1.5}\right]$ $10{,}000 \leq r_v \leq 15{,}000$ (ft) (3.7)

Peak shock overpressures were not computed in the fireball region. The velocity-distance data are presented in Table 3.8 and Fig. 3.13. The peak shock overpressure-distance data for both vertical* and surface data are presented in Table 3.8 and Fig. 3.14. It should be noted that the region ranging from 4500 to 7500 ft was over land and the pressures obtained in this region were high. Since these pressures were calculated from the Rankine-Hugoniot relationship, they were dependent upon the assumed speed of sound. It is reasonable to believe that the temperature of the air and, hence, the speed of sound were higher over the land than over the water; but no account was taken of this possibility in the calculations. If these higher temperatures, in fact, existed then the calculated pressures would have been higher than the actual pressures which existed. (See Section 3.9.4 and reference 13).

3.4 SHOT 3

No usable films were obtained on this shot because of the poor visibility and the unexpectedly low yield.

3.5 SHOT 4

The three films obtained for Project 1.1a were of very good quality and were all used in the analysis. The horizontal aiming angles were not as indicated but it was possible to make the necessary corrections. Films taken for Project 13.2 were used to extend the coverage.

---

* The vertical peak shock overpressure-distance data must be treated with caution. The uncertainty is quite large (~20 per cent). (See Section 3.9.5). The meteorological data used in the calculation may be found in Appendix B.

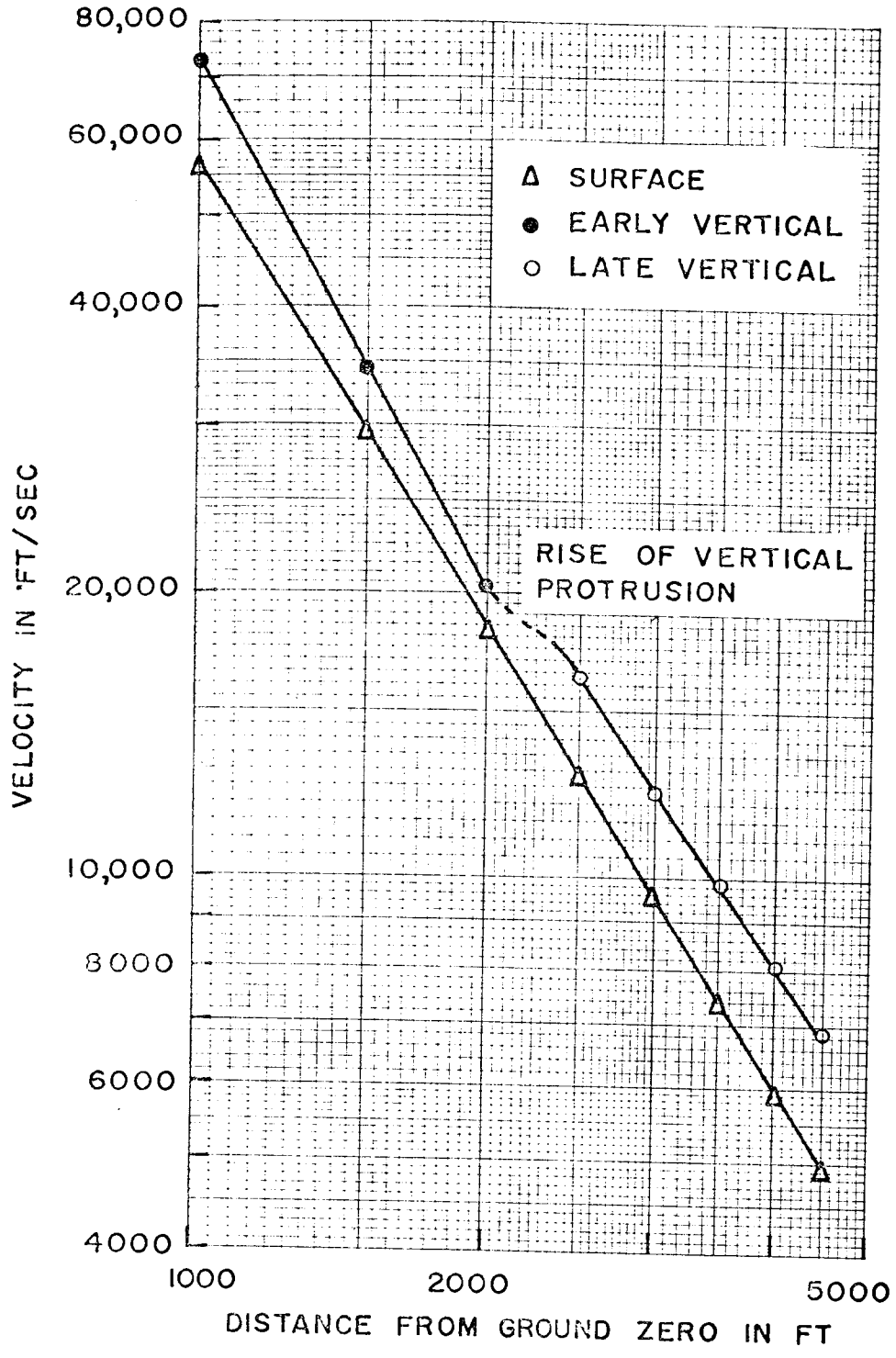

Fig. 3.13 Fireball Velocity vs Distance, Shot 2

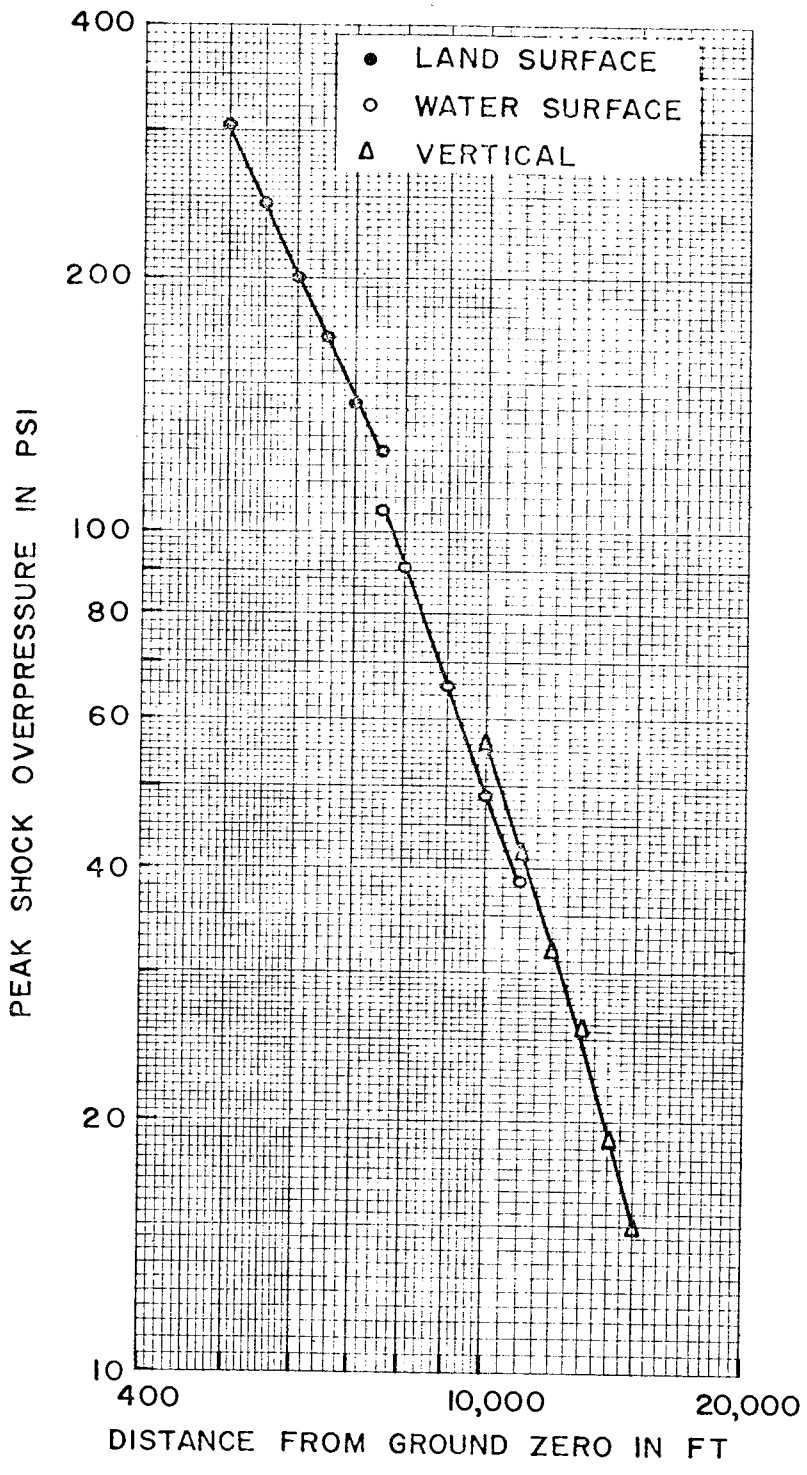

Fig. 3.14 Peak Shock Overpressure vs Distance, Shot 2

TABLE 3.8 - Arrival Time, Velocity and Peak Shock Overpressure, Shot 2

Distance From GZ (ft)	Arrival Time (sec)			Velocities (ft/sec)			Peak Shock Overpressures lb/in²		
	Land Surface	Water Surface	Vertical	Water-land Surface	Water Surface	Vertical	Water-land Surface	Water Surface	Vertical
1000		0.0068	0.0048		56620	72920			
1500		0.0195	0.0153		29280	34310			
2000		0.0415	0.0348		18360	20120			
2500		0.0746	0.0618		12770	16300			
3000		0.1204	0.0971		9500	12440			
3500		0.1803	0.1423		7390	9900			
4000		0.2561	0.1982		5950	8130			
4500		0.3487	0.2658		4917	6823			
5000	0.4431			4890			304		
5500	0.5508			4417			245		
6000	0.6693			4040			201		
6500	0.7982			3734			170		
7000	0.9370			3482			144		
7500	1.0852	1.0920		3271	3051		125	106	
8000		1.2620			2838			91	
9000		1.6386			2498			65.4	
10000		2.0621	1.6631		2234	2649		48.8	56.1
11000		2.5305	1.062		2033	2377		38.3	41.8
12000			2.504			2161			31.8
13000			2.987			1985			25.5
14000			3.511			1840			19.0
15000			4.074			1719			14.8

TABLE 3.9 - Observed Arrival Time Data Shot 4

Time (sec)	Distance From GZ (ft) Surface	Vertical	Time (sec)	Distance From GZ (ft) Surface
0.0070	912	994	0.3883	4330
0.0160	1243	1320	0.3986	4376
0.0249	1476	1539	0.4089	4430
0.0428	1832	1917	0.4193	4462
0.0517	1979	2058	0.4296	4523
0.0607	2107	2207	0.4502	4625
0.0697	2219	2343	0.4605	4659
0.0786	2331	2456	0.4708	4717
0.0876	2426	2564	0.4811	4767
0.0965	2511	2664	0.4914	4805
0.1055	2610	2772	0.5017	4851
0.1144	2692	2886	0.5120	4878
0.1234	2763	2989	0.5223	4917
0.1323	2844		0.5326	4976
0.1413	2912	3153	0.5429	5019
0.1502	2976	3232	0.5532	5055
0.1581	3043		0.5635	5095
0.1592	3049	3328	0.5738	5114
0.1617	3077		0.5944	5222
0.1666	3105		0.6150	5272
0.1681	3107	3405	0.6356	5359
0.1771	3171	3485	0.6562	5432
0.1860	3233	3574	0.6666	5461
0.1950	3297	3657	0.6769	5507
0.2039	3355	3729	0.6975	5559
0.2091	3385		0.7181	5623
0.2176	3418		0.7387	5696
0.2235	3438		0.7593	5750
0.2260	3466		0.7696	5802
0.2338	3483		0.8005	5871
0.2441	3572		0.8211	5981
0.2515	3600		0.8417	6034
0.2647	3636		0.8623	6094
0.2685	3705		0.8726	6146
0.2854	3815		0.8932	6213
0.2853	3824		0.9138	6255
0.3024	3906		0.9242	6305
0.3059	3926		0.9448	6367
0.3265	4027		0.9654	6420
0.3368	4087		0.9860	6484
0.3471	4125		0.9997	6505
0.3677	4239		1.0096	6514
0.3780	4288		1.0066	6541

TABLE 3.9 - Observed Arrival Time Data, Shot 4, (Cont'd)

Time (sec)	Distance From $\overline{GZ}$ (ft) Surface	Time (sec)	Distance From GZ (ft) Surface	Time (sec)	Distance From $\overline{GZ}$ (ft) Surface
1.0195	6542	1.7933	8592	2.5770	10,348
1.0272	6604	1.8330	8595	2.7754	10,535
1.0592	6634	1.8032	8625	2.7853	10,554
1.0394	6645	1.8230	8629	2.8448	10,584
1.0900	6675	1.8528	8659	2.9837	10,648
1.0493	6679	1.8032	8695	2.9738	10,683
1.1088	6768	1.8826	8712	3.0333	10,849
1.1584	6810	1.9024	8726	3.9936	10,955
1.0989	6832	1.9520	8779	3.1325	11,041
1.1286	6899	1.9024	8796	3.2317	11,274
1.1082	6984	1.9123	8840	3.3309	11,348
1.1980	6998	1.9927	8886	3.3706	11,380
1.2079	7075	1.9828	8948	3.4499	11,574
1.2873	7265	2.0016	9081	3.3904	11,596
1.3567	7306	2.0520	9157	3.3805	11,669
1.2972	7307	2.1107	9202	3.5670	11,942
1.2774	7317	2.1206	9214	3.5789	11,982
1.3468	7436	2.1603	9225	3.5888	12,005
1.3866	7499	2.1306	9266	3.7376	12,159
1.4163	7566	2.2000	9341	3.7773	12,322
1.4956	7841	2.1802	9394	3.8467	12,380
1.4858	7854	2.1901	9435	3.7872	12,443
1.5850	7933	2.3000	9483	3.9757	12,495
1.5453	7942	2.3190	9644	3.9658	12,733
1.5552	7942	2.3984	9752	4.0253	12,733
1.5155	7944	2.3786	9783	3.9856	12,778
1.5949	8000	2.3885	9795	3.9558	12,806
1.6048	8105	2.3587	9837	4.2733	12,966
1.6048	8107	2.3984	9918	4.1245	13,130
1.6842	8244	2.4381	9968	4.2237	13,126
1.6941	8298	2.4579	9968	4.3229	13,408
1.7040	8324	2.4976	10,016	4.2634	13,445
1.7536	8444	2.5274	10,158	4.2832	13,467
1.7040	8460	2.6166	10,169	4.5808	13,564
1.7833	8516	2.5869	10,184	4.5610	13,586
1.7535	8542	2.6067	10,212	4.8585	13,978
				4.8684	14,118
				4.8784	14,233

TABLE 3.10 - Arrival Time, Velocity and Peak Shock Overpressure Shot 4

Distance From GZ (ft)	Arrival Time (sec)		Velocity (ft/sec)		Peak Shock Overpressure lb/in^2
	Surface	Vertical	Surface	Vertical	Surface
1000	0.0092	0.0071	42700		
1500	0.0258	0.0234	22800	26060	
2000	0.0538	0.0475	14580	17110	
2500	0.0950	0.0822	10320	12350	
2750		0.1026		11870	
3000	0.1513	0.1248	7780	10640	
3500	0.2241	0.1768	6130	8760	494
4000	0.3186		5173		340
4500	0.4229		4460		250
5000	0.5428		3921		188
5500	0.6779		3501		146
6000	0.8283		3166		117
6500	0.9936		2895		94.1
7000	1.1809		2708		79.5
7500	1.3718		2536		68.2
8000	1.5749		2391		58.7
9000	2.0157		2161		44.6
10000	2.4992		1986		35.2
11000	3.0215		1850		28.3
12000	3.5790		1742		23.5
13000	4.1687		1654		19.1
14000	4.7873		1581		16.4

3.5.1 Arrival Time Data

The same general effects that were observed in the fireball region of Shot 2 were noted on this shot. There were indications of the vertical protrusion as early as 30 msec which became definite at approximately 60 msec. The rupture began at about 280 msec. (Refer to Fig. 3.15).

The vertical fireball data were fitted in two parts and both surface and vertical data were fitted by equation 1.4. The equations were found to be:

Vertical $\quad r = 5498t^{0.345} \quad 1000 \leq r_v \leq 1500$ (ft)

Vertical $\quad r = 6893t^{0.406} \quad 1500 \leq r_v \leq 2500$ (ft)

Vertical $\quad r = 7537t^{0.443} \quad 2500 \leq r_v \leq 3700$ (ft)

Surface $\quad r = 6292t^{0.392} \quad 1000 \leq r_h \leq 3500$ (ft)

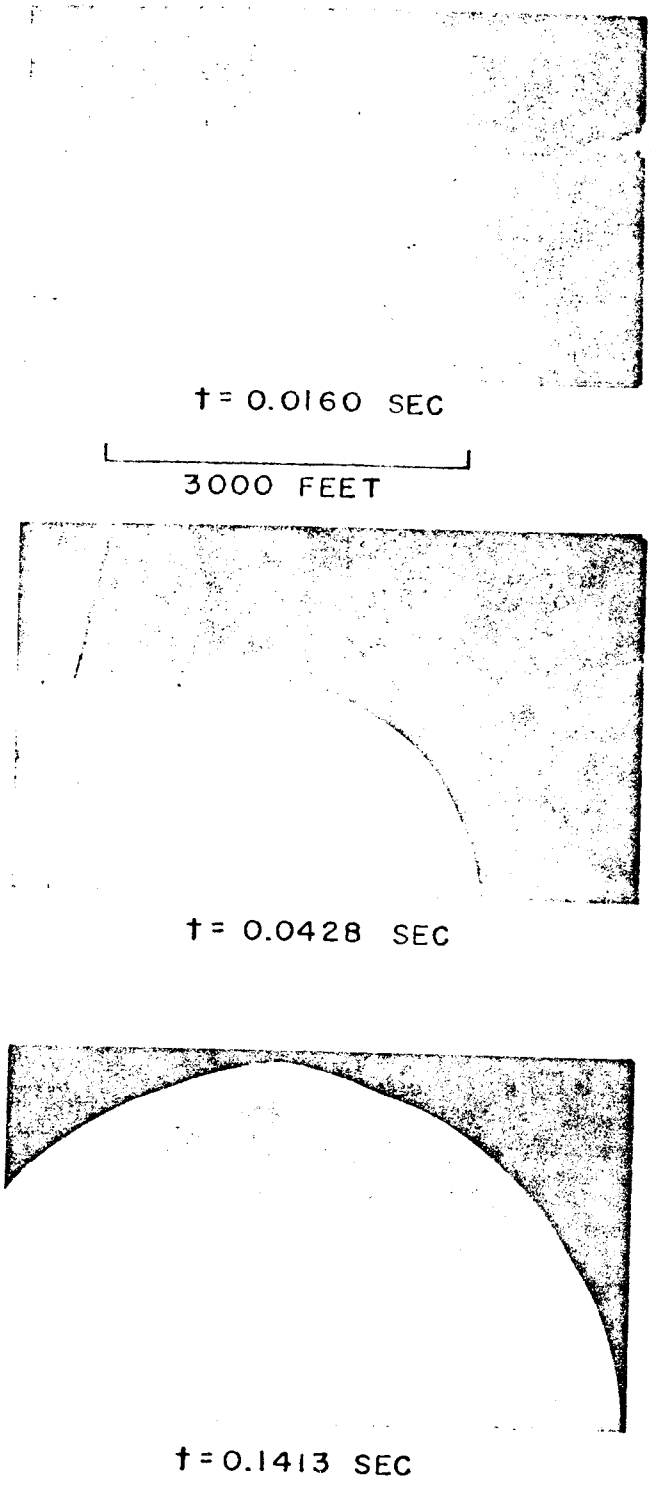

Fig. 3.15 Fireball Photographs Showing the Vertical Protrusion of Shot 4

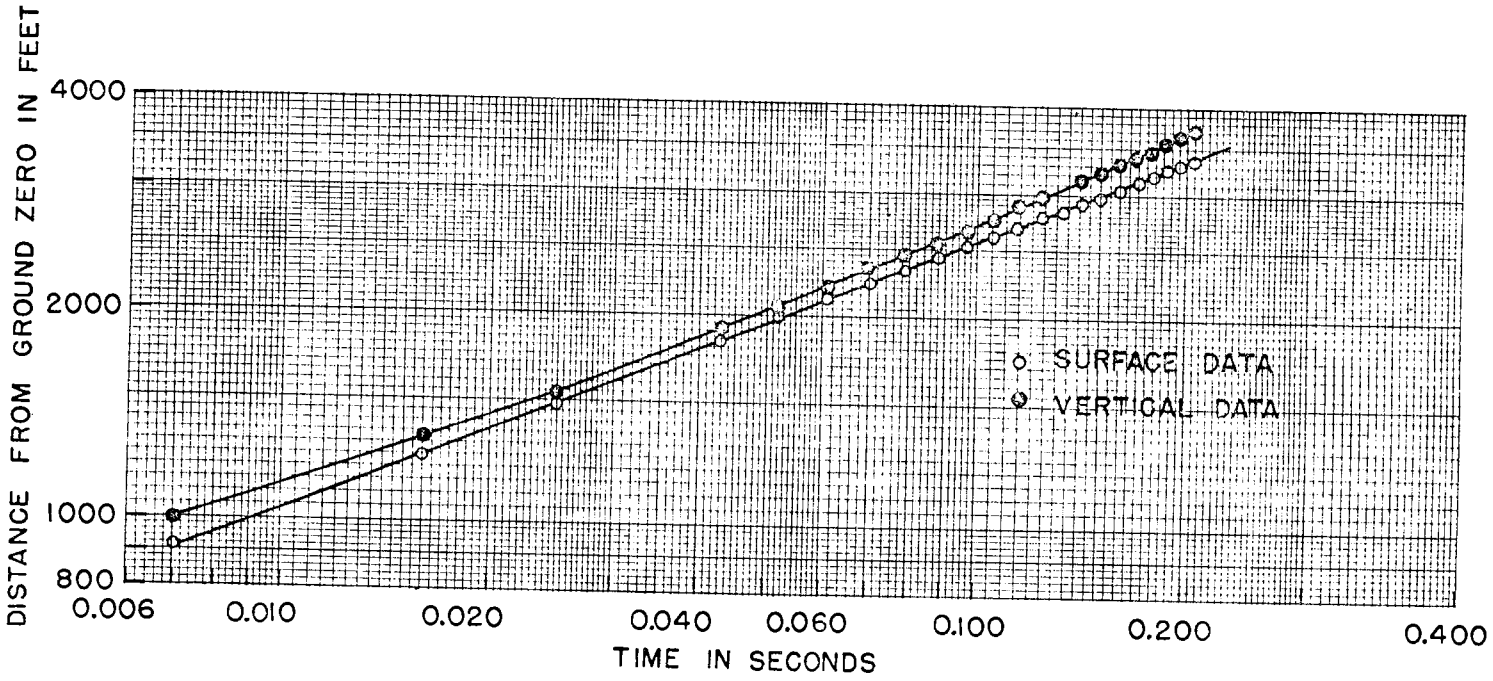

Fig. 3.16 Fireball Arrival Time Data, Shot 4

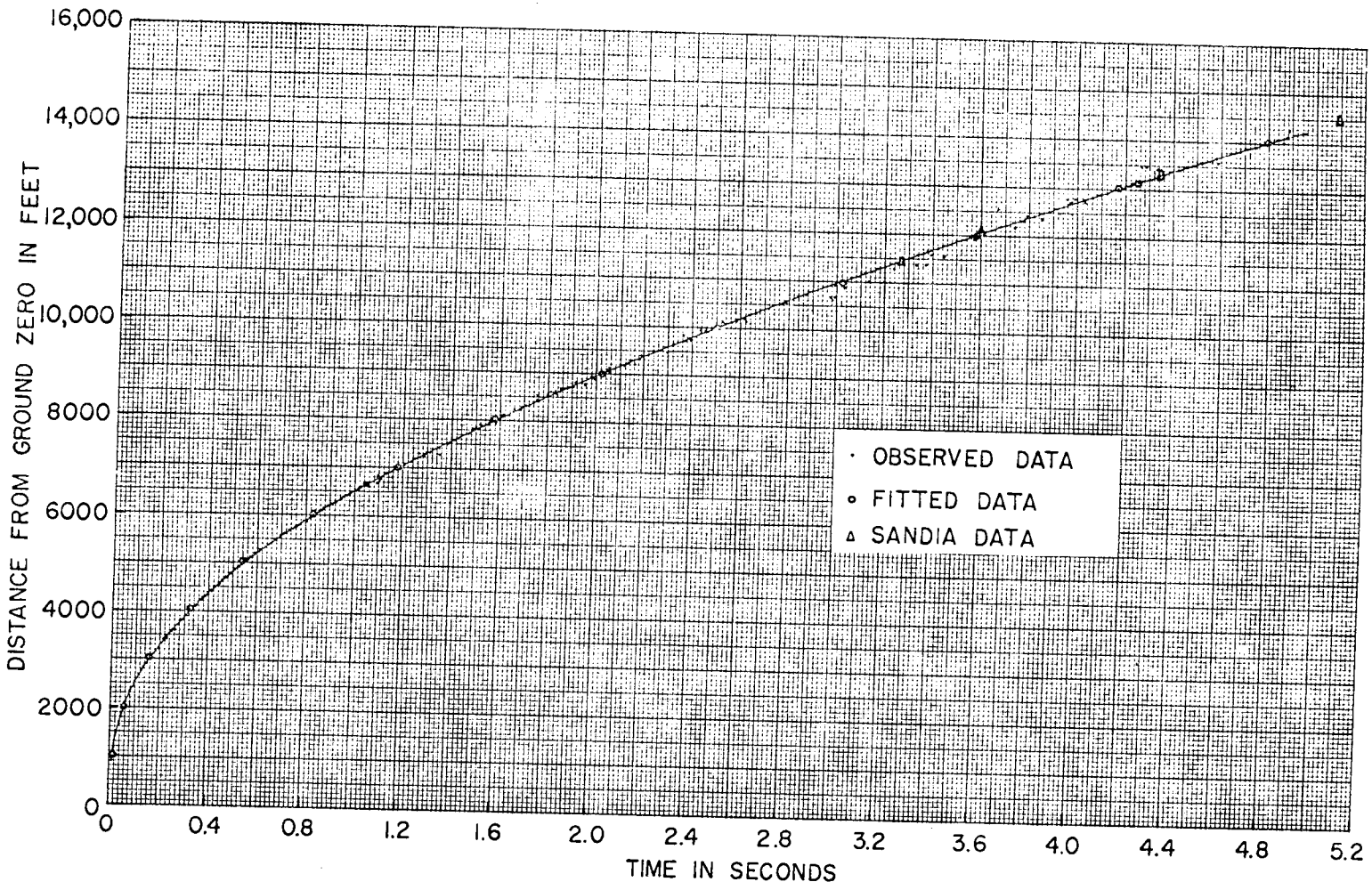

Fig. 3.17 Surface Shock Arrival Time Data, Shot 4

The surface shock-arrival data presented were derived from films 24,180, 24,181, 24,182, and 24,150 (Project 13.2). The Project 1.1a data covered the first 6600 ft, and the usable data from the Project 13.2 film covered the region from 6600 ft to 14,000 ft. Shock breakaway is believed to have occurred between 0.2 and 0.3 sec. All data were obtained over a water surface and ground zero was on the horizon. There were no vertical data obtained in the shock region.

The shock arrival time data were fitted in two parts by equation 1.6 and the constants were found to be:

$$A = 770.7 \quad B = 12{,}782 \quad C = -9.6 \quad 3500 \leq r \leq 6500 \quad \text{(ft)}$$

$$A = 965 \quad B = 10{,}381 \quad C = -26.2 \quad 6500 \leq r \leq 14{,}000 \quad \text{(ft)}$$

The observed and calculated arrival time data are presented in Tables 3.9 and 3.10 and are shown in Figs. 3.16 and 3.17.*

3.5.2 The Velocity and Peak Shock Overpressure-Distance Data

The fitting functions were differentiated to obtain expressions for the instantaneous velocities, U, at the desired distances. For the fireball region the following was obtained:

Vertical $U_v = 2799t^{-0.594} = 1149 \times 10^6 r^{-1.462}$ $1500 \leq r_v \leq 2500$ (ft) (3.8)

Vertical $U_v = 3337t^{-0.557} = 253.9 \times 10^6 r^{-1.259}$ $2750 \leq r_v \leq 3700$ (ft) (3.8a)

Surface $U_h = 2466t^{-0.608} = 1923 \times 10^6 r^{-1.551}$ $1000 \leq r_h \leq 3500$ (ft) (3.9)

For the shock region the following was obtained:

$$U = 770.7 \left[1 + \left(\frac{12{,}782}{r}\right)^{1.5}\right] \quad 3500 \leq r \leq 6500 \text{ (ft)} \quad (3.10)$$

$$U = 965 \left[1 + \left(\frac{10{,}381}{r}\right)^{1.5}\right] \quad 6500 \leq r \leq 14{,}000 \text{ (ft)} \quad (3.10a)$$

Peak shock overpressures were not calculated in the fireball region. The velocity-distance data are presented in Table 3.10 and Fig. 3.18. The peak shock overpressure data are presented in Table 3.10 and Fig. 3.19.

3.6 SHOT 5

Three of the four cameras used to obtain the Project 1.1 data on Shot 5 jammed before zero time. The film obtained from the fourth

---

* The Sandia Corporation data shown with this curve were obtained from the preliminary version of reference (14).

camera (24,280) was fogged by radiation and was of no great value.* Films 24,250 and 24,253, which were obtained for Project 13.2, were used in the analysis of this shot. All data obtained for this shot were in the fireball region.

3.6.1 Fireball Data

The two Project 13.2 films used in the analysis were taken from different camera stations. (Refer to Table 2.3.) Fireball diameters were measured along the surface from the two films and the resulting measurements did not agree. It appeared that the rate of growth of the fireball was non-uniform along the surface.** The growth as viewed from Station 1300 appeared greater than that viewed from Station 1302.02. No reasonable estimate could be made of shock breakaway from these films. A similar disagreement was noted on the vertical measurements. The disagreement was the result of film anomalies resulting from overexposure during the fireball period (the films were not designated for fireball measurements)*** and small errors in the copying process. Film 24,250 was considered to be the more accurate.

Both sets of data were fitted by equation 1.4 and the equations were found to be:

Vertical	24,250	$r = 8105t^{0.398}$	$1500 \leq r_v \leq 4500$ (ft)
Surface	24,250	$r = 7229t^{0.404}$	$1500 \leq r_h \leq 4000$ (ft)
Vertical	24,253	$r = 8663t^{0.395}$	$1500 \leq r_v \leq 4500$ (ft)
Surface	24,253	$r = 7990t^{0.408}$	$1500 \leq r_h \leq 4500$ (ft)

These observed and calculated data are presented in Tables 3.11 and 3.12 and Fig. 3.20.

3.7 SHOT 6

Two usable films (24,477 and 24,478) were obtained for this shot and both were used in the analysis. The primary film (24,477) was of fair quality. The other was extremely good.

3.7.1 The Arrival Time Data

The fireball arrival time data were obtained from film 24,477,

---

* The fireball was not completely visible and the horizontal aiming angle was in doubt. Consequently, the position of ground zero was not known.

** Ground Zero was in the foreground in both films.

*** These films were exposed under conditions to obtain data at late times; consequently they were overexposed in the fireball region. According to EG&G the maximum image spread would be of the order of 0.06 mm on the film (~150 ft in the plane of measurement).

TABLE 3.11 - Observed Arrival Time Data, Shot 5

Film 24250			Film 24253		
Time (sec)	Distance From $\overline{GZ}$ (ft)		Time (sec)	Distance From $\overline{GZ}$ (ft)	
	Surface	Vertical		Surface	Vertical
0.0096	1107	1300	0.0101	1216	1384
0.0197		1763	0.0202	1652	1895
0.0298	1745	1978	0.0304	1939	2182
0.0399		2204	0.0405	2176	2457
0.0499	2145	2542	0.0506	2363	2756
0.0600		2678	0.0607	2550	2906
0.0700	2467	2712	0.0708	2718	2993
0.0801		2938	0.0911	2993	3280
0.0901	2709	3074	0.1113	3247	3661
0.1002		3220	0.1316	3491	3903
0.1203	3074	3503	0.1518	3690	4115
0.1404		3672	0.1720	3896	4340
0.1505	3356	3831	0.1923	4051	4464
0.1606		3887	0.2125	4232	4726
0.2008	3777	4283	0.2328	4424	
0.2511	4181	4667	0.2530	4580	

TABLE 3.12 - Calculated Arrival Time, Shot 5

Distance From $\overline{GZ}$ (ft)	Film 24250 Arrival Time (sec)		Film 24253 Arrival Time (sec)	
	Surface	Vertical	Surface	Vertical
1500	0.0205	0.0144	0.0165	0.0118
2000	0.0417	0.0296	0.0334	0.0245
2500	0.0724	0.0519	0.0578	0.0431
3000	0.1136	0.0822	0.904	0.0684
3500	0.1663	0.1210	0.1320	0.1010
4000	0.2008	0.1694	0.1831	0.1416
4500		0.2277	0.2445	0.1907

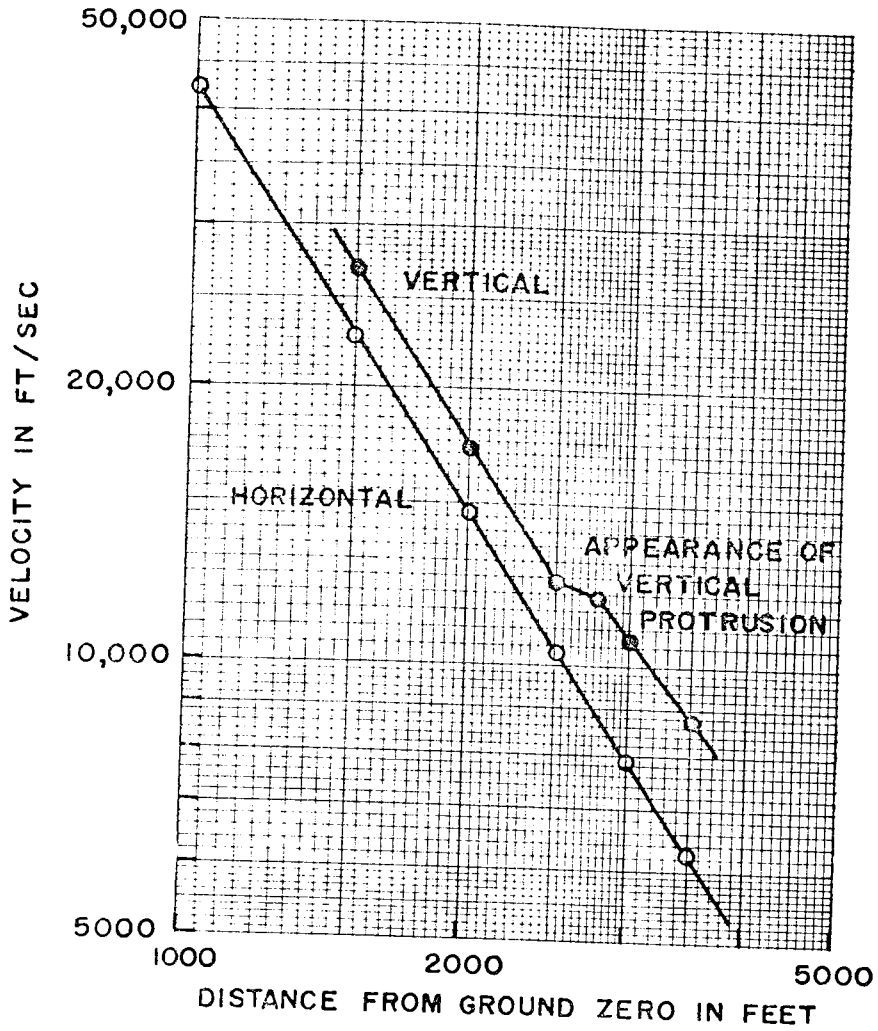

Fig. 3.18 Fireball Velocity vs Distance, Shot 4

in which the fireball was not visible in its entirety (Fig. 3.21) and the horizontal aiming angle of the camera was in doubt. Further, ground zero was below the horizon and the height of the camera above the ground was not accurately known. As a result the correction for the vertical data (the distance that ground zero was below the horizon) could only be approximated (~ 50 ft). The uncertainty in the ground zero position was large. The error could have been as large as 100 ft, which would be serious in the fireball region.

The vertical fireball growth was found to be greater than the horizontal. (This was observed on film 24,408). The west side of the fireball near the surface, as viewed from Yvonne Island, appeared flattened. The vertical protrusion appeared between 65 and 75 msec. The time of the beginning of the rupture of the protrusion was difficult to establish. Refer to Fig. 3.21.

The fireball arrival time data were fitted by equation 1.4 and the equations were found to be:

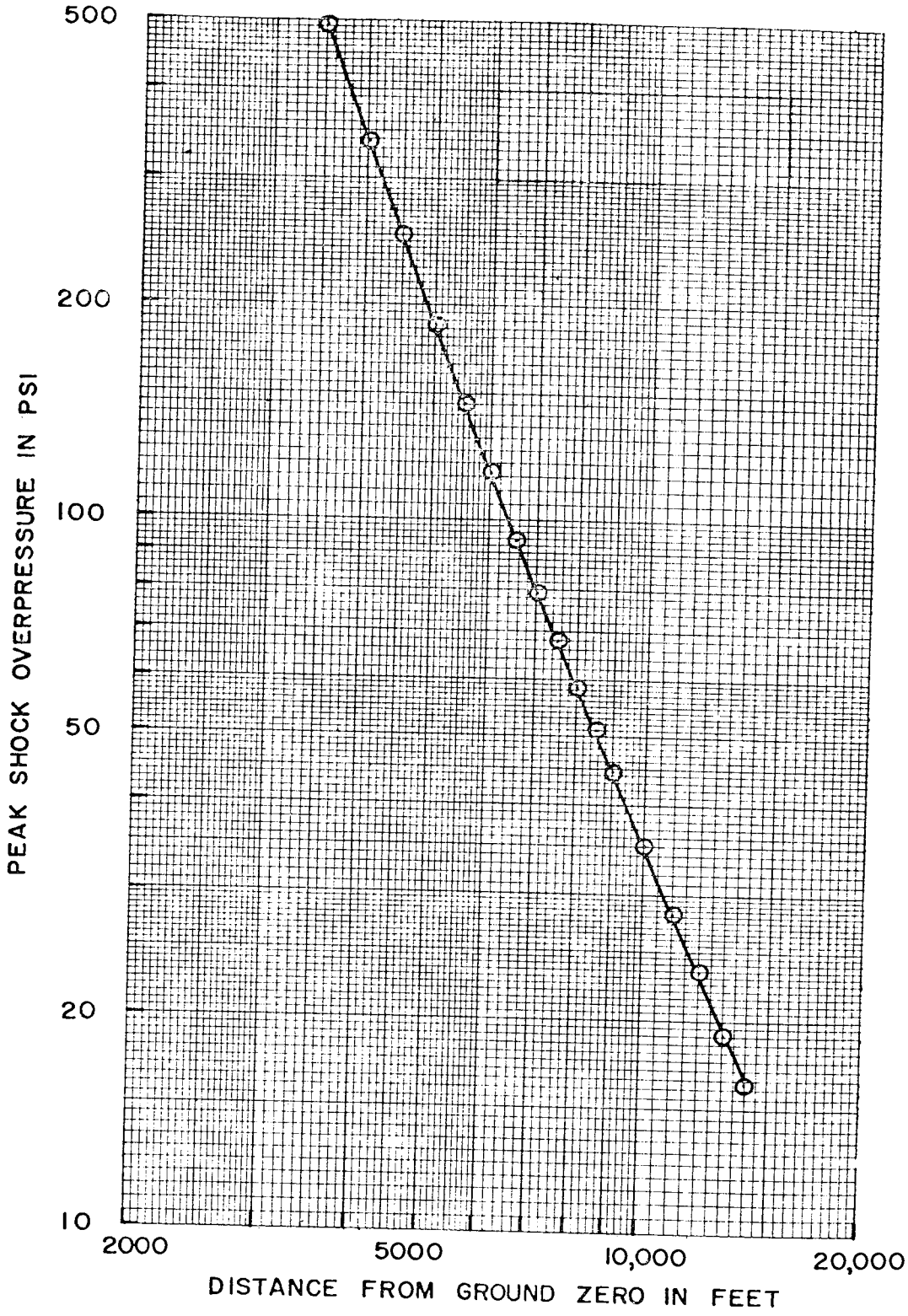

Fig. 3.19 Surface Peak Shock Overpressure vs Distance, Shot 4

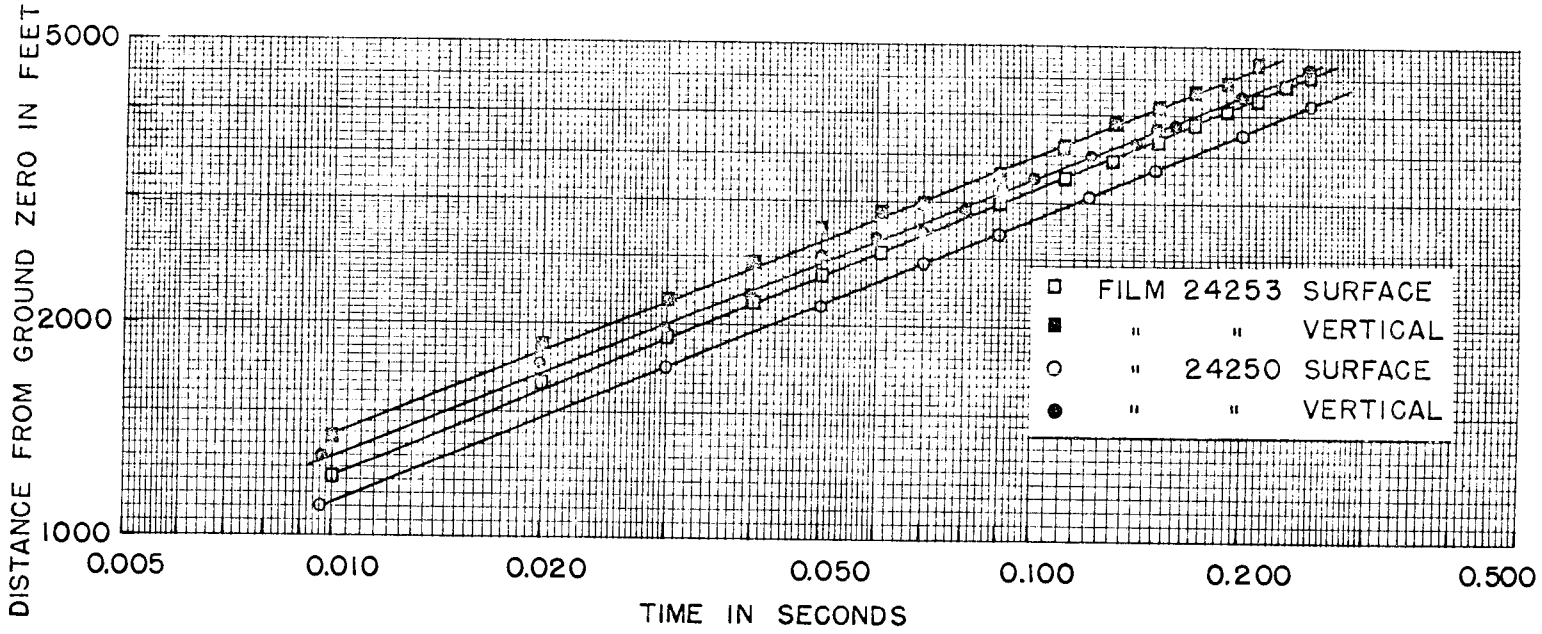

Fig. 3.20 Fireball Arrival Time Data, Shot 5

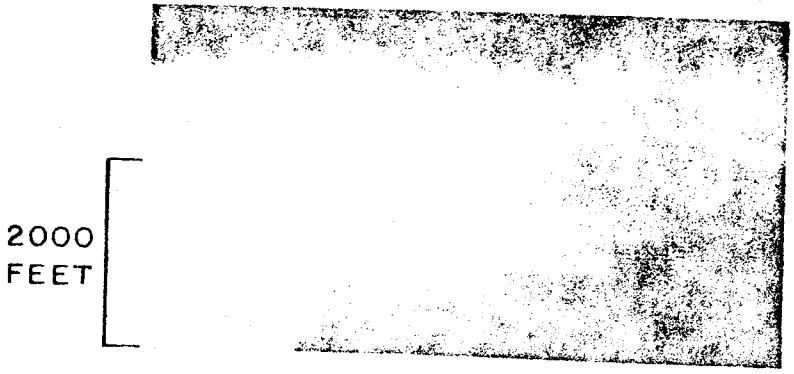

t = 0.0594 SEC

t = 0.1306 SEC

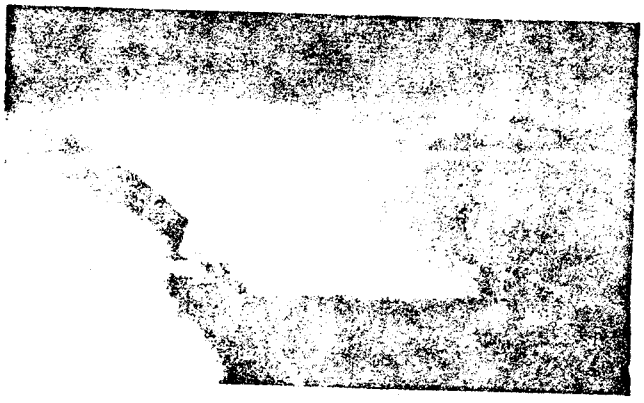

t = 0.2830 SEC

Fig. 3.21 Fireball Photographs Showing the Vertical Protrusion of Shot 6

TABLE 3.13 - Observed Arrival Time Data, Shot 6

Time (sec)	Distance From GZ (ft)	
	Surface	Vertical
0.0086	724	
0.0188	1026	
0.0289	1215	1245
0.0391	1349	1387
0.0492	1469	1525
0.0594	1573	1644
0.0696	1685	1742
0.0797	1780	1854
0.0899	1867	1933
0.1001	1955	2041
0.1102	2029	2137
0.1204	2091	2217
0.1407	2209	2371
0.1611	2305	2505
0.1814	2403	2643
0.2017	2501	
3.1194	9080	
3.1700	9170	
3.2205	9256	
3.2711	9336	
3.3216	9409	
3.3722	9499	
3.4227	9583	
3.4733	9660	
3.5239	9730	
3.5744	9815	
3.6250	9905	
3.6755	9970	
3.7260	10,062	
3.7767	10,132	
3.8272	10,212	
3.8778	10,289	
3.9283	10,365	
3.9789	10,440	
4.0294	10,522	
4.0800	10,594	
4.1306	10,670	
4.1811	10,749	
4.2317	10,818	
4.2822	10,895	
4.3328	10,972	
4.3833	11,040	
4.4238	11,093	

TABLE 3.14 - Arrival Time, Velocity and Peak Shock Overpressure, Shot 6

Distance From GZ (ft)	Arrival Time (sec) Surface	Vertical	Velocity (ft/sec) Surface	Peak Shock Overpressure (lb/in^2) Surface
1000	0.0174			
1500	0.0502	0.0471		
2000	0.1073	0.0956		
2500	0.1951	0.1596		
3000	0.3132		4059	201
*3500	0.4476		3439	140
*4000	0.6035		3006	103
*4500	0.7798		2689	78.7
*5000	0.9749		2450	61.7
*5500	1.1875		2264	50.8
*6000	1.4162		2115	42.0
*6500	1.6598		1995	35.6
*7000	1.9171		1896	30.2
*7500	2.1869		1813	26.7
*8000	2.4683		1743	23.4
9000	3.0622		1631	18.2
9500	3.3732		1585	16.4
10000	3.6925		1546	14.6
10500	4.0196		1511	13.1
11000	4.3539		1480	12.0

* Interpolated Data

Vertical	$r_v = 4830t^{0.383}$	$1250 \leq r_v \leq 1700$ (ft)
Vertical	$r_v = 5555t^{0.435}$	$1700 \leq r_v \leq 2500$ (ft)
Surface	$r_h = 4640t^{0.380}$	$1000 \leq r_h \leq 2500$ (ft)

The shock arrival time data were derived from film 24,478. The same uncertainties in the position of ground zero that existed in the data of film 24,477 are present in the data obtained from 24,478. These data however, cover the region from 9,000 ft to 11,000 ft and an error of 100 ft would not be serious. Time could not be expressed in absolute terms. The first frame of this record was assigned a time of 5 msec. The data derived from this film were obtained in late frames and the RMS variation in the film speeds was found to be 0.05 msec per frame. The maximum timing uncertainty would range from 20 msec for the earliest usable frame to 25 msec for the last usable frame.

The horizontal shock arrival time data were fitted by equation 1.6 and the constants were found to be:

$A = 1052 \quad B = 6041 \quad C = -16.1 \quad 2500 \leq r \leq 11{,}000$ (ft)

It should be noted that the fitted curve covers the dataless region. Arrival time data obtained from the preliminary version of reference (14) are shown with these data (both the interpolated and the observed data) in Fig. 3.23. The agreement is surprisingly good.

All observed and calculated arrival time data are presented in Tables 3.13 and 3.14. These data are shown in Figs. 3.22 and 3.23.

3.7.2 The Peak Shock Overpressure-Distance Data

As a result of the large uncertainties in the fireball region it was felt that the presentation of the fireball velocities would be unjustified. Shock breakaway was estimated to have occurred between 0.16 and 0.18 sec.

The following was obtained for the shock region:

$$U = 1052 \left[1+\left(\frac{6041}{r}\right)^{1.5}\right] \qquad 2500 \leq r \leq 11{,}000 \text{ (ft)} \qquad (3.11)$$

In the region extending from 9000 ft to 11,000 ft there were several points at which these data could be compared with other data given in the preliminary versions of references (13) and (14). The BRL data fell on both sides of the curve and the Sandia Corp. data were ~10 per cent lower.

The pressure-distance data are presented in Table 3.14 and Fig. 3.24.

3.8 SURFACE EFFECTS

No precursors were observed in the films. On all shots* what appeared to be a dense cloud of water was generated immediately behind the shock. It was particulary evident in the Project 1.1 films of Shots 2 and 4.

On Shot 4 the effect was clearly observed (see Fig. 3.25) to a distance of 6600 ft, which was the extent of the coverage of the Project 1.1 films. As a result of the low magnification of the Project 13.2 films the actual generation of the cloud was not visible at any time in these films. However, there were indications of the existance of the effect at much greater distances. What appeared to be the cloud after it had increased in height was visible in film 24,150. It is impossible to place a limit on the persistence of this effect on this shot. However, there are indications that the effect existed at a distance of the order of 20,000 ft (~ 10 psi region). On Shot 2 the effect was particulary well developed in one of the 1.1 films (24,578) which was not usable in the arrival time measurements. The effect was observed out to an estimated distance of 15,000 ft (~ 25 psi), which was the extent of the coverage of the film. On the Project 13.2 films of this shot there were indications of the cloud out to a distance of ~ 23,000 ft (~ 10 psi region).

* The surface over which the shock traveled was visible on Shots 4 and 5 only. On the other shots the water cloud was visible over the horizon.

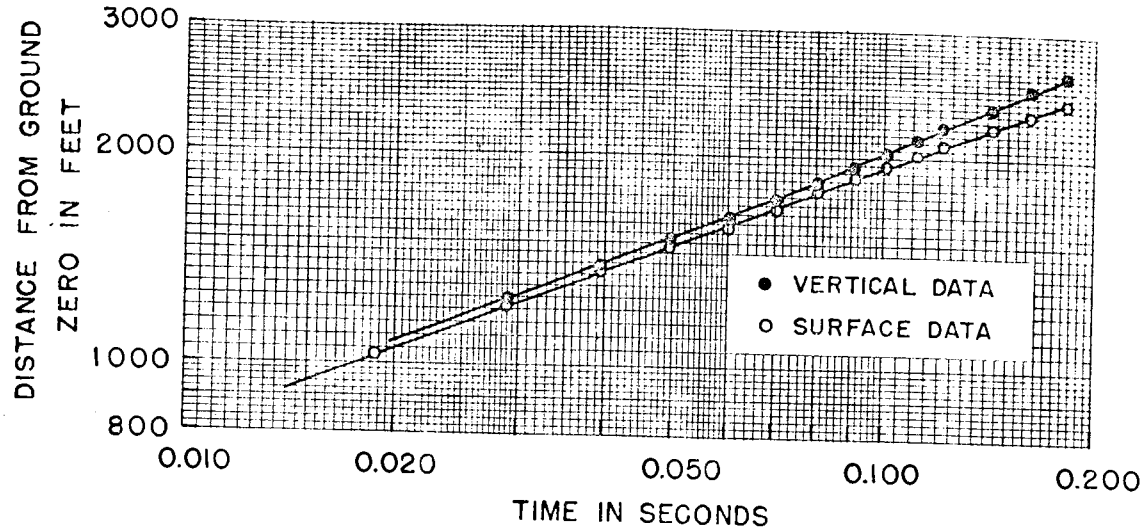

Fig. 3.22 Fireball Arrival Time Data, Shot 6

3.9 ACCURACY OF RESULTS

3.9.1 Sources of Error

There were a number of possible sources of error which were inherent in the photogrammetric method of measurement that was used to determine the arrival time data from which the peak shock overpressures were ultimately derived. They were grouped in three general categories:

1. Sources of Spatial Errors
   a. Reading Accuracy. This was dependent upon the static and dynamic resolutions of the system under actual conditions.
   b. The uncertainty of the position of ground zero in the plane of measurement.
   c. Scaling distances from the film. This was dependent upon the optical system, the camera aiming angles, the position of the camera with respect to ground zero, and the magnification of the device (Direct Projection Recordak) used for the measurement of the film.
2. Sources of Time Error
   a. The correlation of relative time to absolute time. This was dependent upon the accuracy of the early spatial measurements and the accuracy to which the frame rate could be determined.
3. Sources of Pressure Errors
   a. Uncertainties in the curve fitting. This was dependent upon the fitting function and the quality of the distance-time data.
   b. The uncertainty of atmospheric conditions ahead of the shock front.

Most of the error sources and procedures for calculating the errors may be found in reference (4). A thorough discussion of the fitting function may be found in references (7) and (8). The following discussion of spatial, timing, and peak shock overpressure accuracies applies chiefly to Shots 1, 2, and 4. Shot 5 was treated separately in Section 3.6 and Shot 6 was discussed in Section 3.7.1.

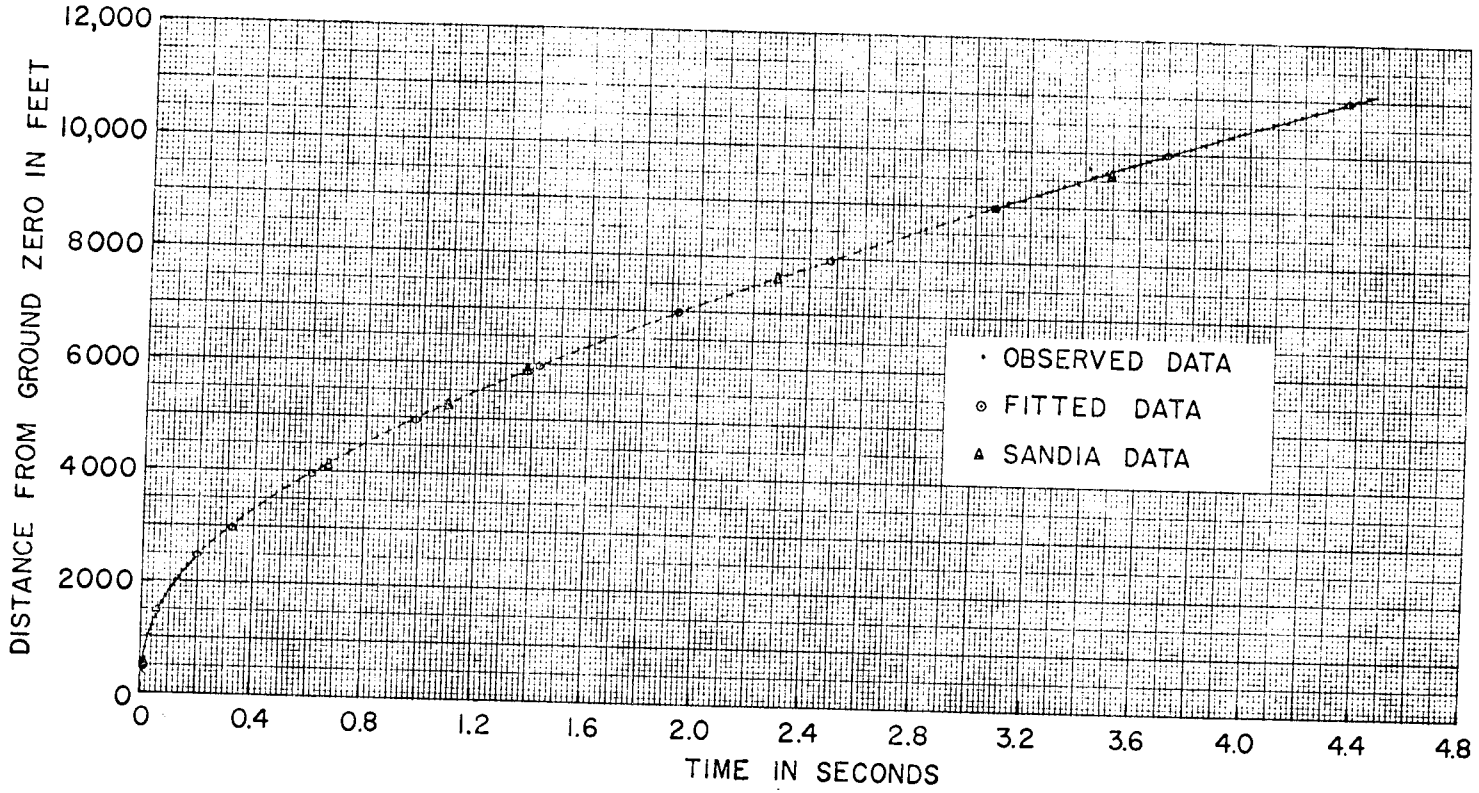

Fig. 3.23 Surface Shock Arrival Time Data, Shot 6

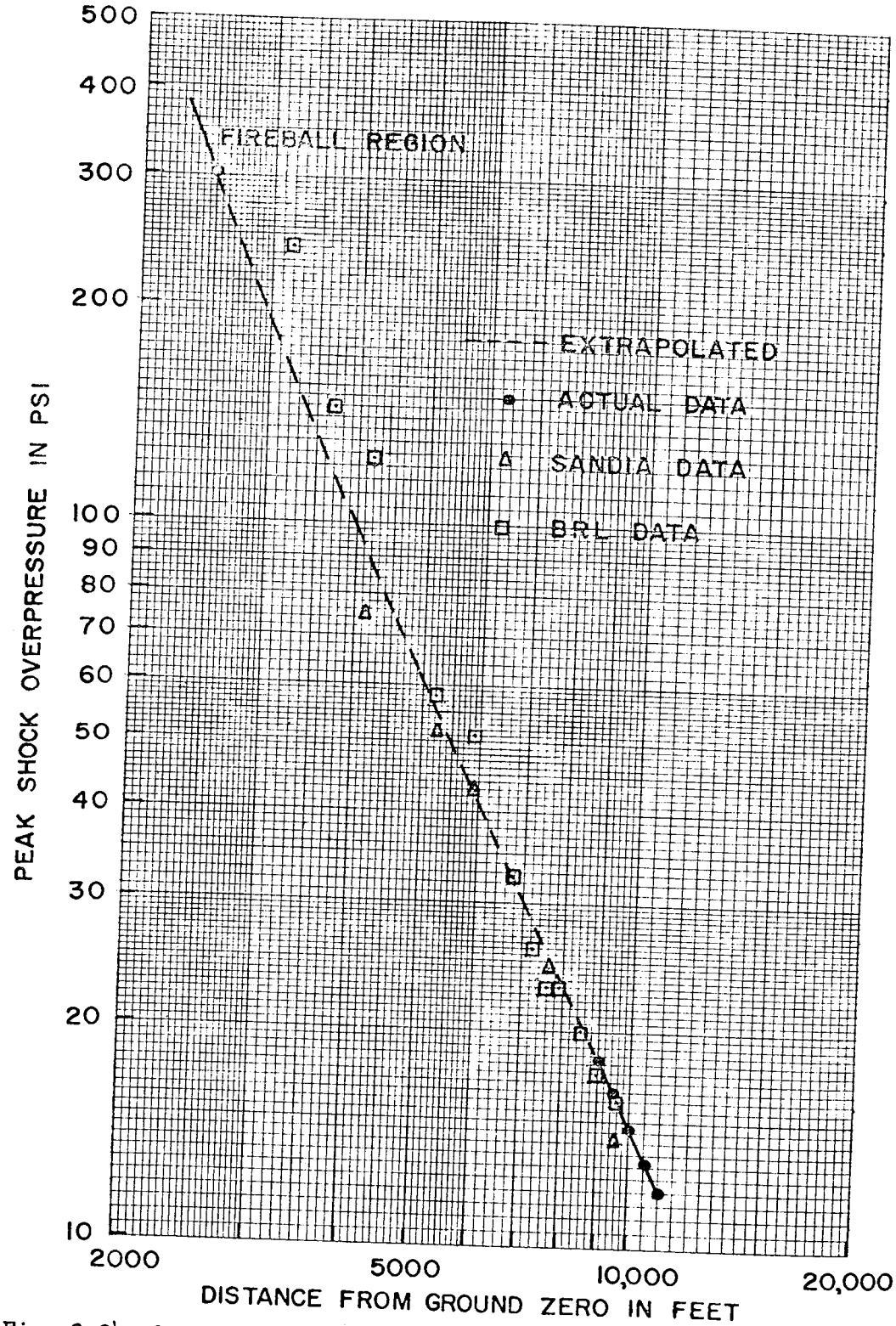

Fig. 3.24 Surface Peak Shock Overpressure vs Distance, Shot 6

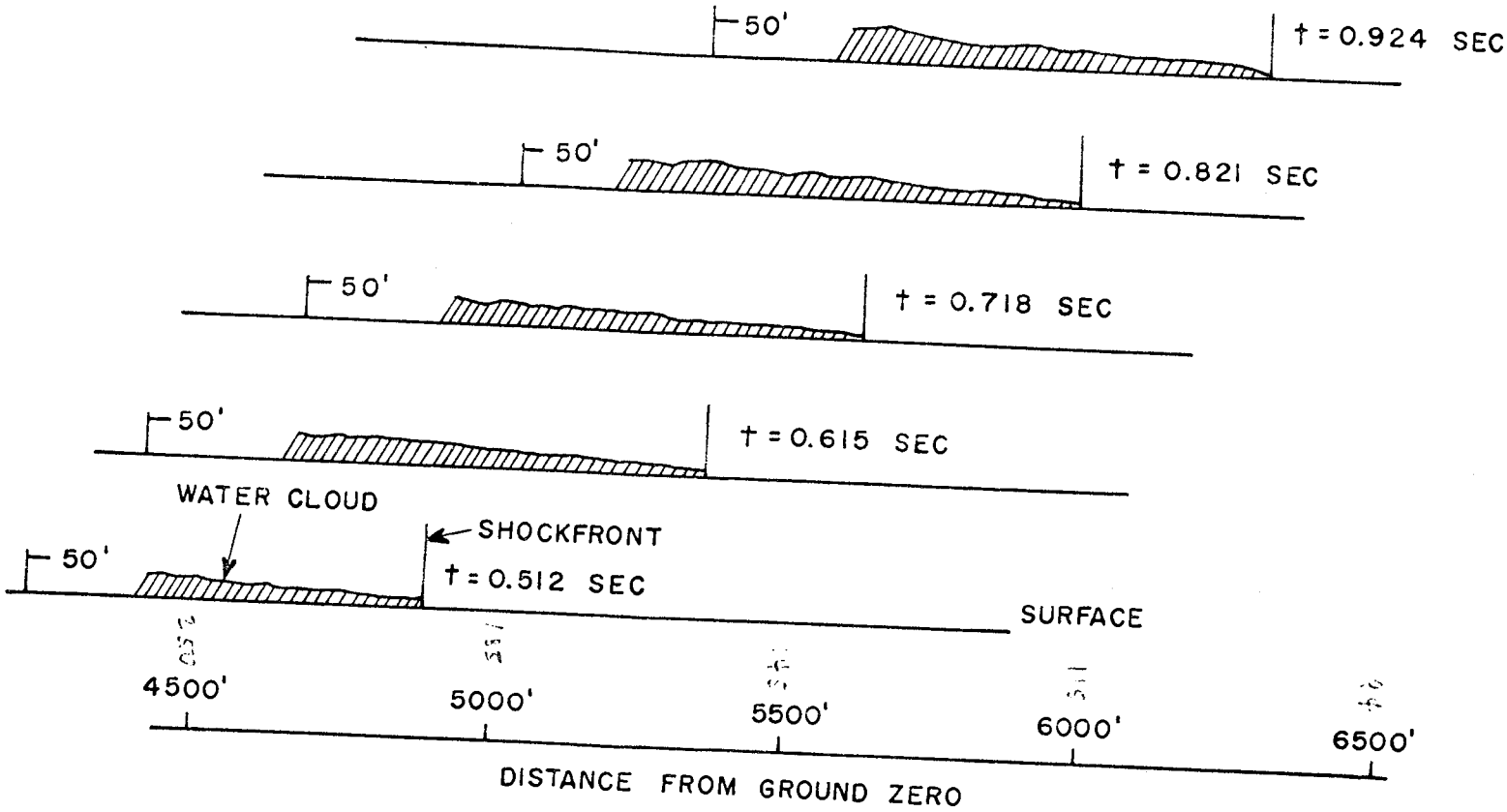

Fig. 3.25 The Growth of the Water Cloud Behind the Shock Front of Shot 4

3.9.2 Spatial Accuracy

Under ideal conditions the minimum spatial uncertainty of any film is limited by the static resolution, which is dependent upon the optical system of the camera,* and the dynamic resolution, which is a function of the shock velocity and the exposure time. The optimum static resolution of the lenses ranged from as high as 50 ft for the short focal lengths to 7 ft for the longer focal lengths. (See Table 2.3.) The dynamic resolution was significant in the early fireball region only. Maximum values of the order of 100 ft were obtained but these rapidly approached the actual static resolution. The effect was negligible after the first few frames of any record.

The conditions under which these films were obtained were not ideal. With few exceptions** the reduction of the records was difficult during and after shock breakaway because of low contrast brought about by the scattering of light in the humid atmosphere. As a result the stipulated static resolution of the lenses for ideal conditions cannot be stated as the correct lower limit. It is felt that the actual lower limit was at least twice*** the ideal static resolution.

The method used to establish ground zero was dependent upon the symmetrical growth of the fireball along the surface. A check was made for non-uniform growth along the surface. Fireball diameters obtained from films taken from different camera stations were compared for each shot.**** With the exception of Shot 5 no non-uniformity in the growth of the fireball along the surface was detected (see Section 3.6). However, it should be pointed out that the films (Project 13.2) available for this comparison were obtained through cameras using the short focal length lenses and that the optimum static resolution even in the fireball region was of the order of 50 ft. Further there was image spread and the possibility of small errors in the film copying to be considered (see Section 3.6). Consequently the possibility of non-uniform growth along the surface could not be completely excluded.

Once ground zero was located on either the primary or the 13.2 film, the position was determined with respect to either the sprocket holes or the vertical centerline***** for use in the subsequent frames or records in which the fireball was not usable for establishing ground zero. The maximum variation of the sprocket holes with respect to any

---

* In this case the resolving power of the film exceeds that of the lenses used.

** This was not true of the films obtained for Shot 4. The rocket trails were effective in alleviating these conditions. Parts of film 24,478 also were extremely clear.

*** This does not apply to the fireball region.

**** This was not possible on Shot 6.

***** The vertical centerline lies midway between the sprocket holes on any given frame. The principal optical axis of the lens very nearly intersects this line. The lens and camera combinations used to obtain the 1.1 films were calibrated so that the maximum deviation (in the films used) was 5 minutes of arc. Most of the deviations were 1 minute or less. Corrections were made for this deviation.

given frame center was less than 1 per cent. It was found that the position of ground zero as established in any fireball frame varied from 0.05 millimeter to 0.07 millimeter* with respect to the sprocket holes. This variation was negligible in the case of films obtained with cameras of long focal lengths but it led to uncertainties in the position of ground zero of the order of 150 ft to 200 ft in the later frames of the records obtained by the Project 13.2 cameras.

The uncertainty in the horizontal aiming angles of Shots 2, 4, and 6 led to large uncertainties in the position of ground zero in the planes of measurement of the subsequent films. This uncertainty was of the order to 50 ft in the subsequent films of Shots 2 and 4, and on Shot 6 it could have been as large as 100 ft.

The accuracy of scaling distance from the film was dependent upon the measurements of the focal length of the lens used and the distance from the camera to the object plane. The uncertainties in these measurements were known to be less than 0.1 per cent.

As a result of these considerations the maximum spatial uncertainty assigned to the horizontal distance data obtained from Project 1.1 records, beyond the fireball region, was 50 ft (Shots 2 and 4). The maximum uncertainty assigned to the horizontal data obtained from the Project 13.2 films was of the order of 200 ft.

The uncertainty of the vertical distance data obtained from film 24,554 was of the order of 400 ft. This was due to the extreme difficulty in observing the actual shock wave above ground zero.

3.9.3 Timing Accuracy

If the fireball arrival times contained in the tables are compared with those published by EG&G, a discrepancy in distance will be noted. The EG&G data were obtained by constructing the best fitting semi-circle about ground zero which intersected the fireball at several points. The NOL data were obtained along the surface (or along the vertical axis through ground zero) with no attempt made to average the resulting values. The primary records of Shots 1, 2, and 4** were used by EG&G in conjunction with other films in their analysis of the fireball data. Thus the time base used was the same as that used by EG&G. The frame times on these records were accurate to the nearest 0.01 msec.

The frame rates of the subsequent Project 1.1 films were determined through the timing marks on the films. In all cases the frame rates were found to be very nearly constant before and throughout the region of interest. On Shots 2 and 4 the times were correlated with those of the primary record in the regions of overlap. The agreement was good in all cases. The timing uncertainty ranged from minimum of 1 msec to a maximum of 10 msec.

The Project 13.2 films were placed in terms of absolute time by comparing distance data obtained in the fireball region to the primary records of Project 1.1. The resulting uncertainties were of

---

* The uncertainty introduced amounts to from 5 to 7 per cent of the magnification factor (see Table 2.3).

** Films 24,079, 24,575, and 24,180.

the order of 2 msec. There were no timing marks on the copies of the 13.2 films analyzed. The frame rates were given by EG&G. Figures were given for initial values and terminal values of the frame rate. The maximum difference in the time per frame between the initial and terminal points was found to be 0.1 msec. The uncertainty in time for the data obtained from these films ranges from a minimum of 2 msec to a maximum of approximately 50 msec at late times.

3.9.4 The Accuracy of Peak Shock Overpressures

The error introduced by the curve fitting was found to be slight. The standard deviation of the calculated distances from the observed distances was found to be 1 per cent or less. The maximum uncertainties of the resulting velocities obtained from the fitted data were found to be 1 per cent for the data obtained from the Project 1.1 films and 3 per cent for the data obtained from the Project 13.2 films.

The condition of the atmosphere into which the shock grew during the period of observation was not known. If the atmospheric conditions can be assumed to be the same as those reported by the weather survey then the accuracy of the pressure presented is limited only by the velocity uncertainties, which would lead to pressure uncertainties ranging from a minimum of 3 per cent to a maximum of 10 per cent. With the exception of the Shot 4 data, the probable maximum uncertainty of the pressure data derived from arrival time data obtained over water surfaces was of the order of 10 per cent. The Shot 4 data were somewhat better. The probable uncertainty was of the order of 7 per cent.

The portion of the Shot 2 data was obtained over a land surface. These data were felt to be high as discussed in Section 3.3.2. Pressure results from the Project 1.2b preliminary version of reference (13) bear out this contention.

3.9.5 The Accuracy of the Vertical Data of Shot 2

The determination of the position of the shock front in film 24,554 was extremely difficult. This difficulty resulted in large reading errors which could not be avoided. As a result the data were badly scattered.

These data were fitted by equation 1.6 and the standard deviation in terms of distance varied from 5 per cent at 10,000 ft to 2 per cent at 15,000 ft. The uncertainties in the velocities derived from the fitting function were found to range from 6 per cent at 10,000 ft to 3 per cent at 15,000 ft.

If the atmospheric conditions given by the weather survey were correct, the pressure uncertainties range from approximately 15 per cent at 10,000 ft to 10 per cent at 15,000 ft. Small errors in the meteorological data aloft would have serious results in the pressures. If the weather data were correct to 2 per cent the resulting pressure uncertainites would be of the order of 20 per cent at 10,000 ft and 15 per cent at 15,000 ft.

CHAPTER 4

DISCUSSION

4.1 SCALED RESULTS

All of the surface data, both arrival time and pressure data, were reduced to a yield of 1 KT at standard sea level conditions ($T = 20^{\circ}C$, $p_o = 14.7$ psi). For comparative purposes these data, together with the JANGLE Surface [15,16] and IVY Mike data,[17] were plotted with composite free air curves [8] scaled to 2 KT. The comparison to 2 KT assumed a reflection factor for blast of 2 for a surface shot. No yield based on radiochemistry has been assigned, so that this factor of 2 was used in determining the official yields, and hence no check of the factor was possible. Information relevant to the scaling of these data is given in Table 1.1.

4.1.1 Scaled Peak Shock Overpressure-Distance Data

The scaled peak shock overpressure-distance data of Shots 1, 2, 4, and 6 are given in Table 4.1. These data together with the JANGLE Surface [15] and the IVY Mike [17] data are shown in Fig. 4.1.

Excluding the land surface data of Shot 2, which was known to have been high, all of the data proved to be self-consistent within 5 per cent, which in the case of the CASTLE data was well within the stipulated maximum uncertainty (10 per cent). As compared to the free air composite curve scaled to 2 KT, the data of JANGLE, IVY, and CASTLE are approximately 10 to 15 per cent low in this pressure region ($\sim$500 psi to $\sim$10 psi). However considering the maximum uncertainty of both the experimental data ($\sim$10 per cent) and the free air composite ($\sim$5 per cent) the agreement is not unreasonable.

It would appear then that the use of these scaling laws for weapons of great yield in this region is justifiable. As was stated above, in spite of the reasonable agreement with the composite curve, scaled to 2 KT, these data did not demonstrate the validity of the assumption that the blast yield of a surface burst is effectively twice the free-air yield, because the methods used to determine the official yield are dependent upon this assumption.

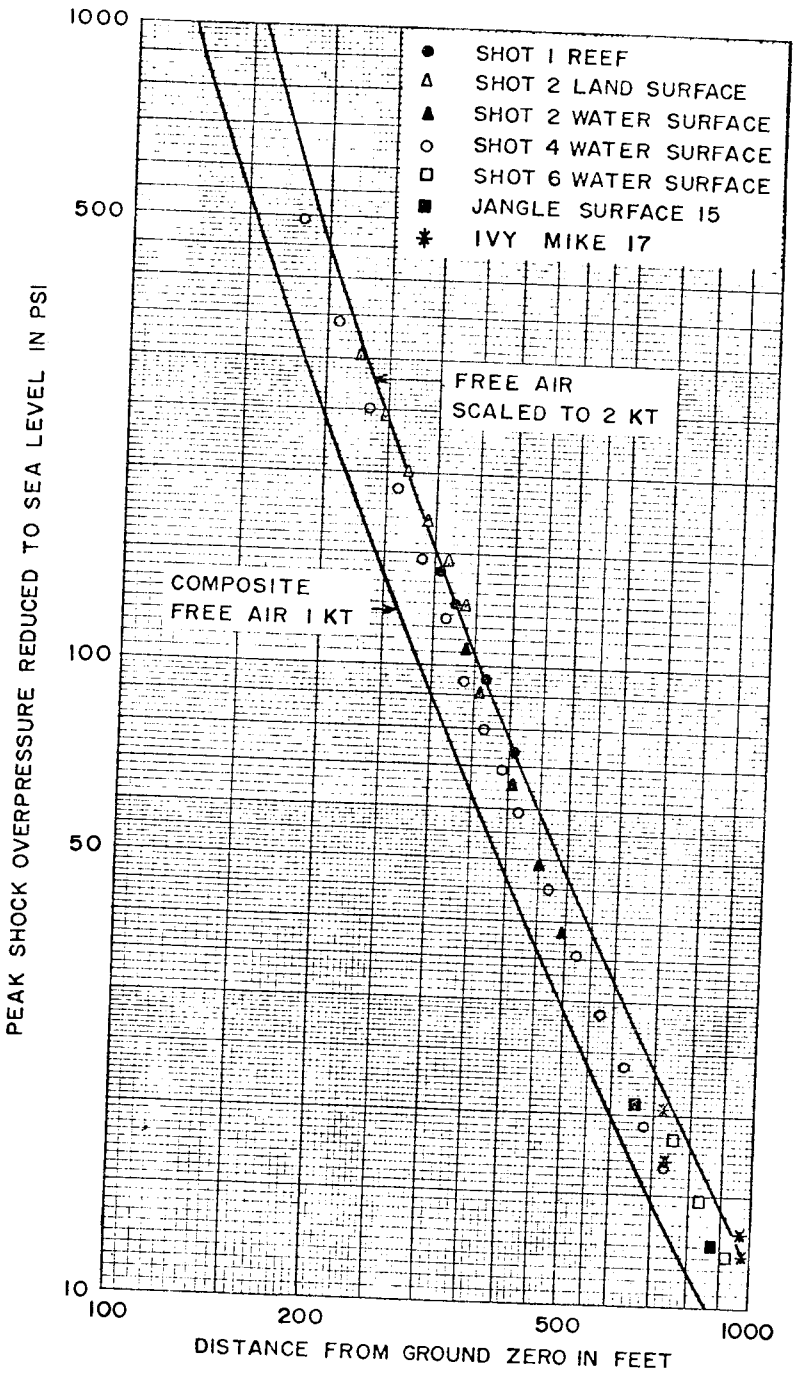

Fig. 4.1 Surface Pressure-Distance Data Scaled to 1 KT at Sea Level

4.1.2 The Scaled Arrival Time Data

Data given in reference (8) were used to derive the composite free-air arrival-time curve; they are shown in Table 4.2.

The scaled arrival time data for CASTLE are presented in Table 4.3 and are compared to the free air curve for 2 KT in Fig. 4.2. The scaled CASTLE general time data were self-consistent. The deviation of these data was of the order of 1 per cent or less. The scaled arrival time data varied from 1 to 3 per cent low as compared to the corresponding distances on the 2 KT curve. The JANGLE surface, with the exception of one point,16 / and the IVY Mike data that existed in the observed region compare favorably with the CASTLE data.

4.2 THE VERTICAL DATA OF SHOT 2

In Section 3.3 the vertical data obtained on Shot 2 were presented. Throughout this discussion the pressure-distance data obtained in the region extending from 10,000 to 15,000 ft will be referred to as the low-altitude data. Those data obtained in the 265,000 to 335,000 ft region will be referred to as the high-altitude data.

4.2.1 The Low-Altitude Data

The curves to which the experimental data were compared were obtained through the theory described in references (2) and (3).

In order to derive the theoretical vertical pressure-distance curve it was necessary to determine the radius of a TNT charge equivalent to Shot 2. Both the water surface data (Table 3.8) and preliminary data of Project 1.2a were used. The determination was made through the use of the modified Ledsham-Pike TNT data* given in reference (3). These data are expressed in terms of the dimensionless parameters:

$$Q = \frac{Ps}{P_o}, \quad X = \log \frac{r}{a}$$

Where:

Ps = the peak shock overpressure, psi
P_o = the standard atmospheric pressure, psi
r = distance from ground zero in the homogeneous medium along the surface (ft)
a = radius of an equivalent charge of TNT (ft)

The value of Q was easily determined from the experimental data and the corresponding X was found by interpolating in Table 1 of reference (3). The distance r was known and therefore a, the charge radius, could be determined.

---

* These data are based upon an ambient pressure of 14.7 psi and an ambient temperature of 288 K. The effect of the small difference between the standard temperature and the ambient temperature for Shot 2 could be neglected for the purposes of this comparison.

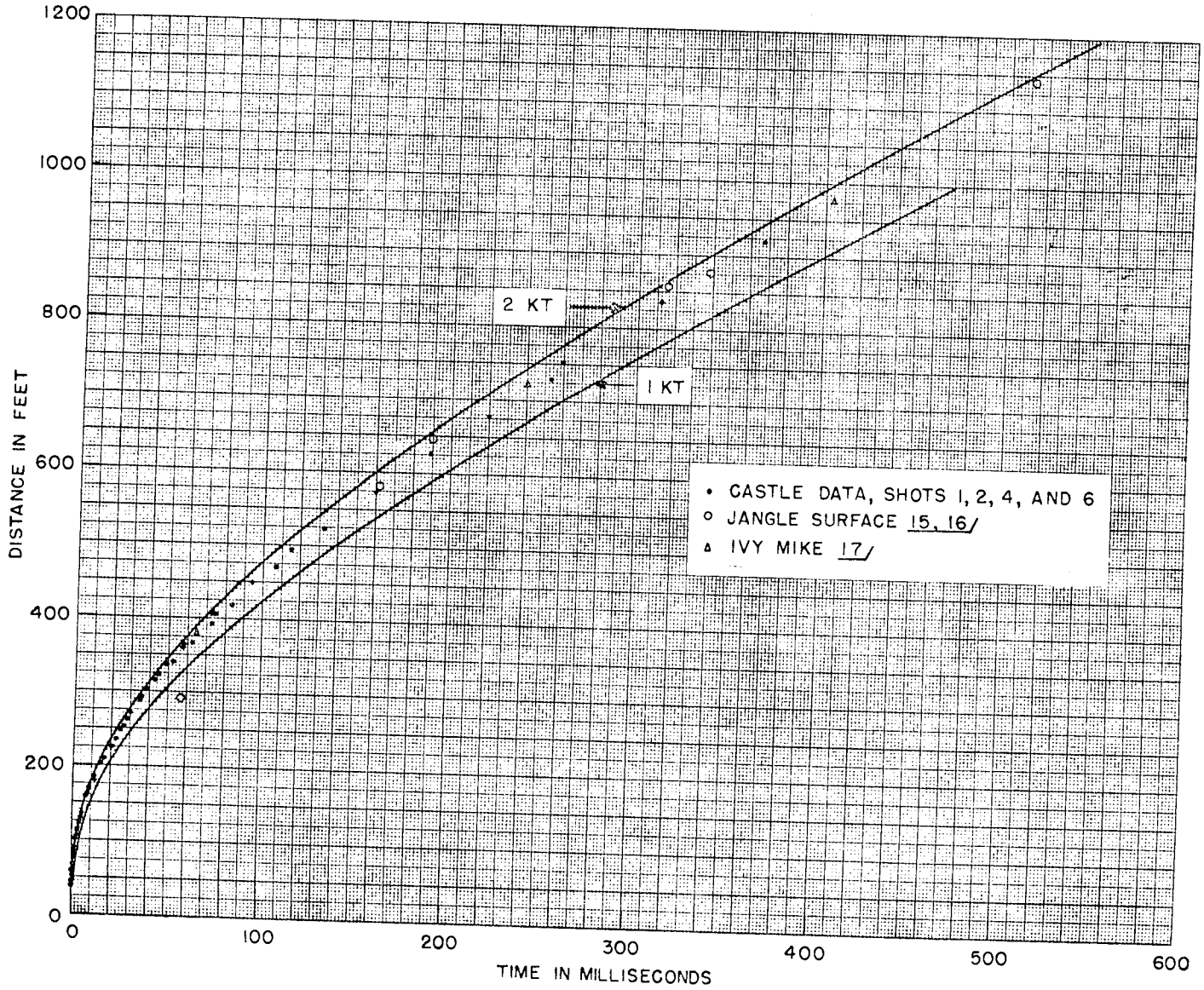

Fig. 4.2 Surface Arrival Time Data Scaled to 1 KT at Sea Level

The average charge radius obtained over the region encompassed by the water surface data (106 psi to 38 psi) was found to be 349 ft ± 3 ft; the average radius over the Sandia Corp. data (2.9 psi to 1.2 psi) was found to be 404 ft ± 11 ft. The arithmetic mean of these radii was 376 ft ± 26 ft. A similar computation was made for the Mike data* [17] (20 psi to 1.3 psi) and the average radius was found to be 387 ft ± 17 ft, which falls within boundaries established by the Shot 2 data and is in effective agreement with the Shot 2 average curve. (The resulting surface curves based on the theory are shown in Fig. 4.3.) Utilizing these equivalent charge radii, vertical pressure-distance curves were found after the methods of reference (3). These curves together with the vertical data of Shot 2 are shown in Fig. 4.4.

The uncertainty of the vertical experimental data was large,** but it should be noted that the predicted values fall within the stipulated experimental accuracy. Another result of the large experimental uncertainty was the inability to determine whether the vertical peak shock overpressures were greater or less than the surface pressures at corresponding distances.

In addition these data cannot be compared to the pressure data obtained aloft on IVY Mike,[18] which was a comparable shot. The CASTLE data were obtained vertically above ground zero whereas the IVY Mike measurements were made along shock radii.

4.2.2 The High-Altitude Data

On Shot 2, two wave fronts were observed between the altitudes of ~265,000 and ~335,000 ft.

The first wave front of the two visible wave fronts (section 3.3.1, Figs. 3.9 and 3.10) was in all probability the shock wave. This contention was checked by approximating the arrival time of the shock wave at the lower level of the data. The arrival time of the shock at 100,000 ft was determined through the low-altitude data and theory.[2,3] Beyond this distance, the shock velocity was assumed sonic and sound velocities obtained from the NACA standard atmospheric data [19] were used. It was found that the observed arrival time and the approximated value agreed within 5 per cent, which was less than the spatial uncertainty.

It will be noticed that the slope of the arrival time curve (Fig. 3.9) of the first wave increases slightly with altitude, which would indicate that the velocity was increasing with distance. (The velocity of sound increases with altitude [20,21] in this region but not as much as the curve indicates.) However, in light of the large spatial uncertainties this was ignored and the data were fitted by a straight line. From this, the average velocity was found to be 1470 ft/sec. Measurements made by EG&G in the same region indicated an aver-

---

* The yield of Mike was given as 10.5 MT; that of Shot 2 was given as 11 MT.

** The uncertainty ranges from 20 per cent at 10,000 ft to 15 per cent at 15,000 ft. Refer to section 3.9.5.

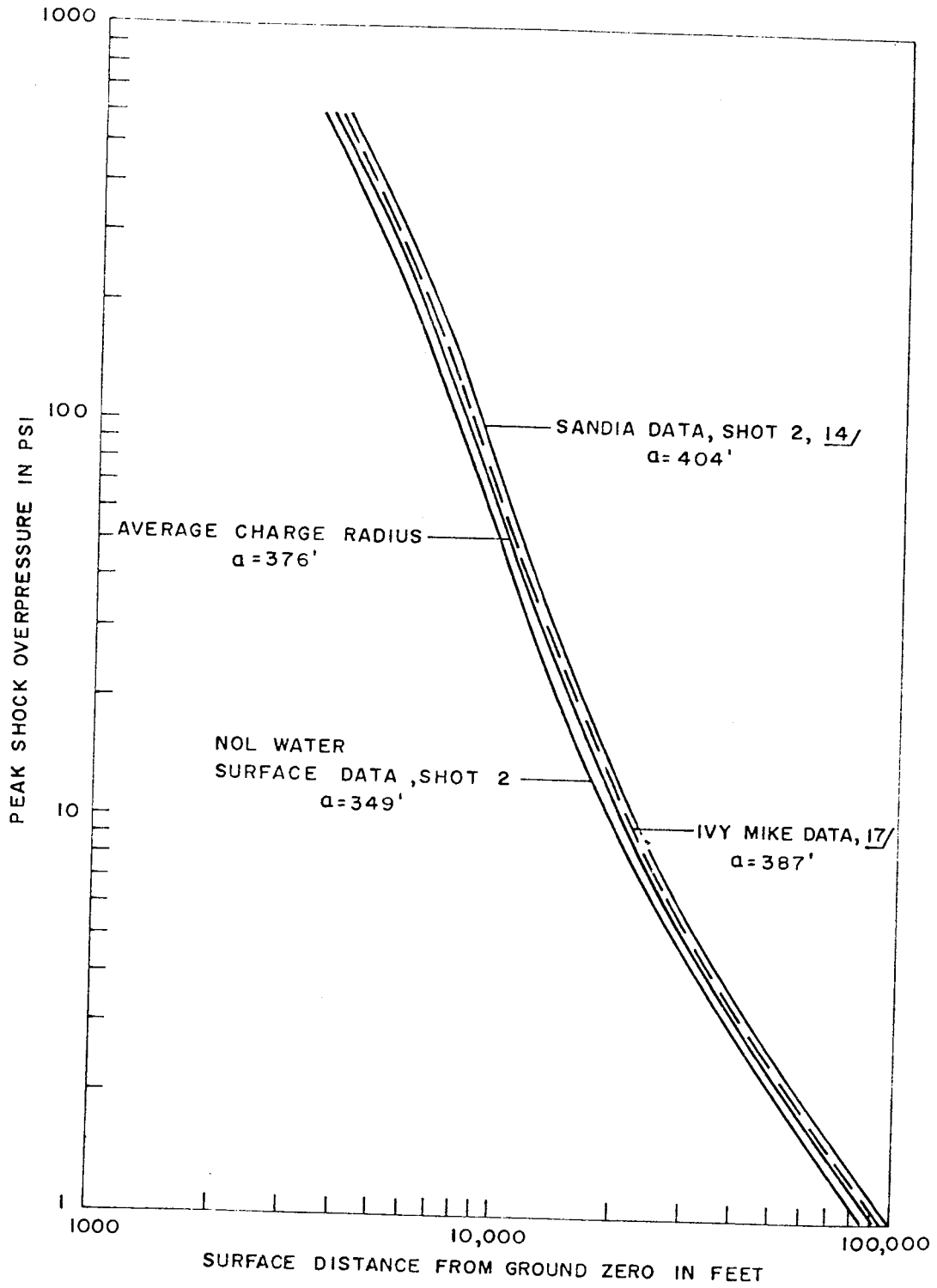

Fig. 4.3 Theoretical Surface Curves Derived from Shot 2 and IVY Mike Data

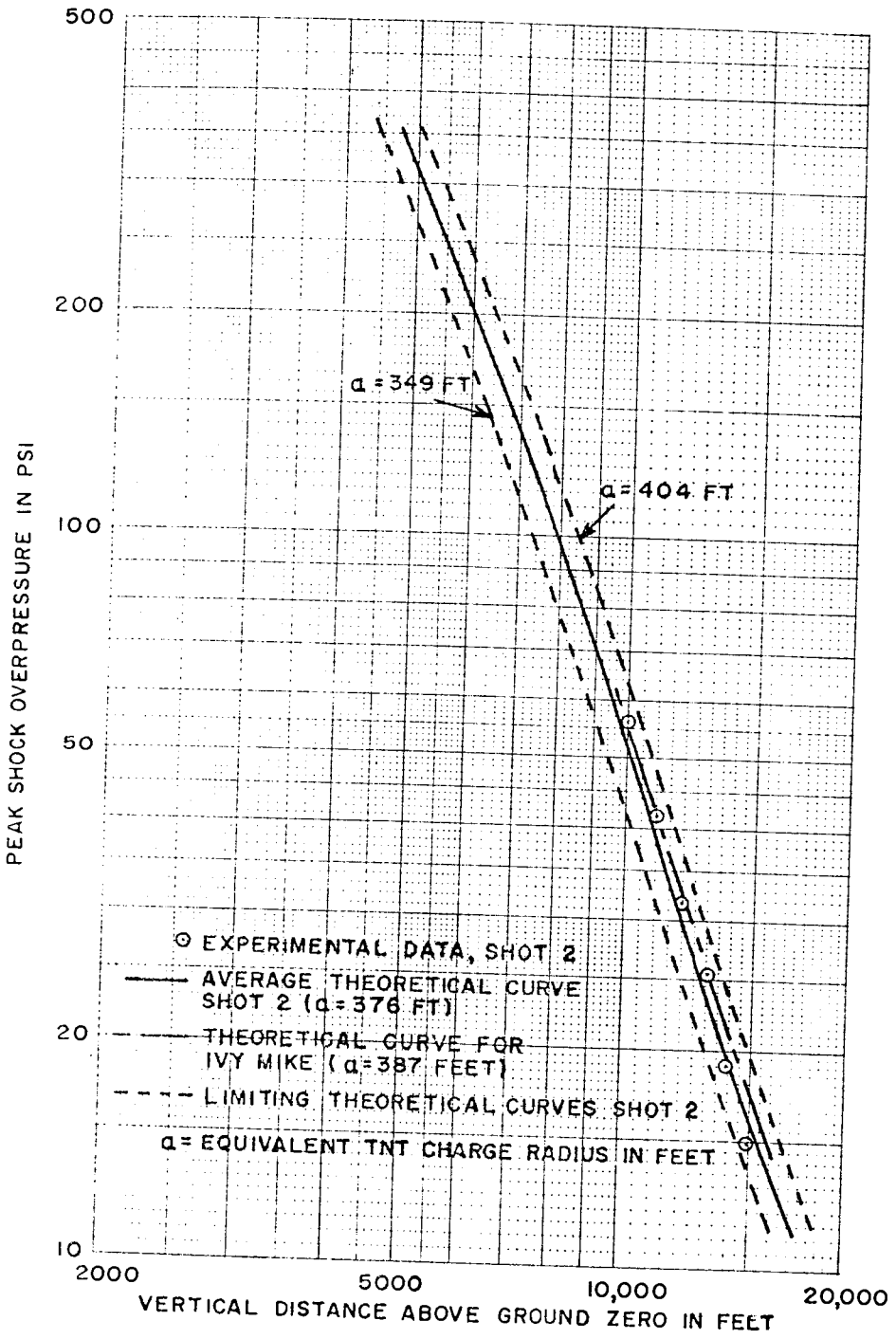

Fig. 4.4 Vertical Pressure-Distance Data of Shot 2 Shown with Curves Predicted from NOL Theory

TABLE 4.1 - Scaled Pressure-Distance Data

Distance From GZ (ft)	Shot 1		Shot 2				Shot 4		Shot 6	
	Water Surface		Land Surface		Water Surface		Water Surface		Water Surface	
	Distance (ft) S_d=0.0405	Pressure (psi) S_p=1.008	Distance (ft) S_d=0.0450	Pressure (psi) S_p=1.001	Distance (ft) S_d=0.0450	Pressure (psi) S_p=1.001	Distance (ft) S_d=0.0522	Pressure (psi) S_p=1.006	Distance (ft) S_d=0.0836	Pressure (psi) S_p=1.007
3500							183	497		
4000							209	342		
4500							235	252		
5000			225	304			261	189		
5500			247	245			287	147		
6000			270	201			313	118		
6500			292	170			339	94.7		
7000			315	144			365	79.9		
7500	303	141	337	125	337	106	391	68.6		
8000	324	125			360	91.1	417	59.0		
9000	364	95.3			405	65.5	470	44.9	752	18.4
10000	405	73.6			450	48.8	522	35.4	836	14.7
11000					494	38.3	574	28.5	920	12.1
12000							626	23.6		
13000							678	19.2		
14000							730	16.5		

TABLE 4.2 - Composite Free Air Arrival Time Data For 1 KT

Scaled Distance (ft)	Scaled Time (sec)
125	0.0063
150	0.0098
175	0.0142
200	0.0194
225	0.0253
250	0.0321
275	0.0400
300	0.0486
325	0.0579
350	0.0679
375	0.0786
400	0.0898
450	0.1138
500	0.1398
550	0.1676
600	0.1969
650	0.2276
700	0.2595
750	0.2925
800	0.3264
850	0.3613
900	0.3970
950	0.4333
1000	0.4703

age velocity of 1180 ft/sec.* The difference between the two velocities was large but not unreasonable (refer to 3.3.1). At these altitudes, it would seem reasonable to believe that the shock velocity would be very nearly sonic. As compared to the sonic velocities shown in reference (20) and those computed from the data given in (21), the EG&G data would seem the more reasonable, although both appear high. (Using these velocities to approximate** over-pressures

* The velocities obtained by EG&G have not yet been published. These data were obtained from Lewis Fussell of EG&G.

** Up to roughly 80 km the composition of the air is virtually unchanged, but beyond this point the composition does change; consequently beyond 80 km the Rankine-Hugoniot relation for pressure can serve as an approximation only. Data from (20) and (21) were used in the approximation.

TABLE 4.3 - Arrival Time Data Scaled to 1 KT at Sea Level

Distance From $\overline{GZ}$ (ft)	Shot 1		Shot 2				Shot 4		Shot 6	
			Water Surface		Land Surface					
	Scaled Distance (ft) S_d= 0.0405	Scaled Time (sec) S_t= 0.0409	Scaled Distance (ft) S_d= 0.0450	Scaled Time (sec) S_t= 0.0455	Scaled Distance (ft) S_d= 0.0450	Scaled Time (sec) S_t= 0.0455	Scaled Distance (ft) S_d= 0.0522	Scaled Time (sec) S_t= 0.0528	Scaled Distance (ft) S_d= 0.0836	Scaled Time (sec) S_t= 0.0845
1000	40.5	0.0002	45.0	0.0003						
1500	60.7	0.0006	67.4	0.0009			52.2	0.0005	83.6	0.0014
2000	80.9	0.0013	89.9	0.0019			78.3	0.0014	125	0.0042
2500	101	0.0024	112	0.0034			104	0.0028	167	0.0091
3000	121	0.0039	135	0.0055			130	0.0050	209	0.0165
3500			157	0.0082			157	0.0080	251	0.0265
4000	162	0.0082	180	0.0116			183	0.0118		
4500	182	0.0110	202	0.0159			209	0.0168		
5000	202	0.0149					235	0.0223		
5500					225	0.0201	261	0.0287		
6000					247	0.0250	287	0.0358		
6500					270	0.0304	313	0.0437		
7000					292	0.0363	339	0.0525		
7500	303	0.0388	337	0.0496	315	0.0426	365	0.0624		
8000	324	0.0448	360	0.0574	337	0.0493	391	0.0724		
9000	364	0.0582	405	0.0745			417	0.0832		
10000	405	0.0731	450	0.0937			470	0.1064	752	0.2591
11000			494	0.1150			522	0.1320	836	0.3120
12000							574	0.1596	920	0.3679
13000							626	0.1890		
14000							678	0.2201		
							730	0.2528		

leads to pressures * that are of the same order of magnitude as the ambient atmospheric pressure.)

The origin of the second wave is unknown but there is evidence which indicates that it was an acoustic wave. It was not possible to make usable measurements of the second wave on the copy of film 24,562. However, EG&G was able to make measurements on the original that led to an average velocity of 1010 ft/sec, which was reasonable as compared to sonic velocity over this region. Further arrival time measurements ** made of Elmer Island showed the existence of an acoustic wave that arrived approximately 100 sec after the first wave, which could well have been the second wave, for if it were assumed that both waves were moving at very nearly sonic velocity (the excessive velocity of the first wave aloft can be accounted for by the large spatial uncertainties) then the spacing of the two waves in terms of time, as estimated from the film copy, was of the same order of magnitude.

4.3 SURFACE EFFECTS

On Shots 4 and 5 a number of anomalies in the wave forms were described in the preliminary version of reference (22) and it was found that the dynamic and stagnation pressures were higher than those calculated from the overpressures. These anomalies were believed to have been caused by water droplets and/or dust particles carried by the shock wave. The observations made in the films of Shots 4 and 5 indicated that the dense water cloud was present in this region which would account for the presence of water droplets.

The generation of this water cloud is believed to be the result of the interaction of the shock and the rough water surface.

The appearance of this effect, which apparently contributed to the anomalous results obtained on Shots 4 and 5, indicates that water does not constitute as ideal a surface as was presupposed.

---

* The approximate average overpressure at 265,000 ft was found to be $(1.4 \pm 0.6)\ 10^{-4}$ psi; at 330,000 ft the average overpressure was $(6 \pm 4)\ 10^{-6}$ psi (ambient pressures were $\sim 7.25 \times 10^{-4}$ psi and $\sim 72.5 \times 10^{-6}$ psi respectively).

** The following observations were made on Fred Island, ~1,041,000 ft from $\overline{GZ}$:

1. + 17 min 55 sec Two sharp reports, close together but resolvable.
2. + 19 min 35 sec A single report of slightly greater duration.

CHAPTER 5

CONCLUSIONS AND RECOMMENDATIONS

5.1 INSTRUMENTATION

5.1.1 Photography 1.1a and 1.1b

The photographic instrumentation for Projects 1.1a and 1.1b was generally successful; however, the analysis would have been simplified if fiducial markers had been used. It would also have been useful to have cameras equipped with lenses of sufficiently long focal lengths at different stations to detect possible asymmetric shock growth along the surface.

5.1.2 Photography 1.1d

The photography of Project 1.1d was unsuccessful. The conditions under which these films were obtained were generally poor: viz., the extreme range at which the aircraft had to operate and the obscuration of the field of view by clouds. However, it is felt that if aerial photography is to be used again for studying blast waves from weapons of great yields, wide latitude film should be used.

5.1.3 Smoke Rockets

The smoke rockets proved to be of great value on Shot 4. There is, however, one change that should be made if similar tests of large weapons are to be made in the future. The rocket battery should be moved, keeping the same plane of fire, to a greater distance from $\overline{GZ}$ in order to increase the coverage.*

* No artificial background is needed in the early shock stages.

5.2 EXPERIMENTAL RESULTS

5.2.1 The Surface Pressure-Distance Data

No asymmetry greater than 200 ft was detected in the growth of the shock waves along the surface.

The surface pressure-distance data obtained have a maximum uncertainty of 10 per cent with the exception of the land data of Shot 2.

The use of the cube root law for scaling blast from yields ranging from 1.7 to 15 MT in the 10 to 500 psi region gave rise to results that were self-consistent and well within the experimental accuracy of the data. As compared to the free air composite curves scaled to 2 KT the reduced data were generally 10 to 15 per cent low in this pressure region, but the uncertainty of both the composite data (5 per cent) and the experimental data (10 per cent) should be considered.

5.2.2 The Vertical Data of Shot 2

The vertical data of Shot 2 were not of sufficient accuracy to be used to confirm or deny the NOL theory of the effect of a non-homogeneous atmosphere on blast. The pressures predicted through the theory fell within the stipulated experimental accuracy of the data. Inasmuch as the data did not confirm or deny the theory further investigation should be made.

The first of the two wave fronts observed at very great altitudes ($\sim$265,000 to $\sim$335,000 ft) was probably the shock wave. The origin of the second wave is unknown, but it was presumed to be an acoustic wave. A further theoretical investigation of the second wave should be made.

5.2.3 Surface Effects

No precursors were observed in the films.

A dense cloud of water, believed to have been the result of the interaction of the shock and the rough water surface, was developed immediately behind the shock. This effect seemed to confirm the existence of water droplets which was postulated by Sandia Corp. as one of the causes for the anomalies observed in the wave forms and dynamic pressures.

It would appear that a water surface does not constitute as ideal a surface as was presupposed.

APPENDIX A

DETERMINATION OF THE HORIZONTAL AIMING ANGLES

A.1.1 SHOT 2

The horizontal aiming angles of the cameras were not as specified in the photographic instrumentation plan (Table 2.3).

The horizontal aiming angle of the primary camera was found as follows: The line midway between the sides of the frame or midway between the inner edges of the two rows of sprocket holes (either basis could be used) was drawn on the drawing and was used as a vertical centerline of the frame. The optical axis was assumed to pass through the center of this line. Ground zero was identified on the drawing, and the distance from $\overline{GZ}$ to the vertical centerline on the drawing was measured. Dividing this distance by the magnification of the Recordak gave the corresponding distance on the film ($\overline{GZ}'\ P_1'$ in the plan view of Fig. A.1).

The horizontal aiming angle is then given by

$$\phi = \tan^{-1}\left(\frac{\overline{GZ}'P_1'}{JP_1'}\right)$$

$$= \tan^{-1}\left[\frac{\overline{GZ}'P_1'}{\left(\frac{JM_1'}{\cos\theta_1}\right)}\right]$$

where $JM_1' = f_1$

= the (known) effective focal length of the primary camera

and θ_1 = the (known) vertical aiming angle of the primary camera

In order to find the horizontal aiming angles of the two subsequent cameras, the point at which a bolt of lightning, visible in all three films, interesected the horizon was used as a fiducial marker.

The distance from the point where the marker appeared in the primary record to the vertical centerline was measured on the

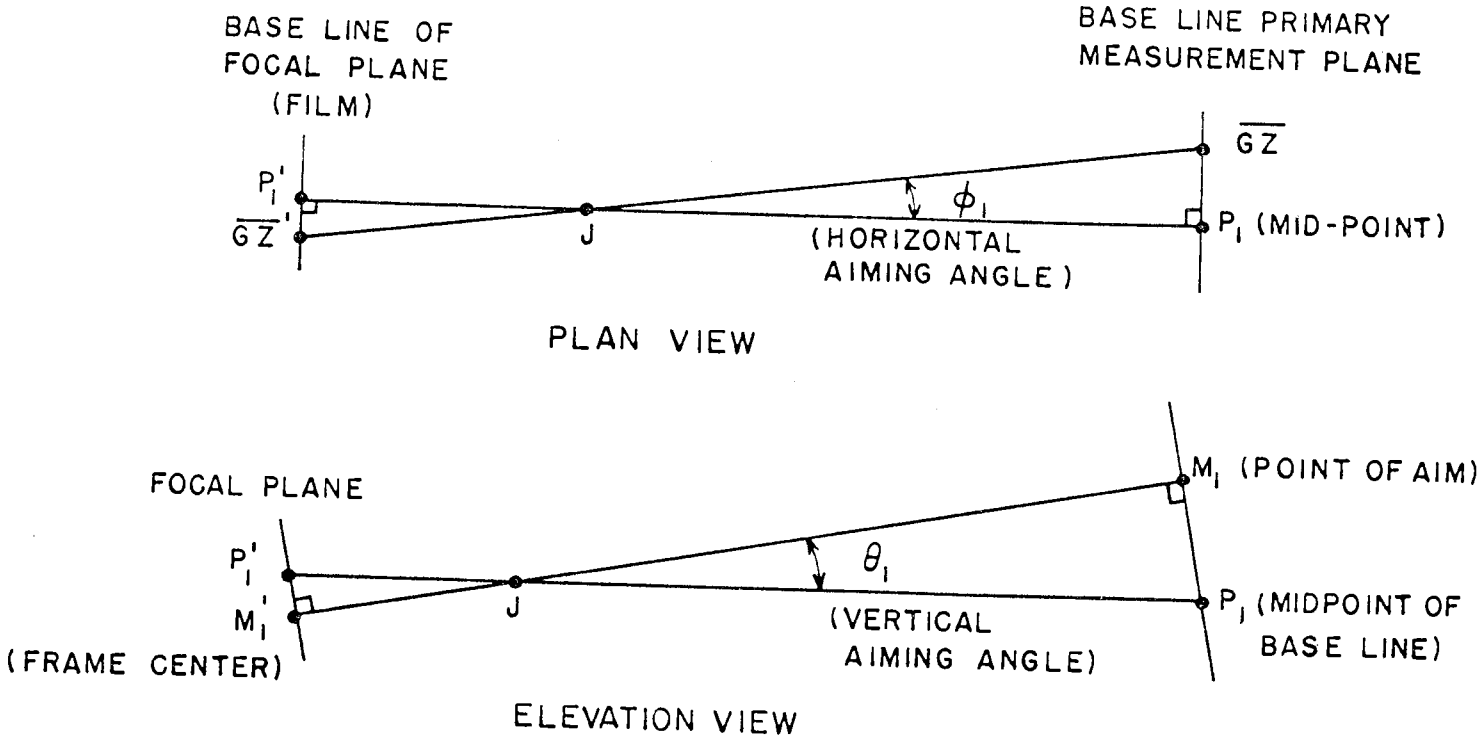

A.1 Plan and Elevation Views of the Geometry of the Optical Axis of the Primary Camera

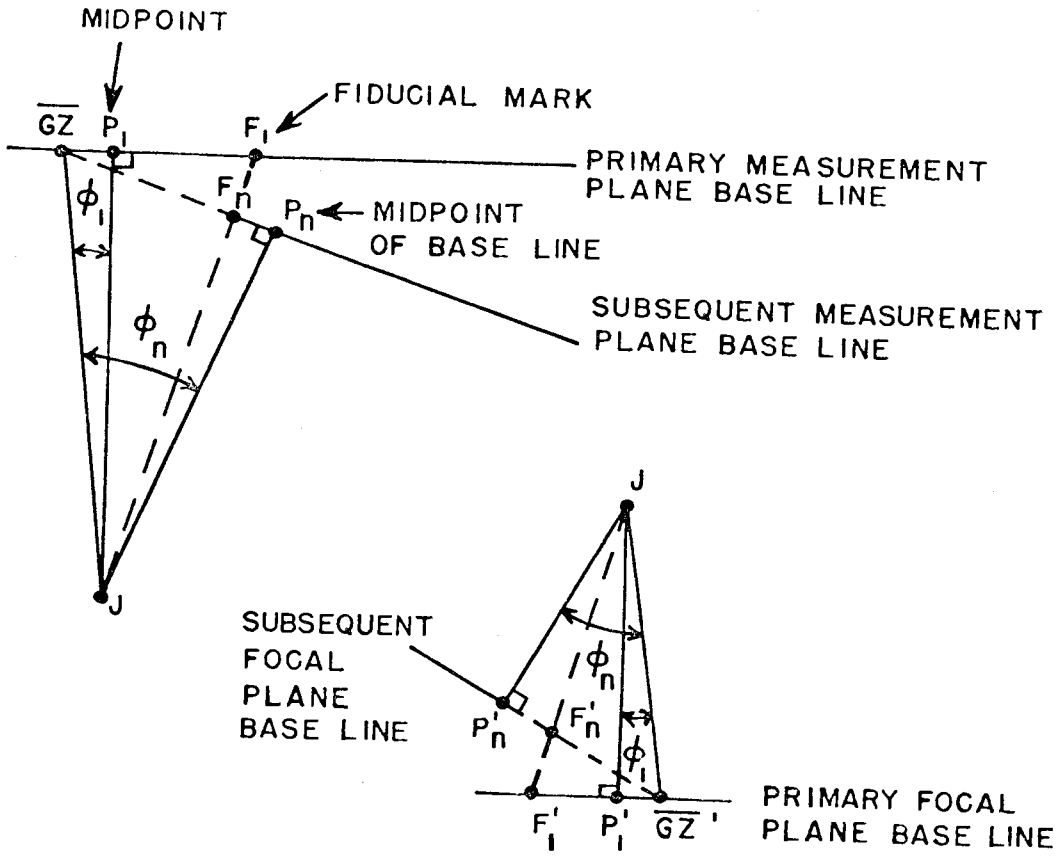

A.2 Use of a Fiducial Marker of Unknown Location

drawing. Dividing this distance by the magnification of the Recordak gave the corresponding distance on the film ($F_1'P_1'$ in Fig. A.2).

$$\text{Then } \measuredangle F_1'JP_1' = \tan^{-1}\left(\frac{F_1'P_1'}{JP_1'}\right)$$

$$= \tan^{-1}\left[\frac{F_1'P_1'}{\left(\frac{JM_1'}{\cos\theta_1}\right)}\right]$$

The distance from the point where the marker appeared in the subsequent record to the vertical centerline was measured on the drawing. Dividing this distance by the magnification of the Recordak gave the corresponding distance on the film ($F_n'P_n'$).

$$\text{Then } \measuredangle P_n'JF_n' = \tan^{-1}\left(\frac{F_n'P_n'}{JP_n'}\right)$$

$$= \tan^{-1}\left[\frac{F_n'P_n'}{\left(\frac{JM_n'}{\cos\theta_n}\right)}\right]$$

$$\text{and } \phi_n = \phi_1 + \measuredangle F_1'JP_1' + \measuredangle P_n'JF_n'$$

A.1.2 SHOT 4

On Shot 4 there was nothing that could be used as a fiducial marker, but the magnification factors of the three films used were known to be very nearly equal.

The horizontal aiming angles were corrected as follows:

The aiming angle of the primary camera was determined in the manner described in the previous section.

Tracings of the fireball from successive frames of the primary record were made on a single sheet of paper. The tracing line and the horizon coincided with those of the previous frames. The portions of the fireball visible in the subsequent record were then projected (at the same magnification) upon the series of tracings obtained from the primary record. The projection of any given frame of the subsequent record was aligned vertically with the tracing (the horizons were made to coincide). Horizontal alignment was attained by moving the projection along the horizon until it appeared to be in the proper position with respect to the tracings. Deformations in the fireball and rocket* trails were used as guides. Once the best position was found, the visible section of the fireball was traced and the position of the left reference** of the subsequent film was marked on the primary tracing. This procedure was carried out through the entire region of overlap between the primary record and the subsequent record in question. The position of the left reference was then approximately known with respect to $\overline{GZ}$ as established in the tracings of the primary record and the approximate horizontal aiming angle of the subsequent camera could be computed. (Refer to Fig. A.2.)

$$\phi_n = \tan^{-1}\left[\left(\frac{D_n}{f_n}\right)\cos\theta_n\right]$$

where D is the distance from $\overline{GZ}$, as established in the drawings from the primary data, to the midpoint of the baseline of the subsequent plane of measurement, i.e., $D_n = \overline{GZ}\,'P_n'/m_R$

m_R is the magnification of the Recordak used in making the tracings of both the primary and the subsequent records.

With aiming angle approximated, the growth of the shock front was measured frame by frame in the plane of measurement of the subsequent record. The resulting distances were then compared to the plotted arrival time data obtained from the primary record and corresponding times were read. The time interval between successive frames was noted and compared to the accurately known time per frame of the record in question. The approximated aiming angle was then adjusted until their times per frame agreed.

---

* The rocket trails were not sufficiently well defined in the primary record to be used as a fiducial marker.

** The left reference was found through the sprocket holes on the left side of the frame. The position of the sprocket holes is always fixed with respect to the frame center. Thus if the position of the reference is known on any given frame, the midpoint of the frame is known. The variation of the sprocket holes on any frame from the frame center is less than 1 per cent. (See reference (4.)

APPENDIX B
METEOROLOGICAL DATA ALOFT FOR SHOT 2

Altitude (ft)	Pressure (psi)	T (°C)	C_o (ft/sec)
0	14.68	26.7	1141
1000	14.17	23.8*	1136
2000	13.69	21.5	1131
3000	13.20	19.7*	1127
4000	12.73	17.8	1124
5000	12.27	16.0*	1121
6000	11.85	14.0	1117
7000	11.43*	12.5*	1114
8000	11.02	14.8	1118
9000	10.63	14.4*	1117
10,000	10.24	13.0	1115
11,000	9.88*	11.0*	1111
12,000	9.51	8.8	1106
13,000	9.17*	7.0*	1103
14,000	8.82	5.2	1099
15,000	8.50*	3.2*	1095

* Obtained by Interpolation

Page 98, deleted